FLORIDA INTERNATIONAL UNIVERSITY

Miami, Florida

THREE-DIMENSIONAL GRAPHENE FOAM REINFORCED EPOXY COMPOSITES

A thesis submitted in partial fulfillment of

the requirements for the degree of

MASTER OF SCIENCE

in

MATERIALS SCIENCE AND ENGINEERING

by

Leslie Embrey

2017

To: Interim Dean Ranu Jung
College of Engineering and Computing

This thesis, written by Leslie Embrey, and entitled Three-Dimensional Graphene Foam Reinforced Epoxy Composites, having been approved in respect to style and intellectual content, is referred to you for judgment.

We have read this thesis and recommend that it be approved.

_____
Norman Munroe

_____
Benjamin Boesl, Co-Major Professor

_____
Arvind Agarwal, Co-Major Professor

Date of Defense: March 27, 2017

The thesis of Leslie Embrey is approved.

_____
Interim Dean Ranu Jung
College of Engineering and Computing

_____
Andrés G. Gil
Vice President for Research and Economic Development
and Dean of the University Graduate School

Florida International University, 2017

DEDICATION

I dedicate this thesis to my Mom and Dad for always believing in me and inspiring me to follow my dreams, to my sister Laci for all the wonderful childhood memories and for never allowing a dull moment, and to my beautiful dog Bear who has been by my side every day for the last decade loving me unconditionally.

ACKNOWLEDGMENTS

First and foremost, I would like to sincerely thank my advisors, Dr. Arvind Agarwal and Dr. Benjamin Boesl for giving me the opportunity to be a part of their amazing research team. I want to thank Dr. Agarwal for challenging me and pushing me to my limits every single day. His leadership, tireless work ethic, and dedication to his students is extraordinary. Because of his mentoring and persistent encouragement, I have accomplished more in the last year and a half than I ever thought possible. He has provided me with opportunities that will influence my life forever, and for that I will always be grateful. I want to also thank Dr. Boesl for his kindness and support throughout the program. His calm and collected approach to problem solving is something to be admired. Dr. Boesl always had a way of helping me put things into perspective when the challenges of research seemed too large to handle. Learning from Dr. Agarwal and Dr. Boesl has helped me develop my skills and talents as a researcher and become the professional I am today.

I would like to personally acknowledge all members of the Plasma Forming Laboratory (PFL) and the Advanced Materials Engineering Research Institute (AMERI) who have helped me in any way through this challenging journey. The members of PLF and AMERI are talented, intelligent, and charismatic individuals who will always hold a special place in my heart. I have made many lifelong friends from this wonderful experience. I want to especially thank Dr. Sadegh Behdad, Dr. Cheng Zhang, Pranjal Nautiyal, and Dr. Alex Franco who kindly welcomed me to the research family and assisted me with the initial adjustment period. Dr. Behdad played a crucial role in helping me understand the basics of polymer science and polymer composites. The depth of knowledge he possesses in these subjects is incredible, and I am lucky to have experienced even a

glimpse of his brilliance while working with him during the first few months of my master's program. Dr. Cheng Zhang has also been very helpful to me since the first day I met him. He patiently answered any and all questions whether it be uncertainties regarding laboratory equipment, scientific processes, or presentation skills. I have learned a great deal from Dr. Zhang, especially how to come up with creative and innovative yet simple solutions as that is his expertise. Pranjal Nautiyal has been an excellent colleague and thankfully has become an even better friend. He has a special gift of deeply understanding science and engineering principles coupled with the ability to express his thoughts in a highly technical yet stylish and elegant manner. His hunger for knowledge, perseverant work ethic, and refreshing sense of humor is contagious. His willingness to help others and work long, hard hours while maintaining an upbeat, positive attitude has definitely served as a motivation and a model for me with my own work. Last but surely not least, I want to thank Dr. Alex Franco for helping me every time I needed anything whether it be answering my many, many questions, taking time to train me on all new equipment, or spending hours with me behind the SEM to further my research. His depth of scientific knowledge, keen ability to teach a variety of topics, ability to manage multiple departments simultaneously, and level of patience and professionalism truly set him apart as an engineer. Although everyone's name is not listed, I have learned so much from each member of these two amazing groups. I will always carry these pieces of knowledge, perspective, and culture with me as I progress through my professional and personal life.

Three other mentors in particular have played a role in my success with my master's program. Dr. Khokiat Kengskool was my first mentor at Florida International University who allowed me to step out of my comfort zone and start building my resume toward

becoming an engineer. After successfully completing his class, he encouraged me to become a tutor and subsequently allowed me to help teach his class during his absence. He has since given me the opportunity to collaborate with him and other students to edit his first Engineering Economy textbook. Dr. KK has demonstrated throughout his career the importance of doing everything with passion and enthusiasm. Consistently receiving awards at FIU such as "Most Caring Professor" and the "Honorable Teaching Award", Dr. KK undoubtedly has touched many students' lives, including my own. I want to say thank you to my previous boss and mentor Dr. Anthony Hui who gave me my first "real" job and allowed me to prosper at Northwest Arkansas Pathology. Dr. Hui leads by example in terms of being the first one in and the last one out of work to drive and maintain his remarkably successful career. Despite his busy schedule, Dr. Hui was always there to give me advice on any subject, and although leaving the medical field was not in line with his best advice, he encouraged me 100 percent to follow what I felt was best for me. I will always admire and respect him for giving me the opportunity to explore my potential. Another person who has had more of an impact on my professional career than almost anyone else is my lifelong mentor Dr. Gay Stewart (my Physics Mom). I met Dr. Stewart in 2001, and she immediately took me under her wing and gave me every possible opportunity in her power. She believed in me and instilled in me a confidence I never knew before. Dr. Stewart taught me the importance of being a role model and leaving my mark on the world. As all other great mentors, she leads by example. She works extremely hard and maximizes every moment of every day to make a positive impact despite her already impressive resume. With each great accomplishment, she sets bigger and better goals, inspiring those around her to do the same. Because of Dr. Stewart, I am here today. She has guided me every step

of the way and reassured me that persistently following my dreams would almost always result in pure happiness and success.

Throughout this journey, the most influential and positive forces have been my beautiful friends and family. My best friend Paige has been like a sister to me for over 15 years. She has been there for me throughout the toughest of times lending me advice along the way whether it be personal or professional. She has taught me the importance of being prepared, patient, and rational in order to make sound, objective decisions. All five of my siblings played a vital role in shaping who I am as a person but most notably my sister Laci. She has shown me how to be independent and stand up for myself. She is a very strong woman, and I am proud to call her my sister. Lastly, and most importantly of all, my parents have made me who I am today. They both worked so hard to make my dreams possible. My Mom taught me how to be loving, caring, sweet, and charming. My Dad encouraged me from childhood to strive for excellence and to get the most out of my education. Mom and Dad instilled in me the importance of standing up for what is right, speaking my mind, and how to be an all-around great person. I owe everything to parents, especially my happiness and success. I truly thank everyone from the bottom of my heart who has contributed to my success throughout this journey. I would not be where I am today without their unconditional love and support.

ABSTRACT OF THE THESIS

THREE-DIMENSIONAL GRAPHENE FOAM REINFORCED EPOXY COMPOSITES

by

Leslie Embrey

Florida International University, 2017

Miami, Florida

Professor Arvind Agarwal, Co-Major Professor

Professor Benjamin Boesl, Co-Major Professor

Three-dimensional graphene foam (3D GrF) is an interconnected, porous structure of graphene sheets with excellent mechanical, electrical and thermal properties, making it a candidate reinforcement for polymer matrices. GrF's 3D structure eliminates nanoparticle agglomeration and provides seamless pathways for electron travel. The objective of this work is to fabricate low density GrF reinforced epoxy composites with superior mechanical and electrical properties and study the underlying deformation mechanisms. Dip coating and mold casting fabrication methods are employed in order to tailor the microstructure and properties. The composite's microstructure revealed good interfacial interaction. By adding mere 0.63 wt.% GrF, flexural strength was improved by 56%. The addition of 2 wt.% GrF showed a surge in glass transition temperature (56^{o}C), improvement in damping behavior (150%), and electrical conductivity 11 orders of magnitude higher than pure epoxy. Dip coated and mold casted composites showed a gauge factor of ~2.4 indicating electromechanically robust composite materials.

TABLE OF CONTENTS

LIST OF TABLES

LIST OF FIGURES

CHAPTER I

INTRODUCTION

The overall objective of this research is to create high strength, low density, electrically conductive nanocomposites by reinforcing epoxy polymer with three-dimensional graphene foam (3D GrF). Two facile synthesis techniques are used in order to vary the GrF content within the polymer matrix. By controlling the GrF to polymer ratio, the mechanical, thermal, and electrical properties may be engineered for the desired applications.

1.1. Motivation for this Research

The discovery of graphene (Fig. 1.1) has sparked intense research interest in recent years due to its superior strength, electron mobility, and thermal properties [1]. Over the last few decades, graphene and other carbon-based reinforcements, such as carbon nanotubes (CNTs) and graphene nanoplatelets (GNPs), have been studied extensively for potential use in high performance polymer composites for a range of applications. Although one and two-dimensional carbon-based polymer composites have many benefits, there are some problems associated with the nanoparticle reinforcements that compromise the integrity of the resulting composite material. Major challenges arise when utilizing carbon fiber, CNTs, and GNPs as matrix reinforcements such as the *tendency of the nanoparticles to agglomerate or restack* and *high inter-sheet contact resistance* between graphene sheets due to the strong intermolecular π-π interactions and interlayer van der Waals forces. These issues can lead to detrimental composite performance because the agglomerated particles act as stress concentration sites and can inhibit polymer chain movement resulting in a

decrease in material flexibility[2]. The electrical and thermal properties are diminished due to the discontinuity of reinforcement pathways within the composite. The two-dimensional structure of GNPs also results in a composite material that is *anisotropic* which may be an unfavorable property depending on the intended application of the material. These challenges are addressed in this study through the use of ultra-low density 3D GrF (0.004 g/cm^3) [3-5] as a polymer reinforcement. By reinforcing polymers such as epoxy with 3D GrF, electrical and thermal conductivities can be enhanced due to the three-dimensional network which provides more seamless pathways for electron and phonon transport. Furthermore, the longevity and survivability of the composite material can also be improved by enhancing mechanical strength and damping behavior.

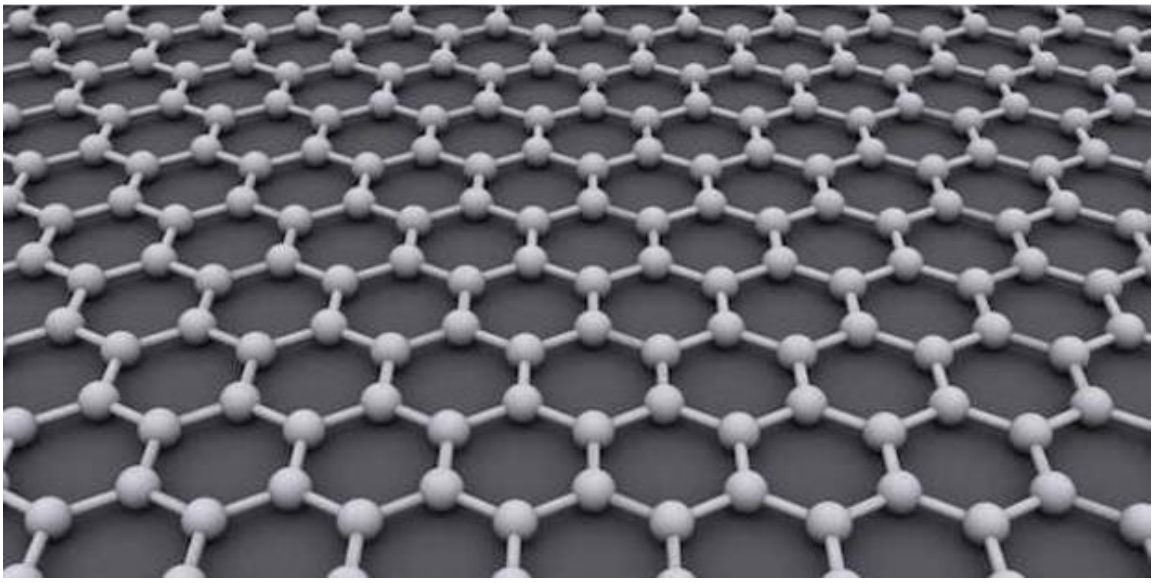

Fig. 1.1. Schematic of graphene's two-dimensional, hexagonal lattice.

1.2. Significant Impacts on Society

1.2.1. Aerospace

The aerospace industry heavily relies on polymer composite materials for improved aircraft performance (Fig. 1.2) while maintaining reasonable operating and maintenance costs. Some of the main concerns of the aerospace industry is overall aircraft weight reduction, improved engine efficiency, electromagnetic interference (EMI) shielding, and extreme weather resistance [6]. GrF-polymer composites may be the key to address each of these problems (Fig. 1.3) with their remarkable mechanical, electrical, and thermal properties. Replacing heavier aircraft components with strong, lightweight composite materials will not only achieve weight reduction but will also result in decreased fuel consumption, improved engine efficiency, and better payload agility [7-9]. GrF-polymer fuselage and wing coatings would protect against extreme weather conditions such as lightning strikes and freezing rain encountered during flight due to their superior electrical and thermal conductivities. GrF-polymers are known to be shock, vibration, and noise dampening materials leading to safer and more comfortable transit [10]. The notable flexibility of GrF-polymeric materials could lead into an era of morphing and self-healing fuselages, airplane wings, landing gear, and unmanned aerial vehicles which would improve survivability of commercial and military aircraft. By enhancing performance and overall lifespan of aircraft systems, manufacturing and operating costs would decrease. This would ultimately drive down costs for passengers which would open opportunities for more frequent and distant travel. Providing a more comfortable trip and ensuring passenger safety against extreme weather would spark more interest in air travel while generating revenue and strengthening the economy.

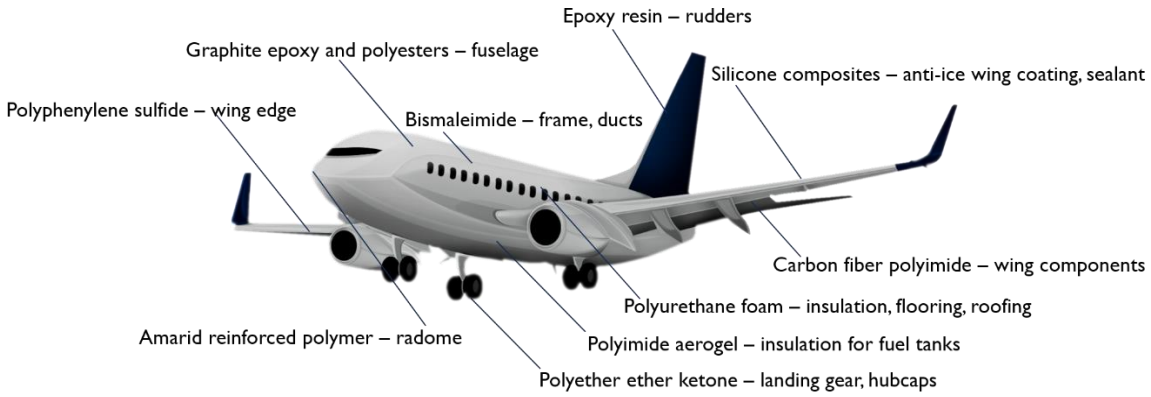

Fig. 1.2. Polymer composites commonly used for commercial aircraft vehicles [11].

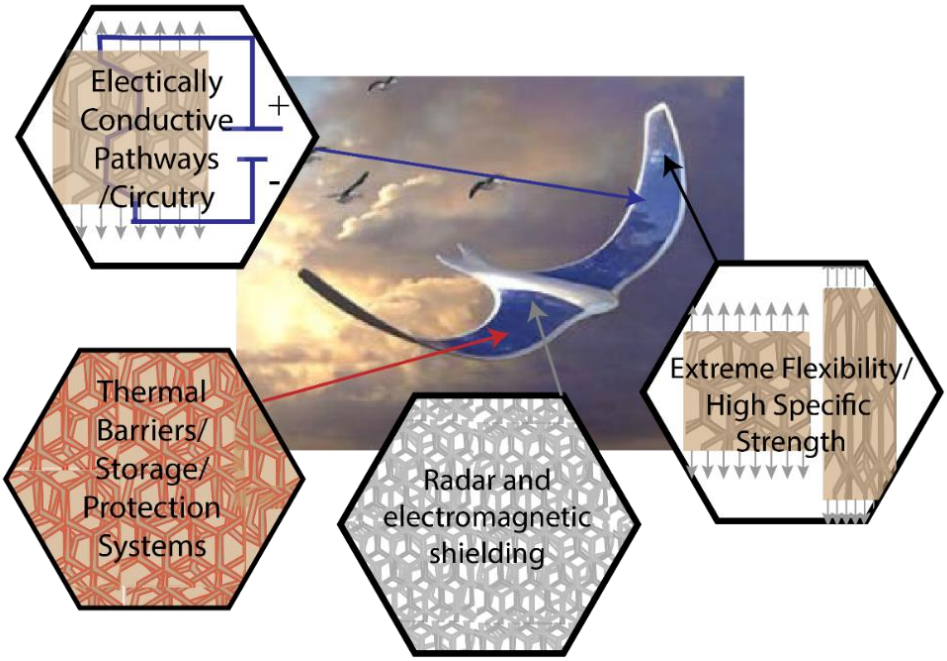

Fig. 1.3. Concept aerospace applications for GrF-epoxy composites [12].

1.2.2. Medical

GrF and its composites have potential applications in the medical field. Flexible, wearable strain sensors made of GrF-polymer composites are a major research focus as these devices have the capabilities to monitor pulse, blood pressure, and respiration rates,

as well as patient medical devices such as insulin and infusion pumps [8, 13-14]. Studies have repeatedly shown that polymers such as hydroxyapatite (HA) and polylactic acid–poly-ε-caprolactone copolymer (PLC) serve as musculoskeletal scaffolds as well as scaffolding for neural stem cells [15-16]. The porous structure of GrF-polymer composites serves as biocompatible and electrically conductive growth media for osteoblasts, myocytes, chondrocytes, and neuronal cells. Not only do the large surface area and porous nature of these GrF-polymer composites provide stable microenvironments for cell proliferation, the GrF itself may be used as electrodes to stimulate the tissue in order to verify cellular functionality [17-18]. GrF-polymer composites are effectively providing a foundation for large-scale cell and tissue bioengineering, musculoskeletal regeneration, and neurological prostheses.

1.2.3. Electronics

The electronics industry undeniably has an impact on the health of the economy, and GrF-polymer composites have great potential at revolutionizing the electronics world. Owing to GrF's outstanding electrical charge and discharge rate, GrF composites have a promising role as supercapacitors and chemical-free batteries. Recently, a 1 mm^2 integrated circuit has been fabricated via standard complementary metal-oxide semiconductor (CMOS) compatible processes with a graphene-based field effect transistor and inductors revealing the probability to develop scalable, ultrafast electronics which would allow people to feel more connected than ever before [19-21]. Continued research and development of GrF and its polymer composites have the ability to change the world of electronics siting

profound impacts on the energy, aerospace, automotive, and entertainment markets across the world.

1.2.4. Environmental

Environmental concerns are on the rise, and GrF-polymer composites could contribute significantly to environmental cleanup, pollution management, and general awareness efforts. The porous nature of GrF along with its ability to effectively move phonons give rise to thermal energy storage applications such as solar cells and other electronic heat sinks [22]. Harnessing the hydrophibicity and adhesion energies of GrF's surface may foster more advanced environmental cleanup procedures. By controlling the pore size and wettability characteristics of GrF and its composites, water desalination, oil-water separation, and gas filtration have been achieved experimentally [23-25].

GrF and GrF-polymer composites have many promising applications across a variety of diverse fields. The development of scalable GrF-polymeric materials would have profound global impacts considering the applications span entertainment and leisure, travel, national and international security, healthcare, and environmental cleanup. These micro and nanoscale materials will inevitably have important macroscopic impacts on the global community.

1.3. Research Objectives

The *overall objective* of this thesis is to reinforce epoxy with three-dimensional graphene foam (3D GrF) to create high strength, low density, thermally and electrically

conductive nanocomposite for various applications. The following points outline the approach taken to meet the overall objective:

- Graphene foam based composites require good interfacial interaction for achievement of superior mechanical, thermal, and electrical properties – *Wettability studies of epoxy against graphene foam are used to investigate contact angle hysteresis.*
- Effective use of GrF as a reinforcement material requires homogeneous distribution of GrF into the epoxy matrix – *Dip coated and mold casting synthesis techniques are employed to produce 3D GrF-epoxy composites efficiently and effectively.*
- Effects of GrF on strengthening and damping behavior of GrF-epoxy composites are evaluated through mechanical testing and nanoindentation experiments – *Microstructural observation is used to illustrate GrF strengthening mechanisms.*
- Superior thermal and electrical conductivities are required of multi-functional aerospace fuselages, wings, skins, and coatings – *Effects of GrF addition on thermal and electrical properties are investigated through differential scanning calorimetry and 4-probe electrical conductivity experimentation.*

In the following chapter, Chapter 2, a review of the state of the art is presented. An evaluation of the evolution of carbon-based polymer reinforcements is presented as GrF is the polymer reinforcement used in this study. Additionally, the progression of synthesis techniques and processing parameters is discussed. Chapter 3 describes the materials and experimental procedures used in the fabrication and evaluation of GrF reinforced epoxy

composites. Chapter 4 presents the results of these experiments and a detailed discussion of the underlying mechanisms governing the observed phenomena. Chapter 5 reviews the major findings and conclusions of this research. Chapter 6 offers suggestions for future directions and further research on 3D GrF-polymer composites.

CHAPTER II

REVIEW OF THE STATE OF THE ART

2. Evolution of Carbon-Based Polymer Composites

Carbon-based polymer matrix composites (PMCs) have been extensively researched since their technical and commercial introduction in the late 1960s [26-27]. Due to their flexible nature, high strength-to-weight ratio, and excellent heat, chemical, and corrosion resistance, carbon-based polymer composites are ideal for many applications [6-7, 22, 28-31]. Polymer composites are easy to manufacture which leads to lower production costs and more complex design freedom. Carbon-based reinforced polymer composites, specifically graphene-polymer composites, are on the forefront of current research interests globally [8, 22]. Fig. 2.1 shows the evolution of composites over time, including the importance of carbon fiber reinforced polymer (CFRP) composites in the engineering field starting at around the year 1980. Published by Ashby [27] in 1987, the diagram also shows how the importance of high modulus polymers and conducting polymers composites are projected to gain much popularity leading up to the year 2020. Furthermore, the associated research on carbon-based composites is shown in Fig. 2.2. Represented in the graph are the number of peer-reviewed journal articles published on carbon fiber, carbon nanotubes, and graphene since 1975. The following sections review the evolution of advanced, high-performance, carbon-based polymer composites from carbon fiber reinforced polymer composites to graphene-based polymer composites.

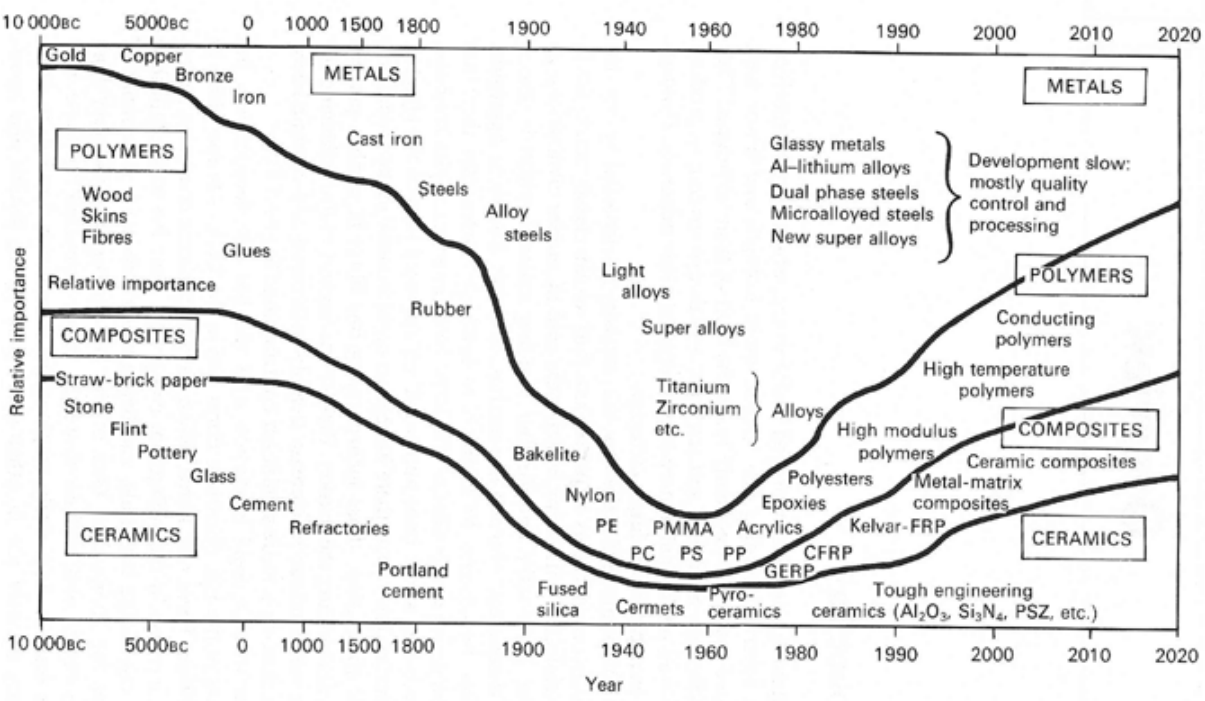

Fig. 2.1. Diagram illustrating the relative importance as a function of time of four classes of materials in the engineering field (metals, polymers, ceramics, and composites [27].

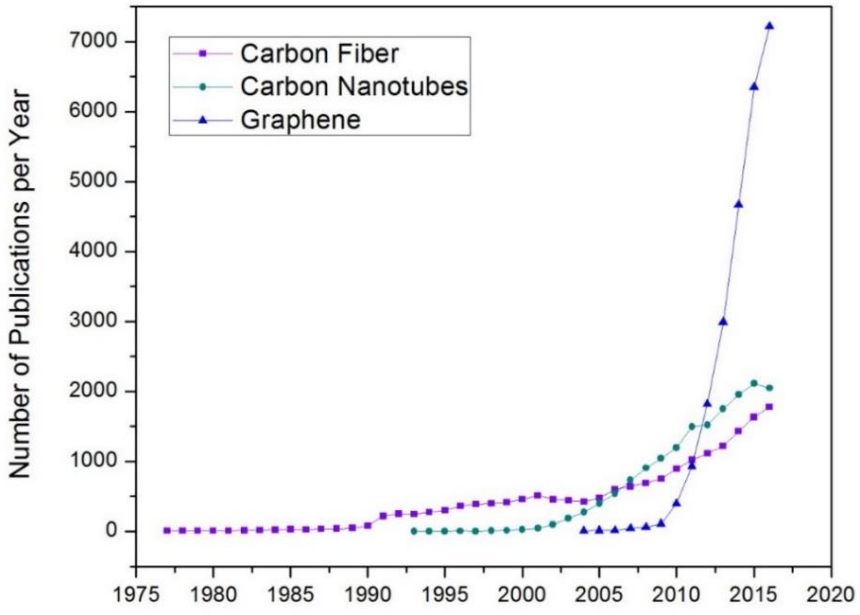

Fig. 2.2. The number of peer-reviewed articles published yearly on carbon fiber, carbon nanotubes, and graphene composites since 1975. Data obtained from Web of Science.

2.1. 1D and 2D Carbon-Based Polymer Composites

The first carbon-based nanofillers, carbon fibers, were introduced commercially in the late 1960s. Carbon fibers, CNTs, and graphene have many appreciable characteristics, but each also have their drawbacks. The characteristics, material properties, composite synthesis method, and polymer composite challenges of carbon fiber, CNTs, and graphene are displayed in Table 2.1. Subsequently, an SEM micrograph of each of the three carbon-based materials are shown in Fig. 2.3.

Table 2.1. A comparison of the properties, synthesis methods, and drawbacks of carbon fiber, CNTs, and graphene.

	Carbon Fiber	**Carbon Nanotubes**	**Graphene**
Year of Introduction	Late 1960s (Technical/commercial introduction) [32]	1991 (Confirmed by SEM) [33-35]	2004 [36]
Dimensions	-1D -Semicrystalline polymeric fibers -Diameter of ~7 microns [30, 37-38]	-1D -Diameters ranging from 1 nm to several centimeters [39]	-2D -Graphene:1 atom thick -GNP: 5-10 nm thickness [40]
Aspect Ratio	Greater than 100 [41-42]	Up to 1000 [39]	Greater than 1200 [43]
Geometries	-Hollow -Patterned -Porous [41]	-Cylindrically shaped -Single-walled geometries: (armchair, chiral, zigzag) -Double-walled -Multi-walled -End cap morphologies [7, 44]	-Single atomic layer -Stacked platelets [41]
Synthesis Techniques	-Pyrolysis of stabilized precursor (Polyacrylonitrile (PAN), petroleum pitch, or rayon) [42]	-Arc-discharge evaporation -Plasma-enhanced CVD [33, 39, 44-46]	-Scotch tape method -Chemical synthesis -Exfoliation -Epitaxial growth -Pyrolysis -CVD on Ni foam [40, 47-49]
Mechanical Properties	-Tensile strength 7 GPa -Tensile modulus 900 GPa -Compressive strength 3 GPa -Density 2 g/cm^3	Along the axial length (not across tube diameter): -Tensile strength 100 GPa -Elastic modulus 1-1.3 TPa	-Tensile strength 130 GPa -Elastic modulus 0.5-1 TPa -Density 1.8 g/cm^3 [52-56]

	[9, 30, 38, 42, 50]	-Density 1.3 g/cm^3 [33, 44, 51]	
Electrical Properties	-Conductivity 900 S/m [42, 50]	-Conductivity 5x10^5 S/m [39, 44]	-Conductivity 2x10^4 S/m [22, 57]
Thermal Properties	-Conductivity 1100 W/mK [42]	-Conductivity 2000 W/mK [58]	-Conductivity 5000 W/mK [28, 59]
Composite synthesis	-Filament winding -Pultrusion -Liquid, compression, and injection molding -Vacuum-assisted resin transfer molding [38, 42, 60]	-Bulk mixing -Melt mixing -Solution blending -Film casting -In situ polymerization -CVD on polymer substrate [45-46, 51, 58, 61-62]	-Melt mixing -In situ polymerization -Hot pressing -Solution mixing [26, 40, 63-64]
Applications (Polymer Composites)	-Auto bodies and seat frames -Sporting goods -Military vehicles and armor -X-ray imaging medical equipment -Water purification -Chemical absorption	<u>Emerging Applications</u> -Sporting goods -Energy storage -Conductive adhesive -Molecular electronics -Air and water filtration	<u>Potential Applications</u> -Flexible, foldable airplane wings -Flexible electronics -EMI and microwave shielding -Anti-ice coatings -Acoustic backing material -Supercapacitors
Challenges	-Nanoparticle agglomeration -Moisture absorption -Brittle fibers fracture -Fiber delamination [9, 30, 38, 50]	-CNT alignment -Nanoparticle agglomeration -Need for surface modification -CNT curling and entanglement -Difficult to strategically orient within polymer matrix [7, 44, 46, 51, 61]	-Nanoparticle agglomeration -Restacking of graphene sheets -Discontinuity of reinforcement in polymer matrix -High intersheet junction contact resistance between layered graphene sheets [4-5, 16, 65-66]

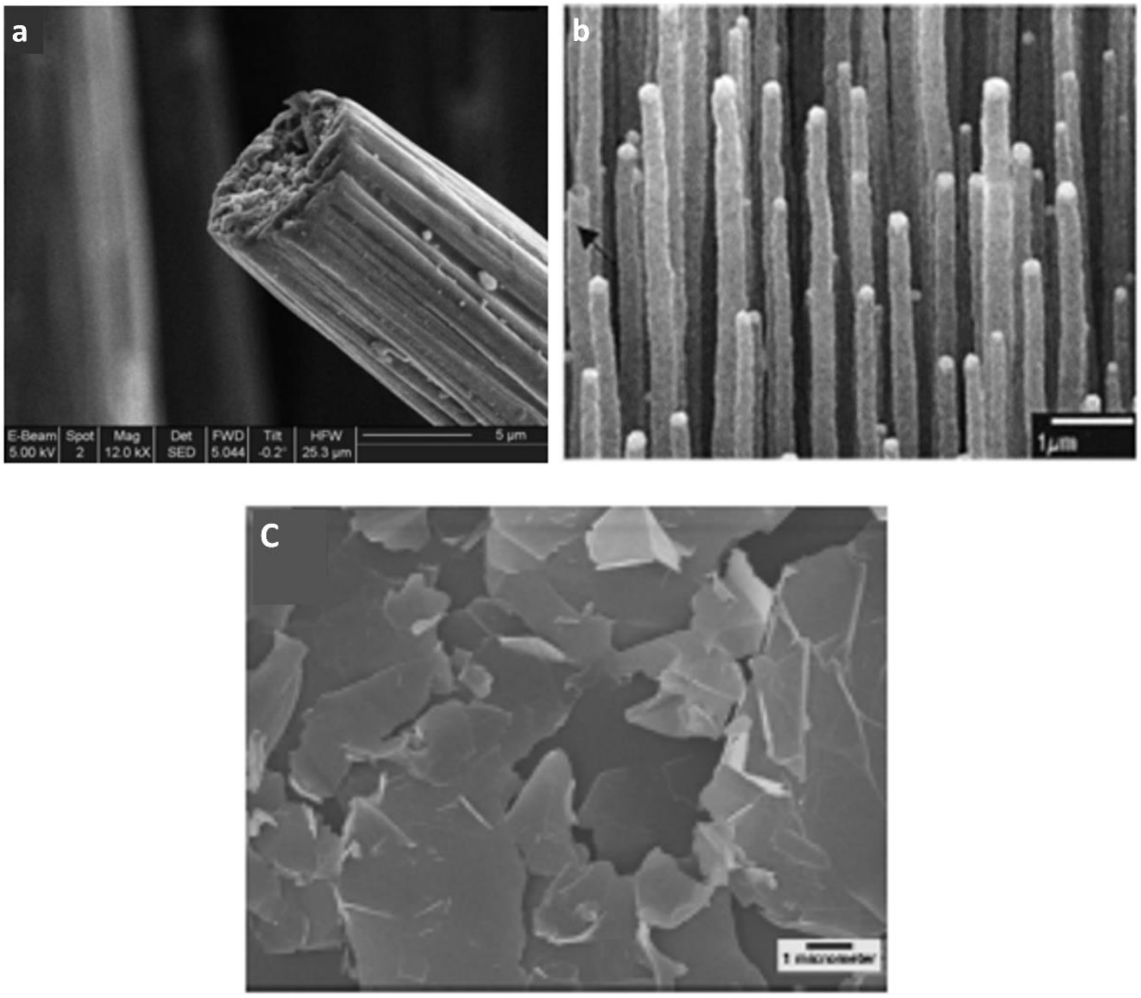

Fig. 2.3. SEM micrographs of (a) a single carbon fiber [67], (b) controlled growth of CNTs [51], and (c) GNP powder [40].

All previously mentioned carbon-based polymer composites have many benefits, but they also have some disadvantages. Carbon fiber reinforced polymer composites are durable, and the carbon fibers may even be recycled. However, the fiber synthesis process is expensive and time-consuming. Carbon nanotubes are now more easily processed leading to lower composite fabrication costs, but the CNTs are difficult to manipulate within the polymer matrix and have the tendency to curl, tangle, and agglomerate. GNPs

have less tendency to agglomerate and have larger surface area than CNTs allowing for enhanced composite performance. However, GNP's two-dimensional nature leads to material anisotropy resulting in inferior through-plane properties as compared to the in-plane properties.

Lastly, while GrF reinforced polymer composites seem to effectively address the problems associated with 1D and 2D carbon-based reinforcements, large-scale manufacturing of GrF is hindering the broader impacts its composites could be having for many structural and multifunctional applications. Concentrated, continuous research is needed to achieve more innovative, cost-effective reinforcement and composite fabrication processes in order to realize the full implications of graphene, GrF, and their associated polymer composites.

2.2. Three-Dimensional Graphene Foam

2.2.1. Properties of 3D Graphene Foam

Three-dimensional graphene foam (3D GrF) is a free-standing, multilayer, cellular structure which retains many of graphene's desirable properties, such as high strength-to-weight ratio, flexibility, elasticity, hydrophobicity, and thermal and electrical conductivities [68-72]. Composed of individual layers of graphene sheets, which are made of sp^2 hybridized carbon atoms with short carbon-carbon bond lengths (~1.418 Å), GrF possesses high strength and elasticity. The out-of-plane, weak van der Waals forces between layers of graphene sheets (separation of ~3.347 Å) allow GrF's surprisingly flexible nature. The ultra-low density of 4 mg/cm^3 [5, 15, 17, 73-74] is due to GrF's hollow interior as well as its porous, foamy, node-branch anatomy. Seamless pathways for rapid

phonon and electron transport are provided by GrF's 3D interconnected network [4, 15-16, 25, 58-59, 74-75]. The regularly-spaced, free-standing structure in addition to the unique mechanical, thermal, and electrical properties make GrF a candidate reinforcing material for composite matrices, eliminating the need for dispersion techniques typically required when using other 1D and 2D carbon-based reinforcement materials.

2.2.2. Fabrication of 3D Graphene Foam

Many synthesis methods of GrF have been reported since its introduction in 2011, including mechanical and chemical exfoliation, hydrothermal synthesis, chemically-driven self-assembly [76-77], lithographic patterning [78], freeze drying [73], and air bubble and silica sphere template-guided synthesis [3, 79]. Among the most common is template-guided growth by chemical vapor deposition (CVD) [4, 57, 80-81]. The CVD method begins with a metal template foam, such as nickel or copper. The foam is placed in a methane or ethylene environment and heated to approximately 700-1000^{o}C. Carbon falls onto the nickel foam as the gaseous molecules dissociate. Following the carbon deposition onto nickel foam, the nickel-graphene foam is removed from the furnace and coated with a stabilizing polymer such as polymethylmethacrylate (PMMA). The nickel is then removed with a wet etchant, followed by completely dissolving away the polymer with acetone. The result is a three-dimensional, porous, freestanding graphene foam [57, 80]. A flowchart of the GrF synthesis process is illustrated in Fig. 2.4. Fig. 2.5. shows SEM images of carbon deposited nickel foam, free-standing 3D GrF, and high magnification images of GrF branches and GrF surface features [17].

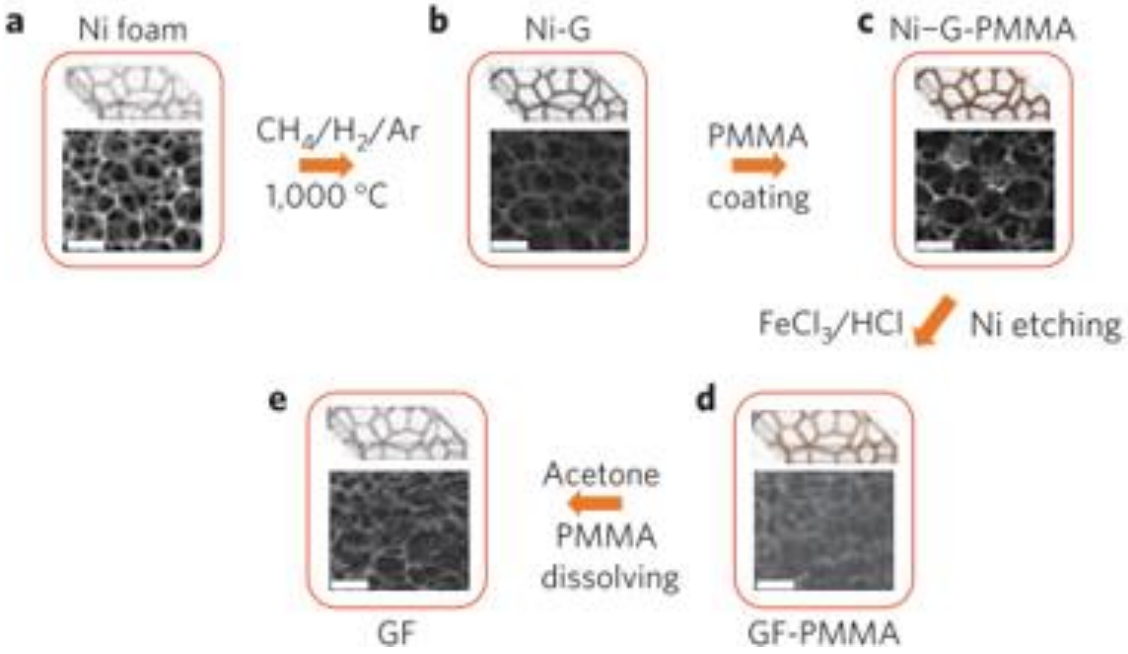

Fig. 2.4. Flowchart of the synthesis of freestanding 3D GrF by CVD method [4].

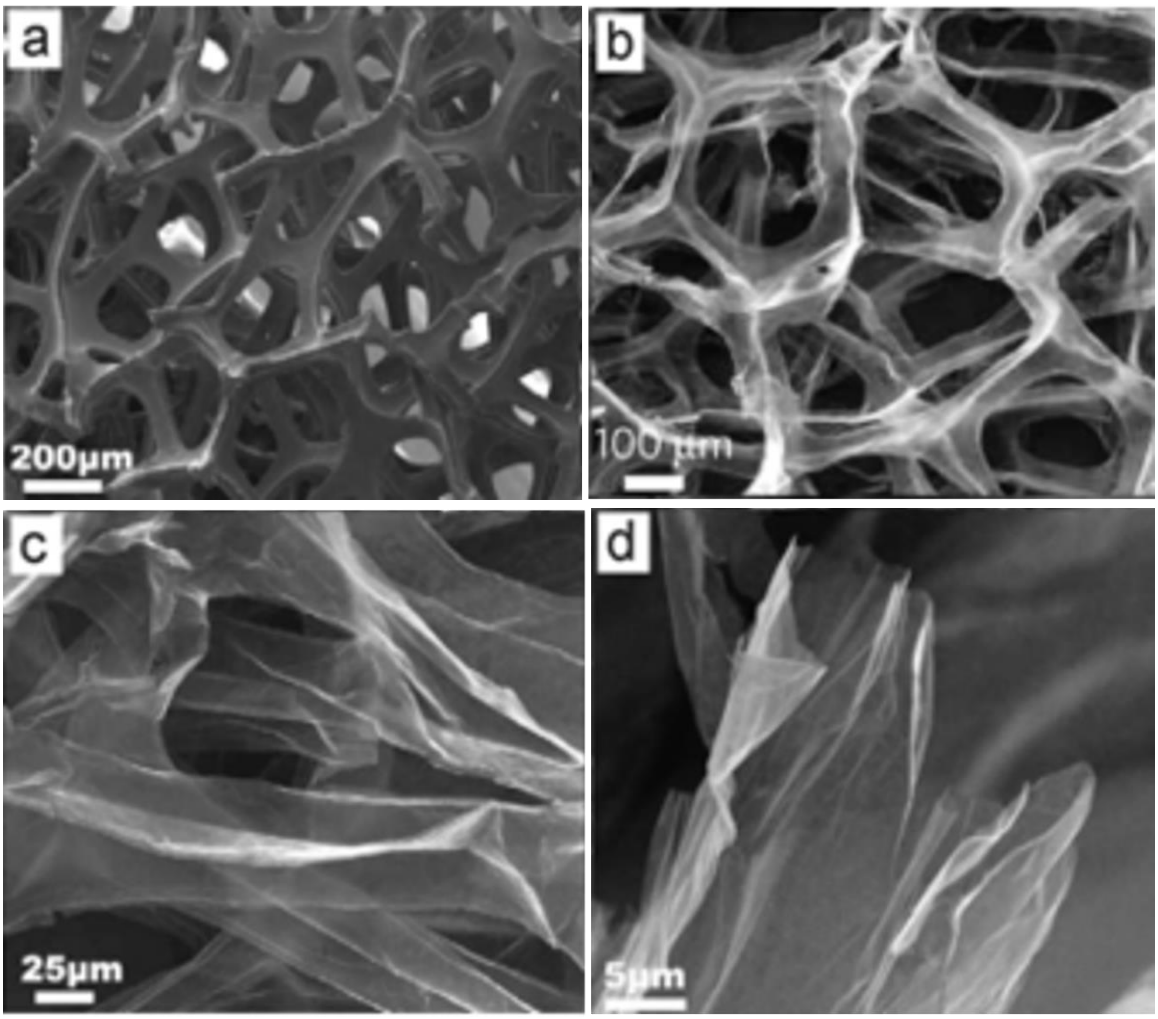

Fig. 2.5. SEM images of (a) carbon deposition on nickel foam, (b) free-standing 3D GrF, (c) high magnification images of GrF branches, and (d) surface features of GrF [66].

Another synthesis method involves combining two synthesis techniques: traditional powder metallurgy and the CVD method [53, 82]. The powder metallurgy template-assisted CVD (PMT-CVD) method is a facile and scalable technique in which sucrose (carbon source) is mechanically mixed with nickel powder in deionized (DI) water and heated to 120^{o}C until the water is completely evaporated. This leaves behind tiny spherical carbon-coated nickel shells which are vacuum dried at 80^{o}C overnight then ground into a fine

powder with a mortar and pestle. The hybrid powder is pressed in a die at 1120 MPa for five minutes to produce pellets which are then loaded into a quartz tube furnace with a H_2/Ar (200 sccm/500 sccm) environment at a pressure of 9 Torr in order to grow graphene. The furnace temperature is raised to 1000^{o}C and the pellets are annealed for 30 minutes. After removing the pellets and cooling to room temperature, the nickel is etched with 1 M $FeCl_3$ aqueous solution for one week, with the solution changed daily. The foam is subsequently soaked in DI water for one week, changing the water daily. A critical point dryer is used to completely dry the PMT-CVD GrF (Fig 2.6). SEM images of PMT-GrF at high and low magnifications are shown in Fig. 2.7.

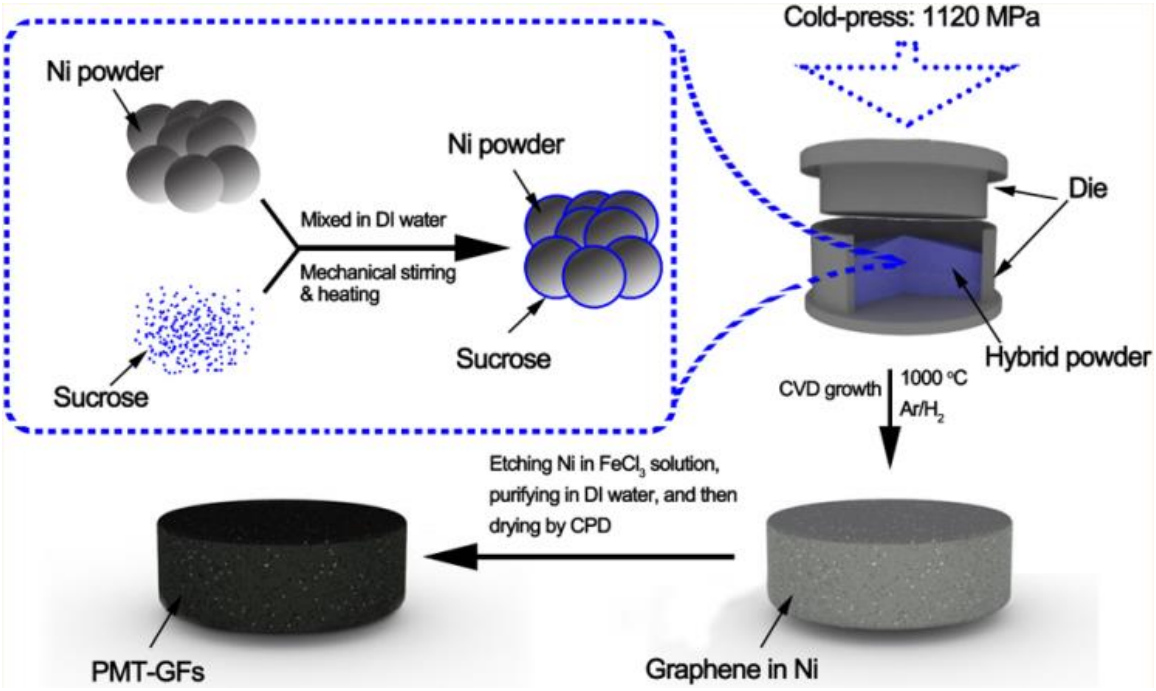

Fig. 2.6. Schematic of the preparation of 3D GrF by powder metallurgy template-assisted CVD method [82].

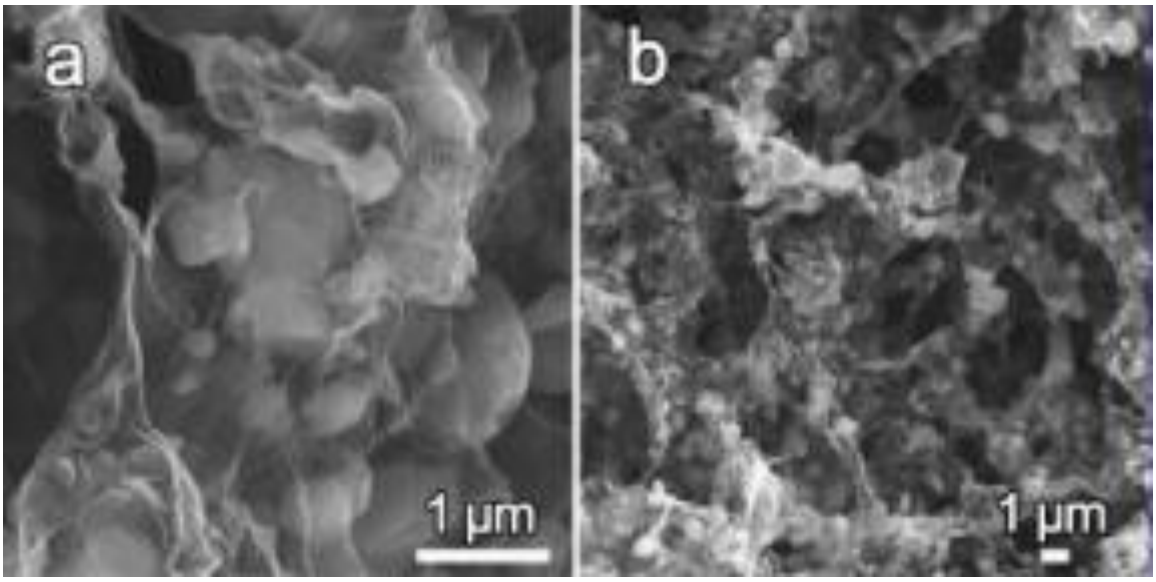

Fig. 2.7. SEM images of PMT-GrF at (a) high magnification and (b) low magnification [82].

Silica sphere template-guided fabrication method is unique in that it allows growth of nano GrF (NGrF) since many CVD template-guided approaches result in GrFs with pores on the scale of several hundred microns. The simple fabrication technique starts by mixing silica spheres (27.7 nm average diameter) modified with methyl groups with graphene oxide (GO) in a neutral aqueous solution. The silica spheres and the GO are both hydrophobic which induces self-assembled lamella structures which is a result of the silica spheres being wrapped between the GO. The GOs are reduced to graphene in an inert environment, and HF etching to remove silica spheres yields NGrF with pore sizes of 32.5 nm, foam thickness of 0.89 nm, and high surface area (851 m^2/g). Fig 2.8 illustrates the fabrication process for NGrF. SEM and TEM images of NGrF are shown in Fig. 2.9.

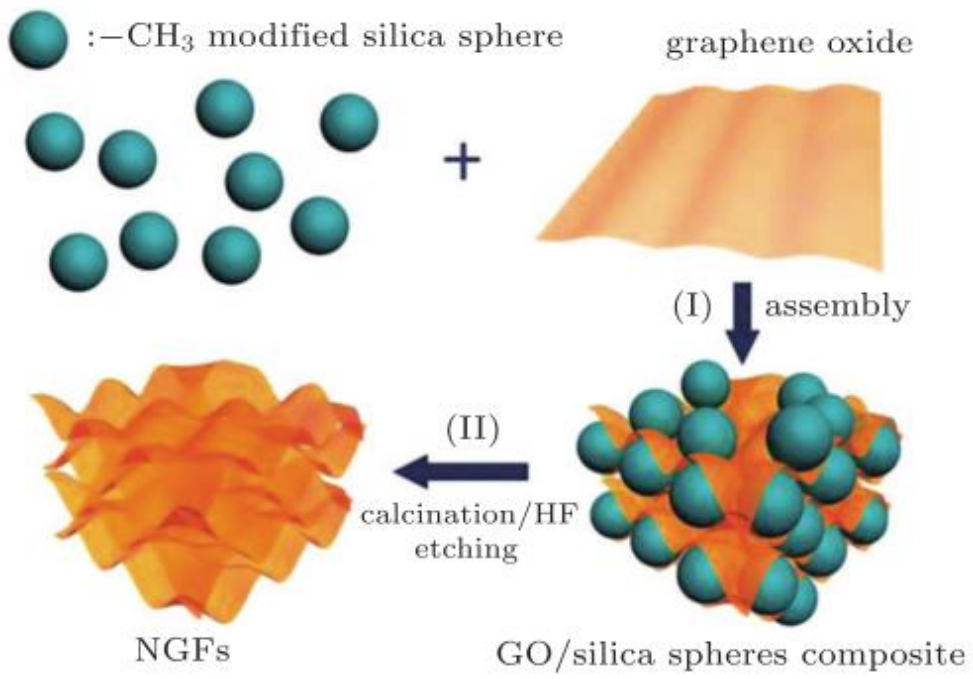

Fig. 2.8. Schematic of fabrication method for free-standing NGrF.

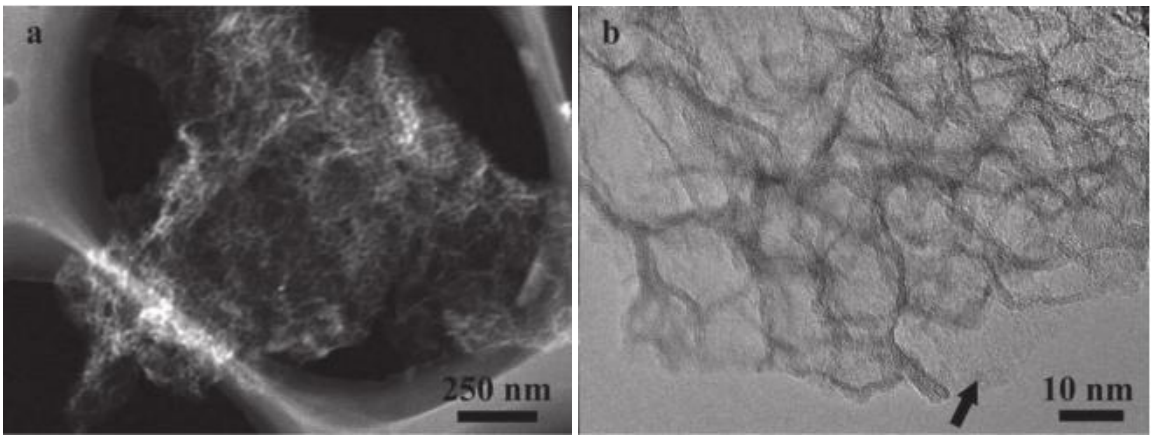

Fig. 2.9. (a) SEM image of NGrF and (b) HR-TEM of NGrF with black arrow differentiating flat foam from raised foam indicating that the NGrF is grown from single graphene sheets.

Other GrF synthesis methods include mechanical and chemical exfoliation [83], hydrothermal synthesis [84], chemically-driven self-assembly [76-77], lithographic patterning

[78], freeze drying [73, 85], breath figure method [85], and air bubble template-guided synthesis [3, 79]. Additional synthesis methods will undoubtedly be discovered as the need for large-scale graphene and GrF production intensifies.

2.3. 3D Graphene Foam-Polymer Composites

2.3.1. Synthesis of 3D Graphene Foam-Polymer Composites

The explosion of interest generated by the discovery of GrF has brought about novel composite materials with remarkable properties. Facile and effective fabrication methods employed for synthesizing GrF include dip coating and vacuum-assisted infiltration. Nieto, et al. [15] used simple dip coating method to synthesize graphene foam-polylactic acid and poly-ε-caprolactone (GrF-PLC) hybrid polymer composites. GrF grown by CVD method was dipped in acetone-diluted PLC solution for controlled time periods and allowed to cure. This facile synthesis technique resulted in GrF branches with uniform PLC coating, and the resulting composite retained GrF's porous, foamy structure.

Dip coating is also carried out in another way to obtain GrF-polymer composites. Chen et al [5] synthesized graphene foam-polydimethylsiloxane (GrF-PDMS) composites by carrying out the CVD approach to grow GrF but eliminating one of the final steps of the process. After depositing carbon on nickel foam, the entire structure was dipped into PDMS. The nickel was etched away, but the stabilizing polymer was not dissolved off of the foam with acetone or similar agent. This approach utilizes the stabilizing polymer as a composite component eliminating further composite synthesis techniques and leaving behind a GrF-PDMS porous, foamy structure.

Vacuum-assisted infiltration has been used to incorporate polymer into GrF's cellular structure. Vacuum-assisted resin transfer molding (VARTM) has long been used to make carbon-based polymer composite laminates. With GrF-polymer composites, vacuum-assisted infiltration may be used in one or two stages of the fabrication process. Samad et al. [86] used vacuum-assisted infiltration of graphene oxide (GO) onto nickel foam before the reducing the GO to GrF. Etching of the nickel substrate resulted in pure GrF which was permeated with PDMS again via vacuum-assisted infiltration and cured.

Typically, a combination of synthesis techniques are used to achieve the most successful composites. Jia et al. [80] combined immersion techniques, vacuum-assisted infiltration, and hot-pressing to fabricate GrF-epoxy composites. Prepregs were made by infiltrating graphene-nickel foam with epoxy resin and curing under vacuum environment. The individual prepregs were stacked and hot-pressed in an aluminum mold. Nickel was subsequently etched away resulting in GrF-epoxy composites.

The same research group utilized hot-pressing to create GrF-glass fiber-epoxy sandwich structure composites. Jia et al. [65] formed prepregs by immersing GrF into epoxy and curing under a vacuum environment. The prepregs were encased into glass fiber-epoxy fabric to form sandwich structures and again underwent vacuum infiltration. Finally the GrF-epoxy/glass fiber-epoxy sandwich structures were hot-pressed in a mold to reveal GrF interleaved glass fiber-epoxy laminate composites.

Centrifugal stirring, application of vacuum force, and a type of mold casting was employed to synthesize 3D GrF-tungsten-epoxy (GrF-W-Ep) composites. Qiu et al. [10] used centrifugal mixing to enhance infiltration of epoxy polymer containing tungsten

spheres as a secondary nanofiller into GrF's cellular structure [10]. Epoxy was placed in the bottom of a test tube to create a smooth, flat surface on which the 3D GrF was to be placed. Small circular pieces of 3D GrF were placed in the bottom of a test tube. A mixture of dilute epoxy and W spheres was vacuumed to remove trapped air bubbles and injected into the bottom of the tubes. The test tubes were centrifuged to embed the W spheres into the GrF cells, and the ethanol was evaporated. Polishing to desired thickness resulted in a GrF-W-Ep film composites.

2.3.2. Properties of 3D Graphene Foam-Polymer Composites

GrF-polymer composites have shown impressive mechanical, thermal, and electrical properties as a result of the synergistic interplay of the individual composite components. Polymers' heat, corrosion, and impact resistance along with their varying degrees of flexibility make them ideal matrix materials. GrF's unique, 3D structure in conjunction with its superior intrinsic properties suggest it to be a candidate reinforcing material. The combination of GrF and polymeric matrices give rise to a promising class of new composite materials to be used for a variety of structural and multifunctional applications. A review of GrF-polymer composites' mechanical, thermal, and electrical properties are presented in detail below.

2.3.2.1.Mechanical Properties

GrF's high strength, flexibility, and deformation mechanisms are primarily responsible for its polymer composites' impressive mechanical properties. Recent studies report enhanced mechanical performance of GrF composites with various polymers as matrix materials. GrF-PDMS composites outperformed pure CNT, pure GrF, and CNT-

PDMS composites (Fig. 2.10) in terms of peak stress, compressive strength (6 times that of CNT-PDMS), and elastic modulus (twice that of CNT-PDMS). Additionally, GrF-PDMS demonstrated highly reversible mechanical behavior up to 100 cycles of compression, including complete elastic recovery and retained energy absorption capabilities at strains of up to 70%. [87]. These impressive findings are attributed to the infiltration of PDMS into GrF porous structure as well as the collapsing of GrF walls under stress leading to higher graphene density. Also, GrF's 3D interconnected structure and its ability to bend and flex in response to applied load allowed effective energy dissipation. Elastic recovery is attributed to the strong interfacial interactions between GrF and PDMS.

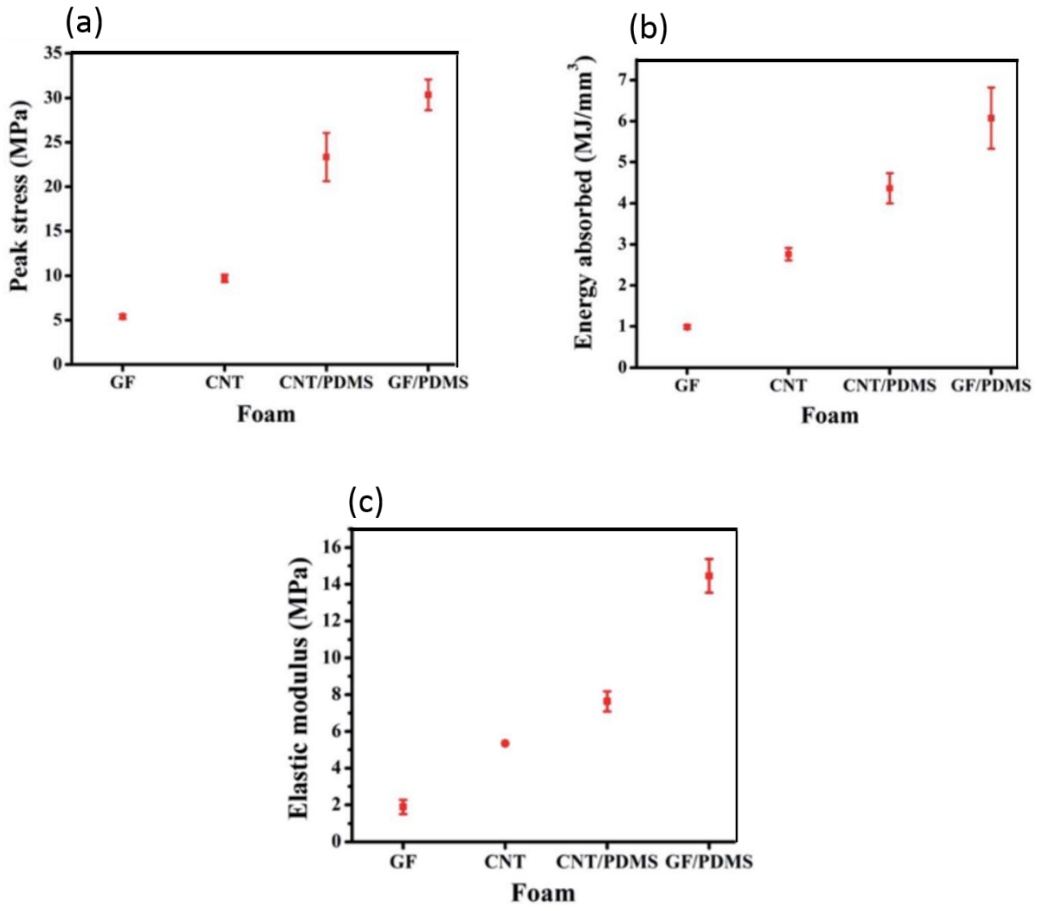

Fig. 2.10. Graphical comparison of (a) peak stress, (b) energy absorption, and (c) elastic modulus among pure GrF, pure CNT, CNT-PDMS, and GrF-PDMS.

Composite strength and ductility were evaluated in another study to understand the effects of GrF on PLC copolymer. Nieto et al. [15] found that GrF-PLC had higher compressive strength, a 3700% increase in ultimate tensile strength, and a 3100% increase in ductility when compared to pure GrF. The compression strengthening mechanisms are owed to the excellent wettability of PLC onto GrF substrate causing a sort of defect healing in which the PLC polymer filled microcracks and voids of GrF upon curing leading to enhanced structural integrity of GrF prior to testing. Furthermore the enhanced strength under tension of the composite are due to the GrF to PLC strong interfacial adhesion resulting in effective load transfer from PLC to GrF. The extreme elasticity of the composite material comes from PLC bridge formations. As the composite system is stretched, the polymer lining the GrF surface and internal cavities demonstrates a "rubber band" type of deformation in which the load is transferred back to the PLC polymer before ultimately fracturing. SEM images of GrF-PLC failure mechanisms are shown in Fig. 2.11.

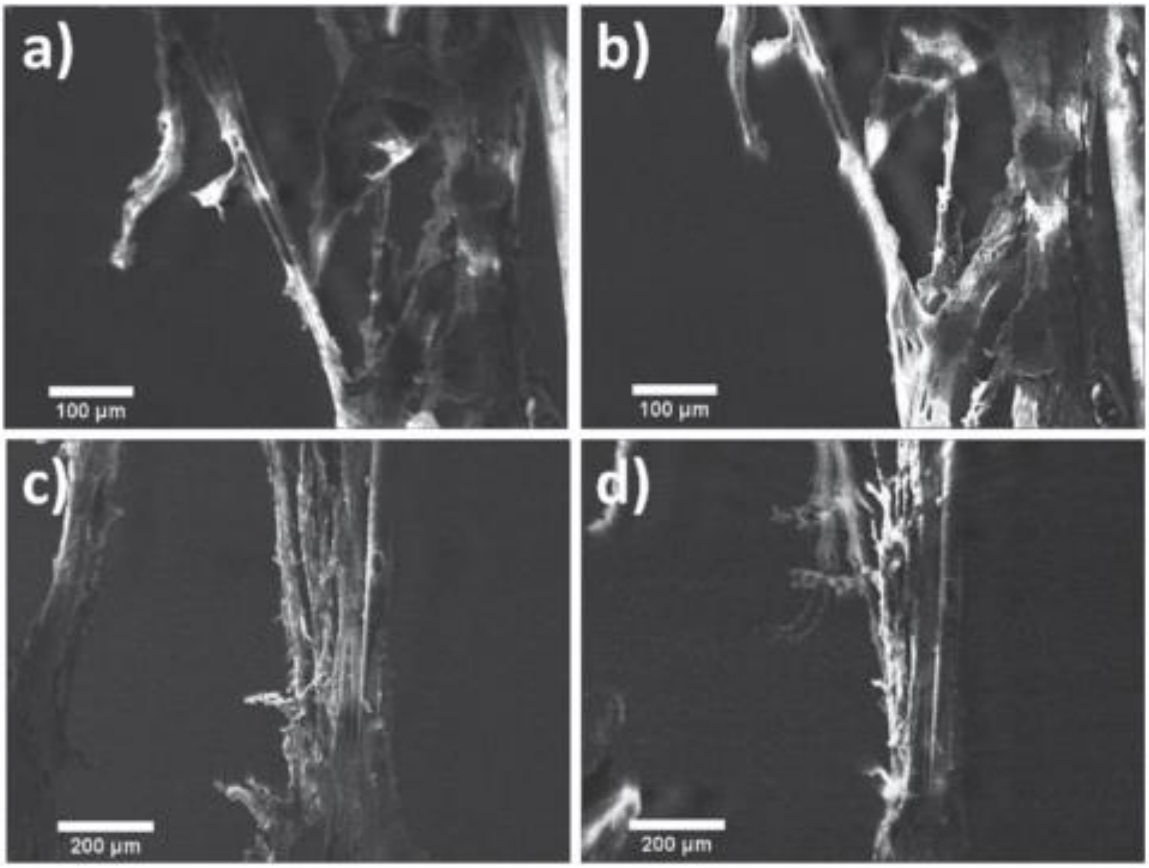

Fig. 2.11. GrF-PLC composite under tension. (a) Initial stretching of PLC bridge. (b) PLC coated GrF branches elongate without fracturing. (c) Branch composed of multiple aligned PLC bridges. (d) Elongated PLC bridges break one-by-one, GrF branch to left has fractured [15].

2.3.2.2.Thermal Properties

PDMS has been utilized as the matrix material for many GrF-polymer composite thermal properties studies. Graphene sheets (GrS) and GrF are incorporated separately into PDMS, and their effects on thermal conductivity and coefficient of thermal expansion of PDMS are investigated [59]. GrF-PDMS composites with mere 0.7 wt% loading drastically enhanced the thermal conductivity of pure PDMS a staggering 300% and proved to be 20%

higher than that of GrS-PDMS at the same graphene loading. This is due to GrF's 3D contingent pathways providing fast phonon transport throughout the composite. Furthermore, the coefficient of thermal expansion (CTE) was found to be much lower than GrS-PDMS and pure PDMS, and the thermal stability of GrF-PDMS was also improved over the pure PDMS and GrS-PDMS materials as seen in Fig. 2.12. For the composite materials, the CTE increased with increasing temperature because the internal stresses accumulated during the curing cycle are released as the materials are heated. The internal stresses within the composites occur because the reinforcement materials interfere with crosslinking during polymerization causing the polymer chains to uncharacteristically bend and twist in order to connect. The CTE of pure PDMS was relatively temperature-independent due to the minimal internal stresses acquired during polymer solidification. Also during heating to higher temperatures, the polymeric materials start to decompose, and the products from the decomposition reaction tend to diffuse throughout the sample in an attempt to escape the material, hence resulting in overall weight loss of the sample. GrF-PDMS enhanced thermal stability is a function of the uniform interconnected architecture. The GrF structure hinders the path of the decomposition products and as a result, they get trapped inside the sample. This leads to an overall improvement in thermal stability over the GrS-PDMS and pure PDMS materials.

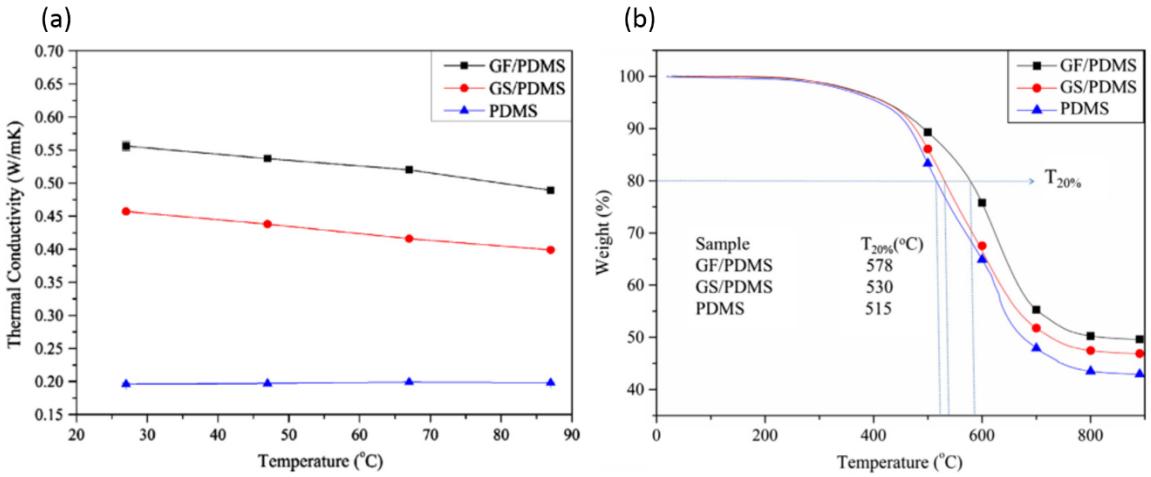

Fig. 2.12. Graphical representations of (a) thermal conductivity and (b) thermal stability of pure PDMS, GrS-PDMS, and GrF-PDMS materials [59].

In another similar study, multilayer graphene flakes (MGrF), GrF, and PDMS were used to make thermally conductive polymer composites. Zhao et al. [88]reports notable synergy between MGrF and GrF to improve thermal conductivity of PDMS. Addition of mere 2.7 vol.% MGrF showed dramatic improvement in thermal conductivity of 80%, 184%, and an astounding 440% over MGrF-PDMS, GrF-PDMS, and pure epoxy, respectively. This is a result of the MGrF adding continuity between the conductive filler materials and by providing higher graphene surface area enhancing contact area for which the PDMS polymer may interact.

2.3.2.3.Electrical Properties

Electrical characterization of GrF-polymer composites has been of high interest due to GrF's ability to rapidly transport electrons effectively and efficiently. Jun et al. [57] prepared GrF from graphite powder, small flake graphite (SFG) and large flake graphite (LFG), and subsequently infiltrated with PDMS. The in-plane and out-of-plane electrical

conductivity values were measured using 2-probe method using a current sweep of -1.0 ampere to +1.0 ampere. The results are summarized in Table 2.2. The GrF-PDMS grown from LFG precursor (0.4 wt.% GrF) proved to be the most successful composite with an in-plane electrical conductivity twice that of the SFG grown GrF-PDMS composite although the composite with GrF grown from SFG had 5 times the GrF content than GrF-PDMS composite with LFG. Additionally, the LFG composite showed 4 times the electrical conductivity of composites with GrF made from graphite powder although the graphite powder composite had 10 times the graphene foam content than the composite with GrF made from LFG owing to the more efficient pathways provided for fast electron mobility through the composite. The GrF grown from LFG underwent fewer defects during GrF production. The graphene sheets showed increasing overlapping areas, indicating less contact resistance and enhanced nanofiller continuity within the PDMS matrix. Finally, due to the larger size of graphene sheets, less contact junctions within the GrF were observed allowing for a more seamless transport of electrons within GrF.

Table 2.2. A summary of the test samples' GrF precursor, composite materials tested with weight percent GrF, and electrical conductivity values.

GrF Precursor	**Precursor Particle Size (μm)**	**Sample with wt.% GrF**	**In-Plane Electrical Conductivity (S/m)**	**Out-of-Plane Electrical Conductivity (S/m)**
LFG	> 100	0.4 - 0.5 wt.% GrF-PDMS	3.2	3.2×10^{-2}
SFG	2-15	1.9 wt.% GrF-PDMS	1.4×10^{-2}	5×10^{-3}
Graphite Powder	Crushed SFG (< 15)	4 wt.% GrF-PDMS	4.2×10^{-5}	4.2×10^{-5}

GrF-PDMS composites were synthesized and tested for electrical properties under bending stress to provide insight on potential large-scale strain sensor applications. As expected, as bending curvature increased, so did electrical resistance. An additional polymer film, poly (ethylene terephthalate) (PET), was used as a substrate for one side of the GrF-PDMS to improve sensitivity to bending deformation. Xu et al. [89] observed that upon bending in the direction of PET, the electrical resistance would increase, but when bending in the direction of GrF, the resistance would decrease. It was found that the GrF-PDMS-PET (Fig. 2.13) composite yielded six times higher relative variation of electrical resistance than GrF-PDMS. The principle of mechanics of the material is employed to understand the baseline resistance variation (GrF-PDMS) as well as the GrF-PDMS-PET behavior in both bending directions. When GrF-PDMS is bended, one side of the GrF is in compression and the other side is in tension, with the resistance effects opposing one another, resulting in almost zero resistance sensitivity. When the GrF-PDMS-PET is bended toward the GrF side, the GrF is put entirely in a state of compression resulting in a resistance sensitivity lower than the GrF-PDMS composite. When the PET substrate is added to one side of the GrF-PDMS material and the entire composite is bended toward the PET side, the GrF is wholly under a state of tension resulting in strain sensor material with high sensitivity (Fig. 2.14).

Fig. 2.13. Optical image of GrF-PDMS-PET composite bended over a beaker [89].

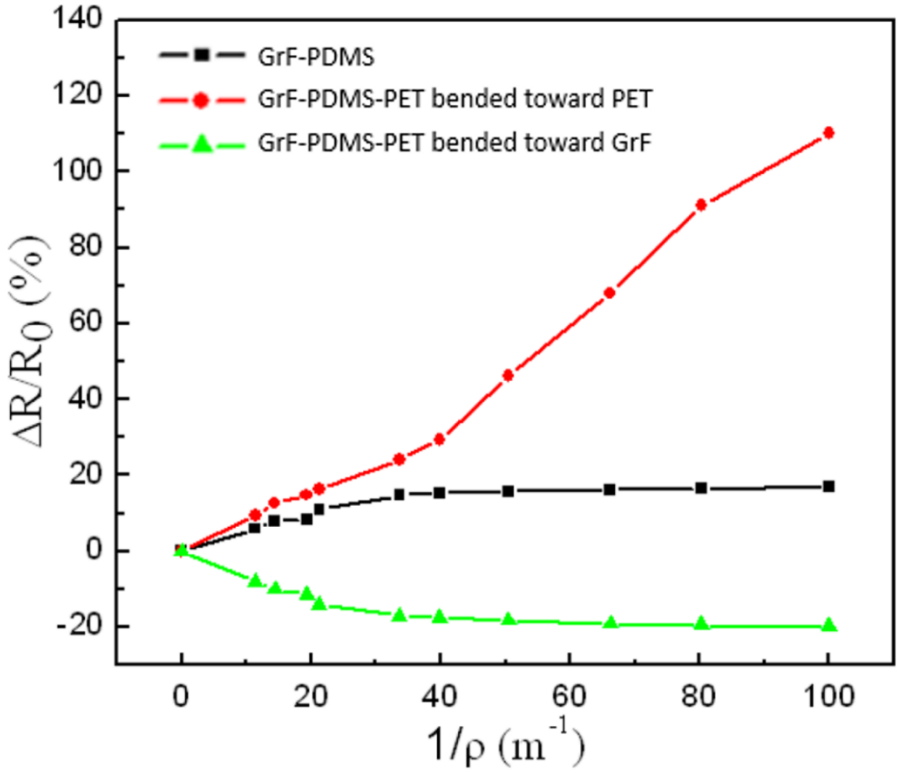

Fig. 2.14. Sensitivity to electrical resistance as a function of bending curvature where ρ is bending radius [89].

Many studies have been carried out with GrF-PDMS composites but, very few works have been published on GrF-epoxy composites specifically. A summary of these studies is presented in Table 2.3.

Table 2.3. Summary of the studies previously done on 3D GrF reinforced epoxy composites.

Materials	**Synthesis Method**	**Major Findings**	**Discussion**	**Ref**
0.1 and 0.2 wt.% GrF-Epoxy	Hot-press stacked prepregs	-Composite electrical conductivity of 3 S/cm -Tg increased by 31^{o}C over pure epoxy -Fracture toughness enhanced 70% over pure epoxy	-3D network and high quality GrF -GrF hinders polymer chain mobility -Interfacial de-bonding yields energy absorption -Roughening of surface, deflection of advancing cracks due to presence of GrF	[80]
2.5 vol.% GrF-Epoxy	Dip coat of GrF into DMF diluted epoxy	-GrF electrical conductivity 125 S/cm -Composite electrical conductivity of 2 S/cm	-Large size and high crystallinity of graphene sheets -3D network allowing fast electron transport	[74]
Glass Fiber-Epoxy / GrF-Epoxy Laminates	Hot-press stacked prepregs	-Mode I and II interlaminar fracture energies increased by 70 and 206%, respectively -36% enhancement of interlaminar shear strength	-GrF deflects and twists advancing cracks, yielding tortuous crack paths with higher surface areas -Interfacial de-bonding allows for more energy absorption during crack propagation	[65]
GrF-W-Epoxy	Sedimentation and centrifugal-assisted assembly	-Densely packed W spheres yield higher impedance and attenuation than loosely packed W spheres inside pores of GrF coated epoxy	-W spheres scatter or reflect acoustic waves -GrF allows for conversion of acoustic waves to thermal energy	[10]

GrF-epoxy has demonstrated extraordinary properties, and these materials have many promising potential applications. Further research on GrF-epoxy composites could advance many fields including aerospace, medical, environmental, electronics, and communications.

2.4. Potential Applications of 3D Graphene Foam Polymer Composites

GrF has been reported to have many potential applications such as electromagnetic interference (EMI) shielding, excellent shock and sound absorption, bio-sensing, and gas sorption [5, 8, 24, 75, 90], ultrathin and foldable electronics, large scale strain sensors, indestructible military armor, flexible and self-healing airplane wings, air and water purification filters, and many other advanced multifunctional applications [8, 22]. These notable material properties in conjunction with ever-accelerating research efforts make GrF a promising matrix reinforcement allowing potential rapid realization of future visions.

CHAPTER III

EXPERIMENTAL DETAILS

In this chapter, the experimental procedures used to synthesize and characterize graphene foam reinforced epoxy composites are discussed. Two facile synthesis techniques were used for composite fabrication, and both methods are described in detail. Microstructural characterization and evaluation techniques of material properties are discussed. Additionally, equipment, software and equations utilized for calculations are presented in the following sections.

3. Materials and Synthesis Techniques

Three-dimensional graphene foam (3D GrF), was obtained from Graphene Supermarket, Calverton, NY, USA. GrF was synthesized using the CVD method on nickel foam substrate [91]. The GrF has a density of 4 mg/cm^3, a thickness of approximately 1.2 mm, and an average pore size of 580 microns. The carbon content of the GrF is 99%. A low magnification SEM image of the as-received GrF is shown in Fig. 3.1.

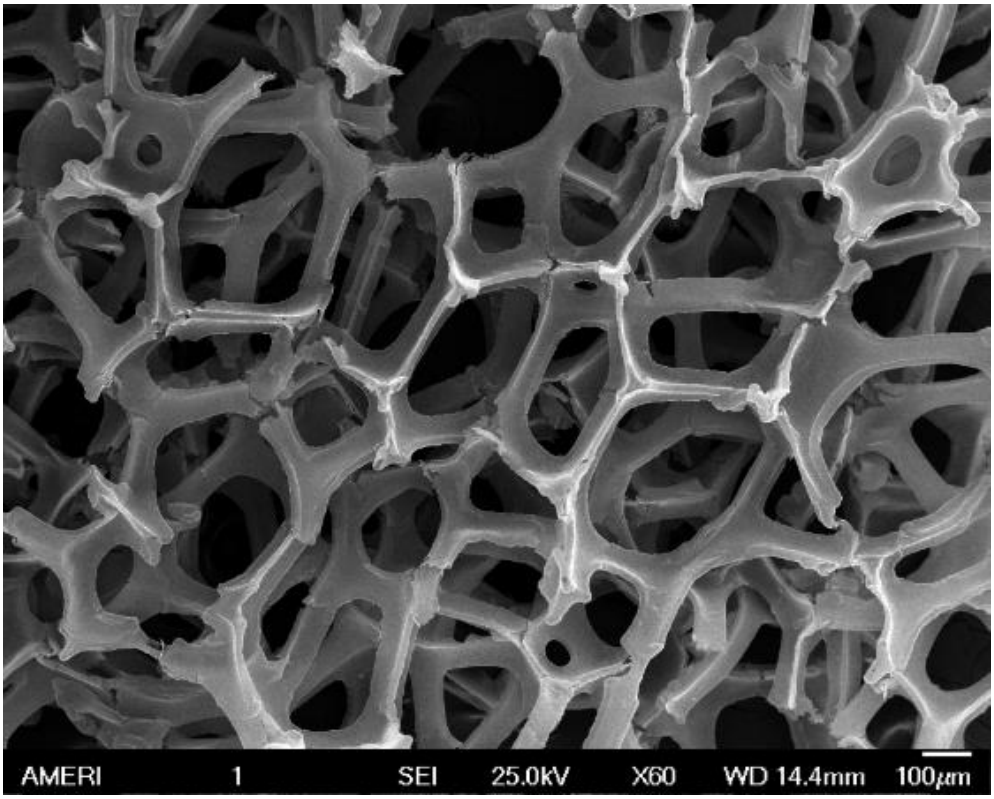

Fig. 3.1. Low magnification SEM image of as-received GrF.

The polymer matrix material used is a multifunctional, two-component, thermosetting epoxy resin and cycloaliphatic hardener system obtained from AeroMarine Products, Inc., San Diego, CA, USA. The epoxy has a mixed viscosity of 600 mPa-s and a working life of up to 30 minutes.

3.1. Wettability Studies of Epoxy Against 3D Graphene Foam

Wetting is indicative of how the GrF reinforcement and polymer matrix will adhere to one another or interact at the interface. Since strong interfacial interaction is crucial to achieving a successful composite with superior properties, wetting studies may provide valuable information. The epoxy system was mixed at a 2:1 volume ratio of resin to

hardener. A sessile drop of epoxy was carefully released onto a 1 x 1 cm^2 piece of GrF. The contact angle as a function of time was measured until the contact angle reached 0 degrees. Sessile drop test was conducted using a KYOWA Contact Angle Meter (model DM-CE1, Saitama, Japan) using FAMAS software.

3.2. 3D Graphene Foam-Epoxy Composite Synthesis

Two facile synthesis techniques were used for composite fabrication. Both methods are described in detail below.

3.2.1. Dip Coat Technique

A facile dip coating method was used to synthesize GrF-epoxy composites. The as-received GrF was cut into five 10 x 4 mm pieces. Each GrF piece was weighed then clipped to a holding device. The epoxy was mixed at a 2:1 volume ratio of resin to hardener and stirred for 20 minutes to initiate polymerization. Each piece of GrF was immersed into the mixed epoxy for varying times of 1, 3, 5, 7, and 9 seconds as a means to vary the weight fraction of GrF in the composite. The clips holding the GrF pieces were suspended from a horizontal cylindrical rod and cured at room temperature for 96 hours. Upon completion of curing process, the composite material samples were removed from the holding clamps and weighed again to compute epoxy content. A schematic of the dip coat method is shown in Fig. 3.2.

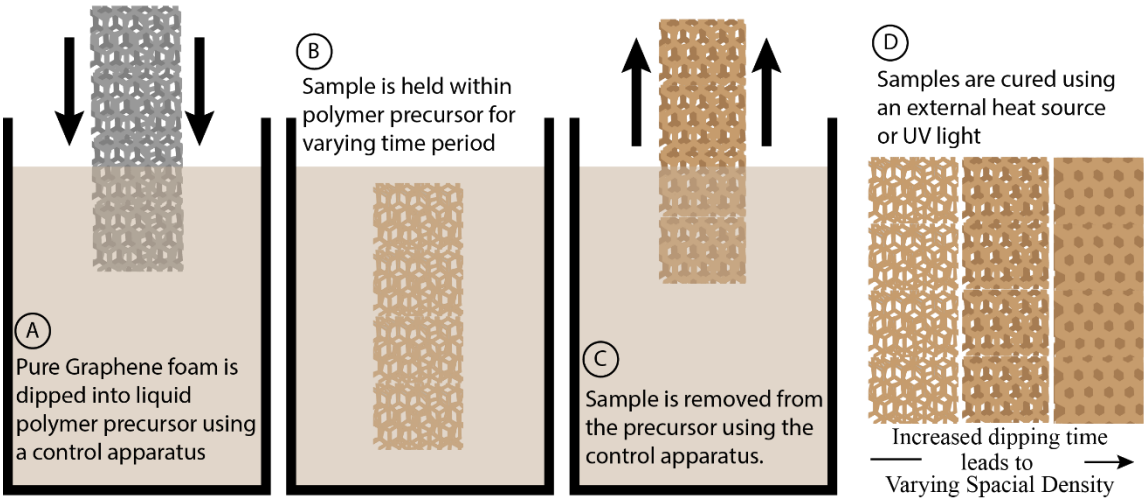

Fig. 3.2. Schematic of the dip coat synthesis technique [15].

3.2.2. Mold Cast Technique

SolidWorks CAD software was utilized to design a casting mold for the GrF-epoxy composites. The CAD design was uploaded to a Form 1+ SLA 3D printer (Formlabs, Somerville, MA, USA), and the casting mold was fabricated with a photo-reactive flexible resin. The mold was coated with mold release agent, and the release agent was allowed to air dry. Multiple strips of GrF were cut into 30 x 4 mm pieces, and each piece was weighed individually. The epoxy was mixed at a 2:1 volume ratio of resin to hardener and stirred for 20 minutes to induce polymerization. A syringe was used to dispense a thick layer of epoxy into the bottom of the casting mold. The GrF strip was placed over the epoxy into the gauge length of the mold (Fig. 3.3). Another layer of polymer was dispensed over the top of the GrF, and the samples were cured for 96 hours at room temperature. To further alter the GrF content, samples were also made with two GrF layers suspended into the gauge length. In this case, a syringe was used to dispense a small amount of polymer onto

the bottom of the mold. GrF and polymer were layered in an alternating fashion until two slightly separated layers of GrF were suspended into the center of the sample mold. Additionally, control samples were synthesized by casting pure epoxy without GrF into the mold. Upon curing for 96 hours at room temperature, the samples were removed from the mold and weighed for further calculations. The GrF contents of each sample for each fabrication method is displayed in Table 3.1.

Fig. 3.3. Schematic of GrF-epoxy mold casted composite.

Table 3.1. Weight percent of GrF within the dip coated and mold casted GrF-epoxy composite samples.

Composite Sample	**Weight Percent GrF**
Dip Coated Samples (s)	
9	1.55
7	1.64
5	1.85
3	1.91
1	1.99
Mold Casted Samples (Number of GrF Layers)	
1	0.07
2	0.13

3.3. Microstructural Characterization

A helium gas pycnometer (Accupyc 1340, Micrometrics Instrument Corporation, Norcross, GA, USA) was used to measure the true density of all samples synthesized by dip coating and mold casting methods. Low magnification top views of the samples were observed with a digital microscope (Dino-Lite, Dunwell Tech, Inc., Torrance, CA, USA). Scanning electron microscopy (JEOL JSM-6330F, JEOL USA, Inc., Peabody, MA, USA) was used at an operating voltage of 15 kV to observe fracture surfaces for GrF-epoxy interfacial interaction analysis and mechanical testing failure mechanisms. ImageJ software was used to analyze the SEM micrographs of the composite samples in order to measure the interfacial spacing between GrF and epoxy.

3.4. Material Properties Characterization

Thermal transformation, mechanical testing, and electrical conductivity characterization were carried out on dip coated and mold casted samples. All tests were run in parallel in terms of fabrication methods except in the case of 3-point bend flexural testing. This test requires sample rigidity, and the dip coated samples were too flexible to perform a successful test. The results for all characterization tests performed are presented and analyzed in the following sections.

3.4.1. Glass Transition Temperature

Glass transition temperature is one of the most important properties for polymers and their composites in order to determine the thermal stability of the material. Thermal analysis was done by using simultaneous Thermogravimetric Analysis and Differential

Scanning Calorimetry (SDT Q600, TA Instruments, New Castle, DE, USA) in an argon environment at a heating rate of 10ºC per minute up to a maximum temperature of 250 ºC. The TGA graphs were plotted using Origin Pro 8 software. The glass transition (Tg) temperatures were obtained as a function of GrF concentration.

3.4.2. Damping Behavior

Understanding the damping behavior of a material is important for reducing or eliminating shock, noise, and other vibrations through effective energy dissipation. Damping tests were carried out using a Universal Surface Tester (UST) (INNOWEP GmbH, Wurzburg, Germany) using a 0.8 mm spherical steel tip. The pure epoxy and dip coated samples were tested at lower loads of 1, 10, 25, and 50 mN due to the thin nature of the material with high GrF content. The pure epoxy and the thicker, more rigid mold casted composites were tested at relatively higher loads of 10, 25, 50, 75, and 90 mN. For each sample, ten trials were performed at each load. The logarithmic decrement values from each trial were recorded, and those values were averaged. The damping behavior was analyzed by calculating the loss tangent (tan δ) using equation 3.1 [60]:

$$tan\ \delta\ = \frac{\Delta}{\pi} \qquad \text{Eqn. 3.1}$$

where Δ = logarithmic decrement.

3.4.3. Flexural Strength

Flexural strength of cast samples was determined by performing 3-point bend testing using a mechanical testing stage (SEMtester 1000, MTI Instruments, Inc., Albany, NY, USA) as shown in Fig. 3.4 [92]. Due to the high flexibility of the dip coated samples, they

were not tested for flexural strength since sample rigidity is required to obtain meaningful 3-point bend flexural strength data. The mechanical testing stage low load cell (440 N) is used to perform flexural testing. The stage is controlled using MTEST Quattro software (ADMET, Norwood, MA, USA). The tests were carried out by holding the sample between 2 contact locations and applying a force at a third central contact location (Fig. 3.5) at a rate of 1 mm per minute.

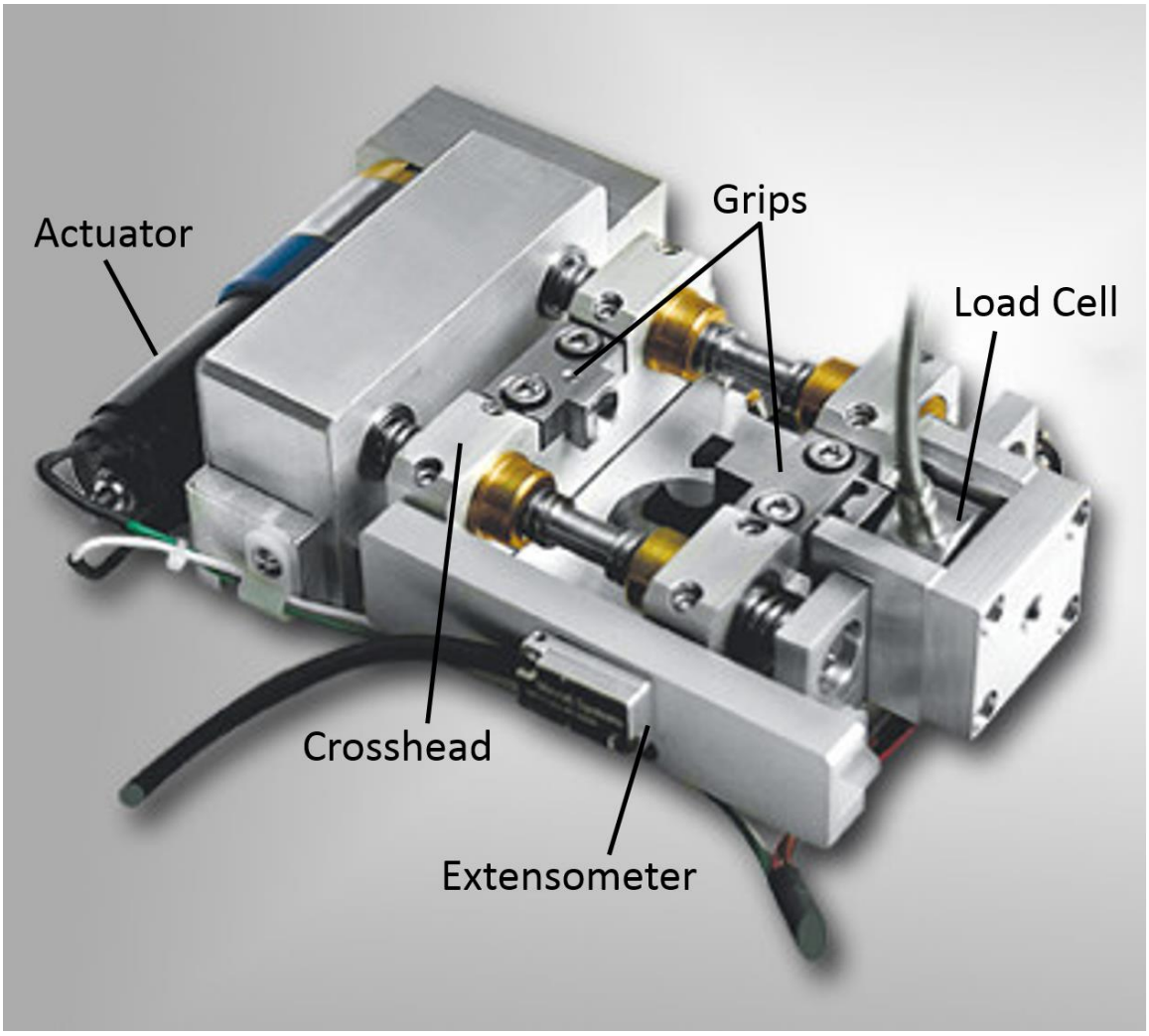

Fig. 3.4. Schematic of the mechanical testing stage used for flexural testing and for electrical testing as a function of tensile strain [93].

The flexural strength was calculated by the following equation:

$$\sigma_f = \frac{3FL}{2bd^2} \qquad \text{Eqn. 3.2}$$

where σ_f = flexural stress, F = force applied, L = length of tested sample, b = width of sample, and d = thickness of sample. The flexural strain was calculated using the following equation:

$$\varepsilon_f = \frac{6Dd}{L^2} \qquad \text{Eqn. 3.3}$$

where ε_f= flexural strain, D = maximum deflection of the sample during testing, d = thickness of sample, and L = length of tested sample. The setup for the 3 point bend tests is shown in Fig. 3.5.

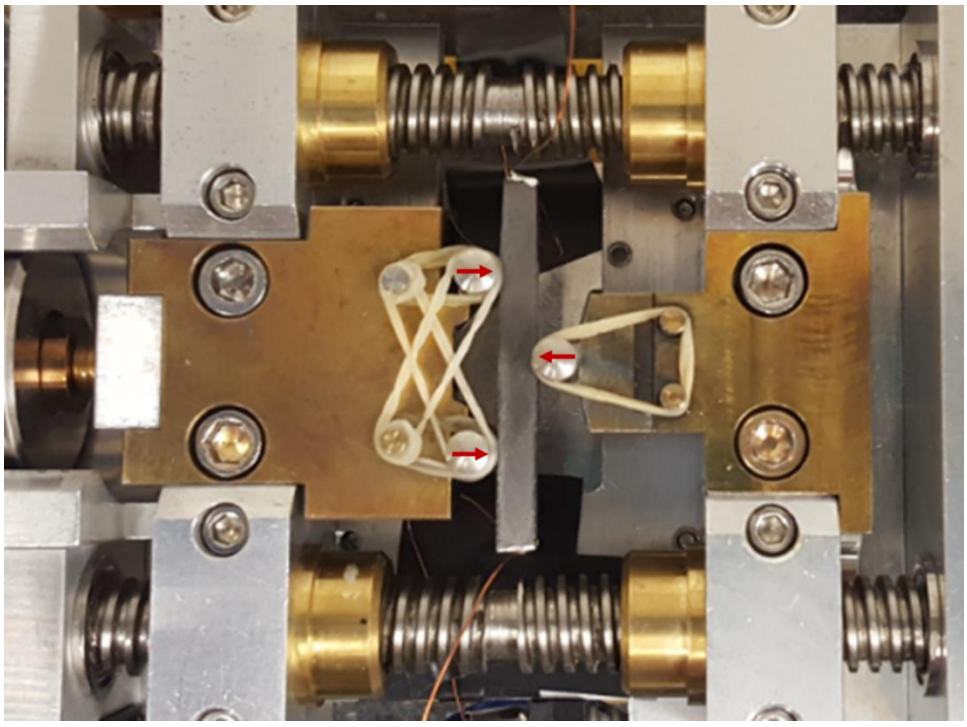

Fig. 3.5. Experimental set up of flexural testing of GrF-epoxy cast sample. Arrows denote points of contact and directions of applied force.

3.4.4. Electrical Conductivity

3.4.4.1. Intrinsic Electrical Properties

The electrical resistance for all GrF-epoxy samples were tested using a four-probe technique. Keithley 2401 SourceMeter Source Measure Unit (SMU) Instrument (Tektronix, Inc., Beaverton, OR, USA) in conjunction with LabVIEW software was used. A four-probe setup was achieved by mounting each sample between copper wires using silver paste. The silver paste was allowed to cure for 24 hours at room temperature. A current of 100 mA was swept through the samples and the resulting voltage was measured. Ohm's law was used to calculate the resistance values:

$$V = IR \qquad \text{Eqn. 3.4}$$

where V = voltage, I = current, and R = resistance. The electrical resistivity of each sample were calculated by using the following equation:

$$\rho = R\,(A/l) \qquad \text{Eqn. 3.5}$$

where ρ = resistivity, A = cross sectional area, and l = length of the sample. Lastly, electrical conductivity, σ, was calculated using

$$\sigma = 1/\rho \qquad \text{Eqn. 3.6}$$

The results were compiled and analyzed using Origin Pro 8 software.

3.4.4.2. Electrical Properties as a Function of Tensile Strain

Electrical conductivity as a function of deformation must be measured in order to better understand the electrical behavior of GrF-epoxy composite under different operating conditions. Dip coated and cast GrF-epoxy composite samples were tested under tensile

strain using a mechanical testing stage (Fig. 3.6) with MTEST Quattro software. The samples were stretched at 1 mm per minute and the electrical conductivities were measured at small incremental displacements based on previous strain analysis which showed similar dip coated samples failing at approximately 5% strain and mold casted samples failing at roughly 10-15% strain. In order to obtain at least 5 data points for each sample tested, electrical resistance was measured at increments of 0.1 mm, and mold casted sample was measured at increments of 0.5 mm. The samples were tested until mechanical failure occurred. Equations 3.4 through 3.6 were used to calculate electrical conductivity values. The results were compiled and analyzed using Origin Pro 8 software.

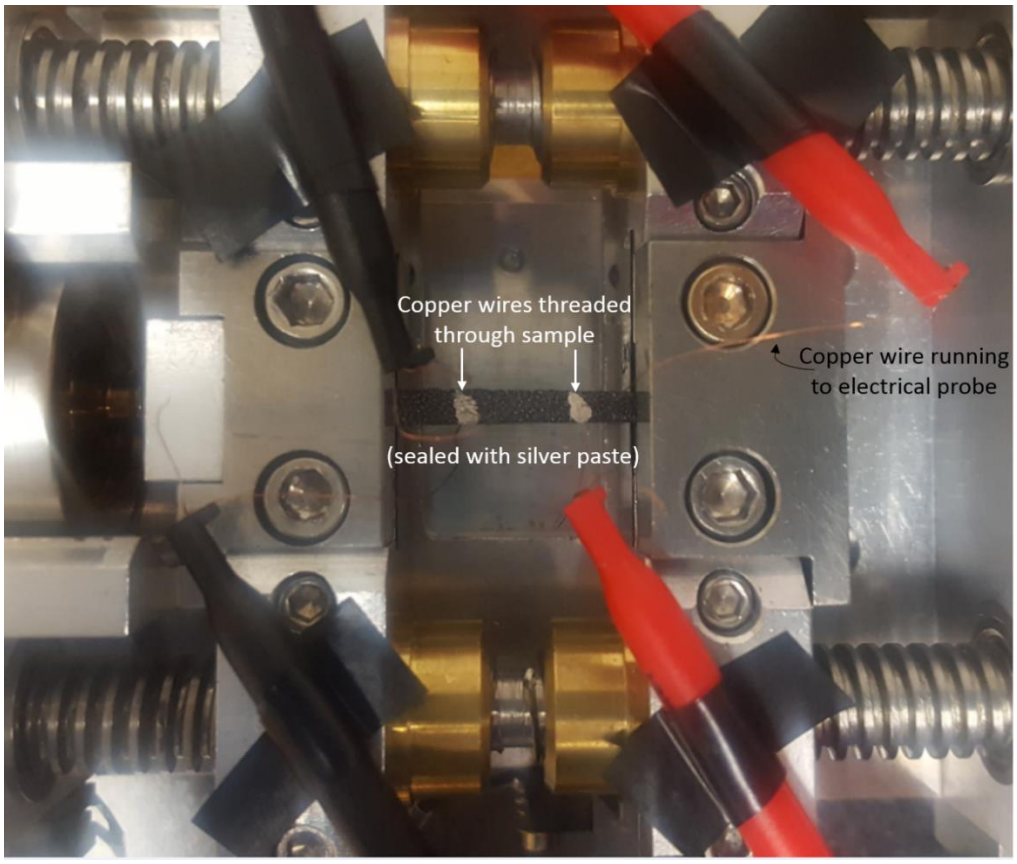

Fig. 3.6. Experimental setup showing a GrF-epoxy dip coated sample being tested for electrical resistance as a function of tensile strain by 4 probe method.

To understand the effects of the synthesis techniques on GrF-epoxy composites, characterization tests were performed in parallel for dip coated and cast samples. Samples fabricated by both techniques were tested for density, interfacial spacing, thermal transformation, damping behavior, and electrical properties. The dip coated samples could not be tested for flexural strength, due to the lack of rigidity of the sample. The completion of the characterization tests for both dip coated and cast samples are presented in Table 3.2.

Table 3.2. Summary of experiments performed for dip coat and mold cast GrF-epoxy composites.

Experimental Studies	**Dip Coated**	**Cast**
Density	✓	✓
Differential Scanning Calorimetry	✓	✓
Damping Studies	✓	✓
3-Point Bend	X	✓
Electrical Conductivity	✓	✓
Resistance Retention as a Function of Tensile Strain	✓	✓

CHAPTER IV

RESULTS AND DISCUSSION

The overall objective of this research is to reinforce epoxy with 3D GrF to create high strength, low density, and electrically conductive nanocomposites. In order to achieve this goal, uniform dispersion of the reinforcement within the matrix material as well as good interfacial interaction must be accomplished. This investigation will reveal how the two facile synthesis techniques employed for this study allow controllability of the GrF to epoxy content therefore affecting the microstructure, properties, and performance of GrF reinforced epoxy composites. The use of GrF's continuous, three-dimensional network aims to alleviate particle agglomeration, restacking, and composite material anisotropy oftentimes observed when using 1D and 2D carbon-based polymer matrix reinforcements. The composite densities and microstructures as well as the mechanical and electrical properties are evaluated. Thermal transformations as a function of GrF content are also investigated. The findings are presented and thoroughly discussed in the following sections.

4.1. Microstructure of 3D Graphene Foam-Epoxy Composites

The microstructure of a material is the direct result of the synthesis techniques and processing parameters employed during fabrication. As a result, the microstructure may be intentionally manipulated by controlling which materials are used, the quantity and ratios of materials used, and the environments in which they are processed. Strongly influencing the material's properties and performance capabilities, the microstructure essentially governs the applications for which the material may be used.

GrF is a porous, ultra-lightweight material (Fig. 4.1 a) with a node-branch anatomy having a density of 4 mg/cm^3. GrF's intrinsic rippled or wrinkled surface features as well as a few slight defects on the surface are observed in Fig 4.1 b. The branches of GrF have a hollow triangular structure (Fig. 4.1 c) assuming the shape of the nickel foam on which it was grown during the chemical vapor deposition (CVD) process. There is also interlayer separation between the stacks of graphene layers in the GrF used for this study as seen in Fig. 4.1 d.

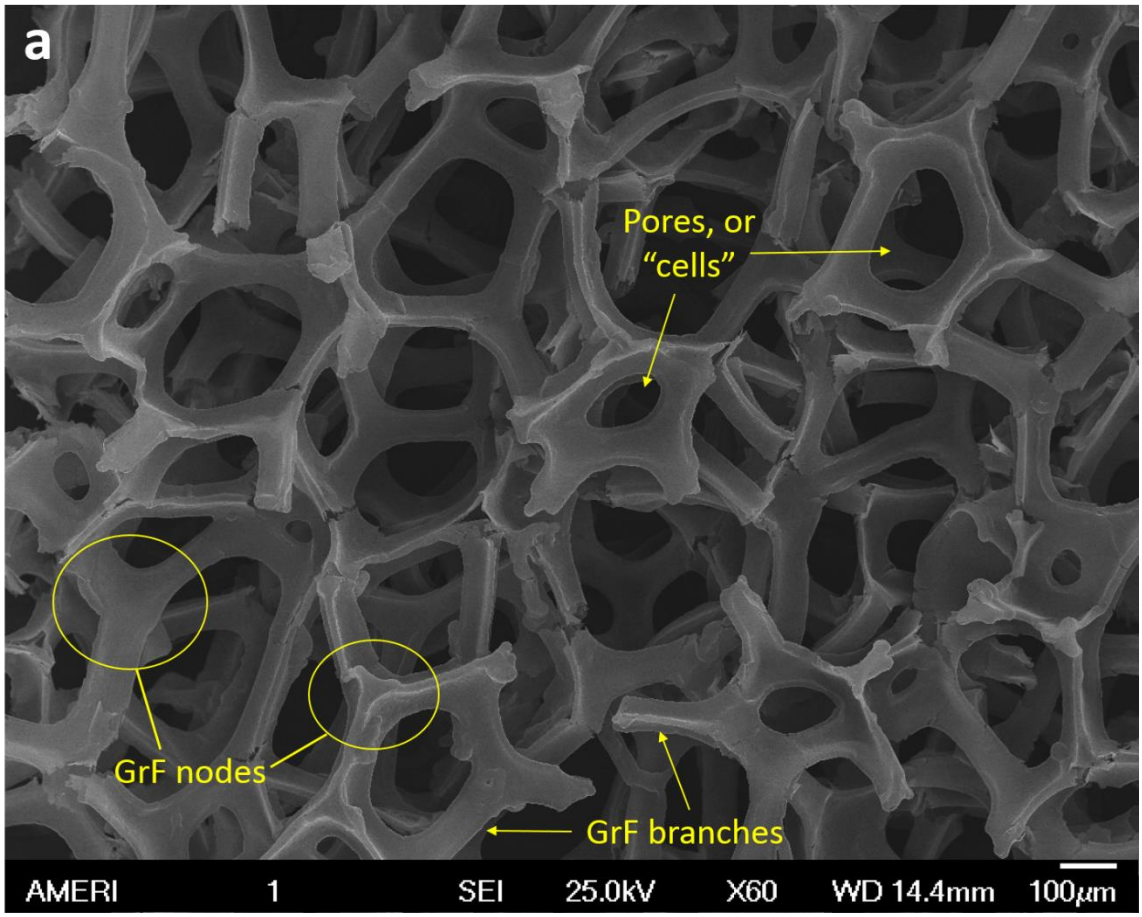

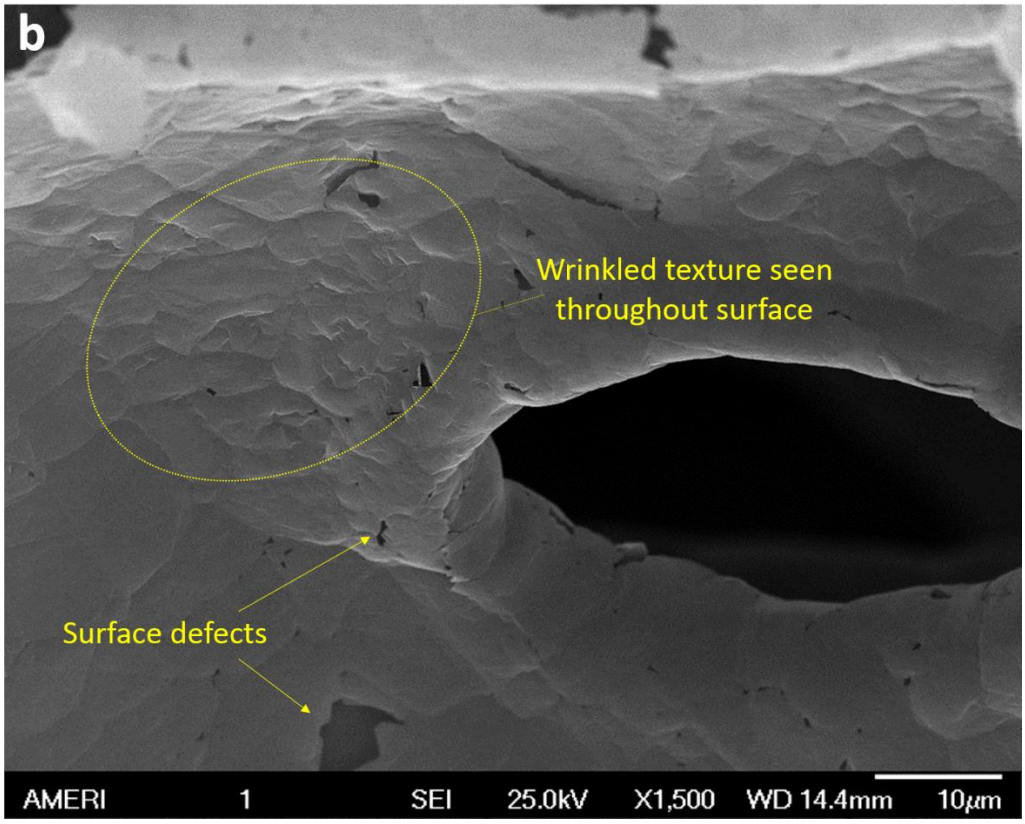
b
Wrinkled texture seen throughout surface
Surface defects
AMERI 1 SEI 25.0kV X1,500 WD 14.4mm 10μm

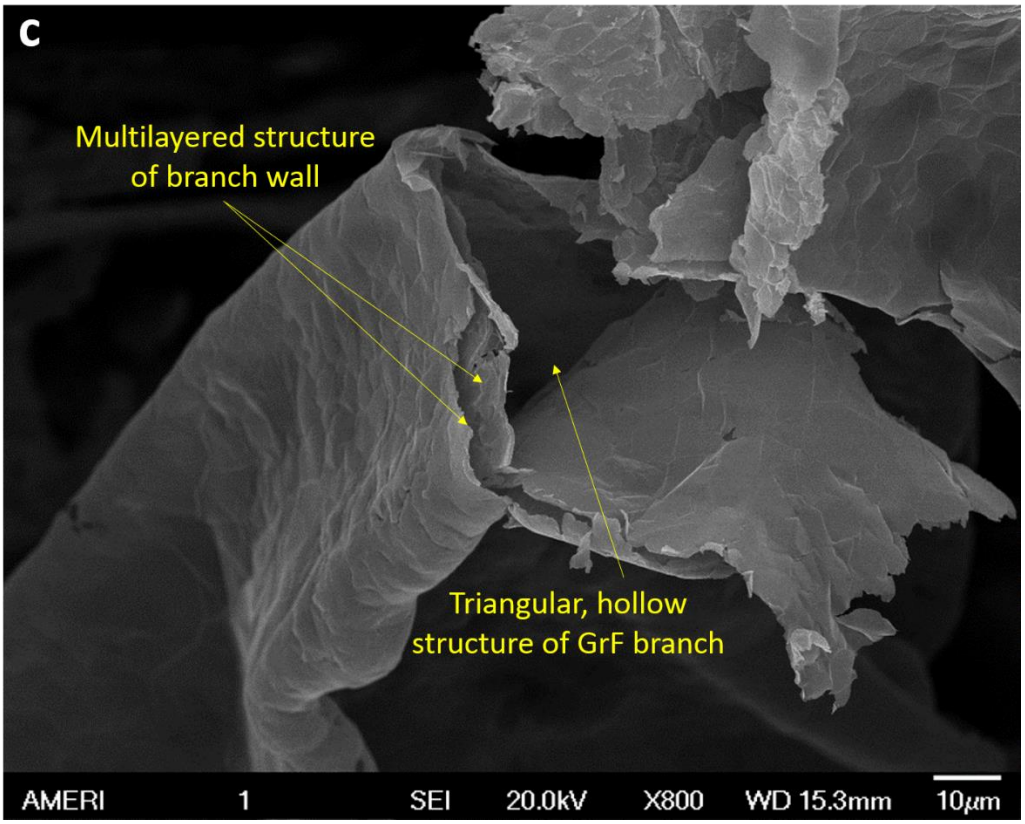
c
Multilayered structure of branch wall
Triangular, hollow structure of GrF branch
AMERI 1 SEI 20.0kV X800 WD 15.3mm 10μm

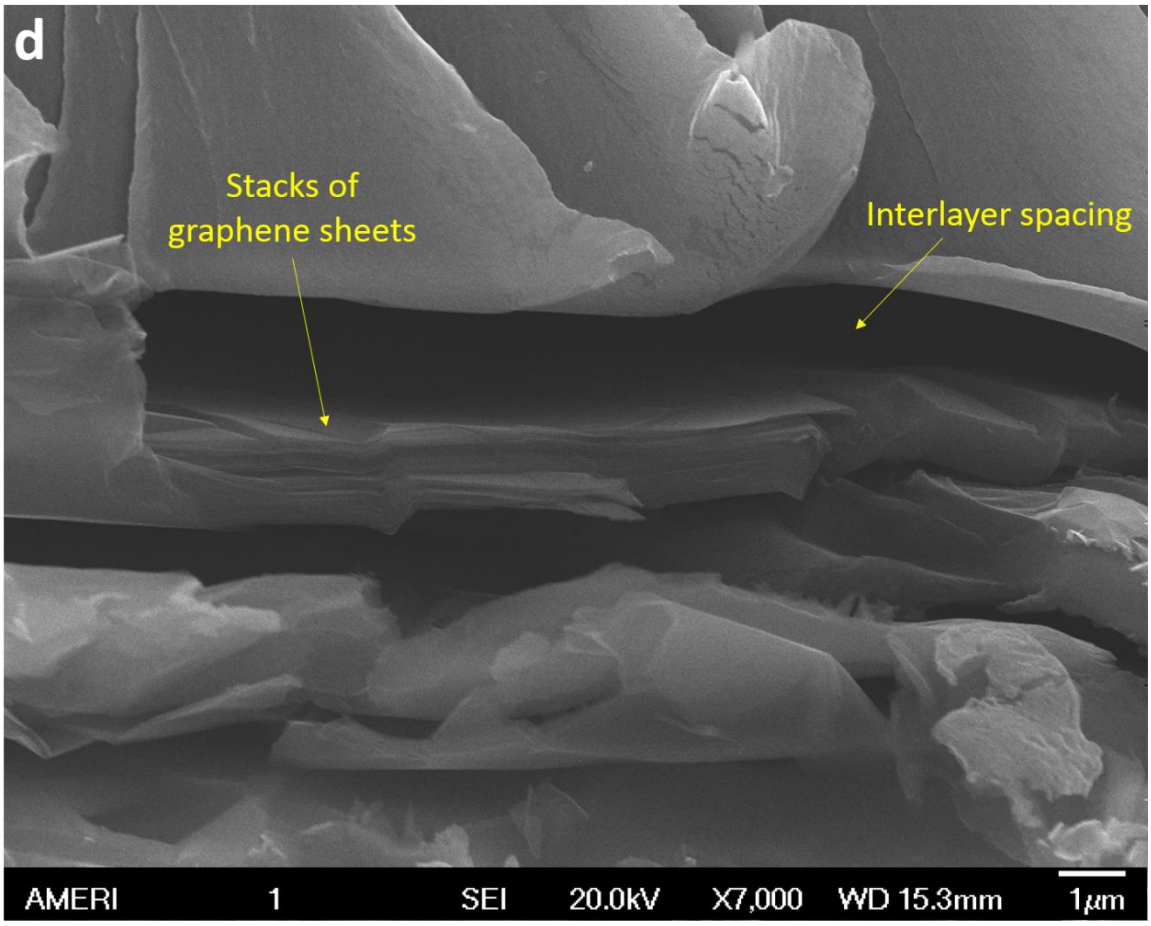

Fig. 4.1. SEM micrographs of (a) top surface of as-received GrF showing the pores, branches, and nodes, (b) GrF's wrinkled surface features and surface defects, (c) hollow, triangular multilayered GrF branch, and (d) high magnification image of stacked graphene sheets which make up the GrF walls.

To understand the interfacial interaction between GrF and epoxy polymer, contact angle studies were performed to investigate the wetting characteristics of epoxy against GrF. The sessile drop method was used and the contact angles as a function of time were recorded. The initial angle upon contact was 67^{o} and the angle quickly diminished to nearly 0^{o} in only 4 seconds (Fig. 4.2).

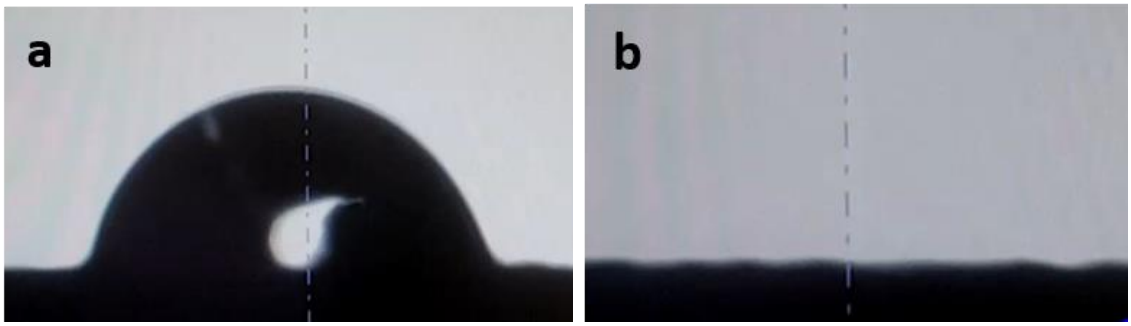

Fig. 4.2. Contact angles of epoxy against GrF at time (a) t = 0 s and (b) t = 4 s.

Good wetting characteristics between GrF and epoxy suggest the potential for good interfacial interaction in future composite fabrication. The results are displayed in Fig. 4.3.

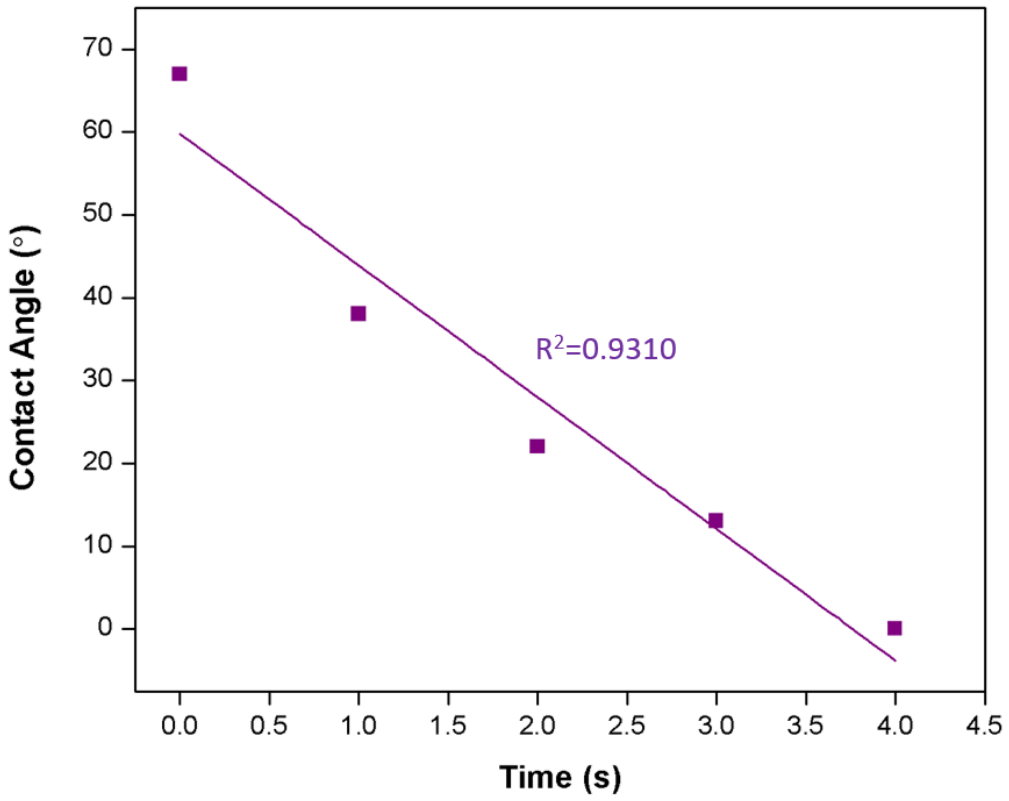

Fig. 4.3. Interfacial contact angle made by epoxy resin against GrF substrate as a function of time.

To demonstrate that the wetting characteristics are a function of the surface energies rather than the porosities of the GrF, comparative wetting tests were also run with deionized water against GrF substrate. The GrF proved to be very hydrophobic with the sessile water droplet having a contact angle greater than 90 degrees.

4.1.1. Dip Coat Technique

The microstructure of a material is determined by the processing parameters and strongly influences the physical, chemical, thermal, and electrical properties of the material. To achieve a successful composite material, the absence of particle agglomeration and uniform dispersion of reinforcing material is key. Optical microscopy (Fig. 4.4) is utilized to observe uniform dispersion and seemingly complete polymer filling of GrF's cellular structure suggesting the potential for superior properties and performance.

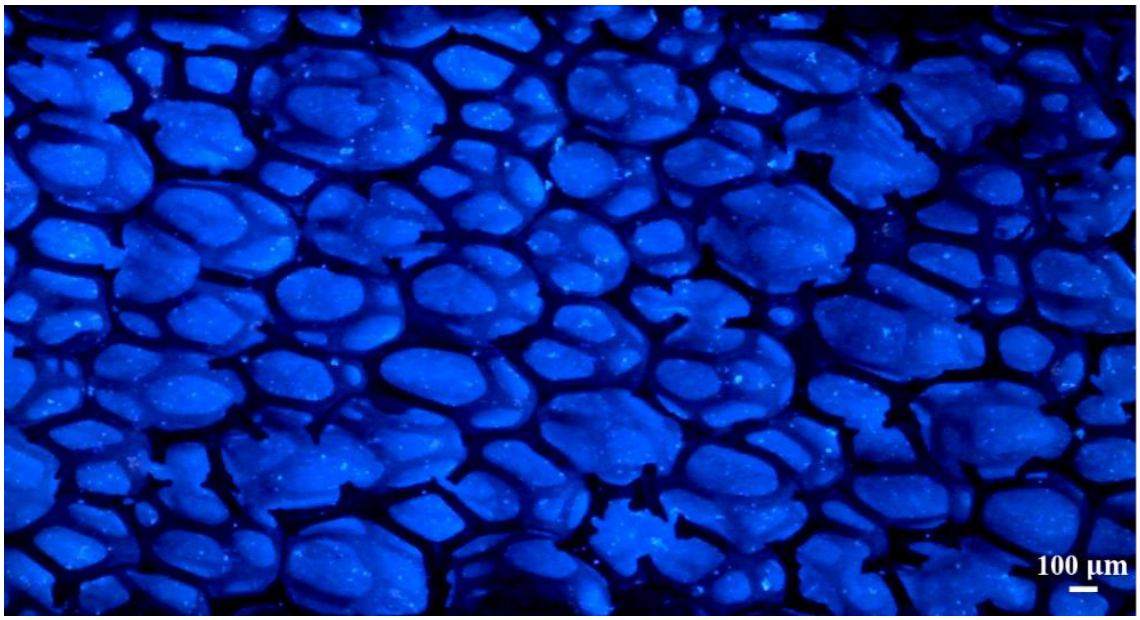

Fig. 4.4. Optical microscope image of dip coated sample showing uniform GrF dispersion within the epoxy matrix. Blue dye was added to epoxy for enhanced visualization.

Dip coated samples showed a decrease in density with increasing GrF content (Fig 4.5). Defects, porosities, and the intrinsic materials of the properties themselves may greatly affect the material's density. The increased porosities of the GrF, including the interlayer spacing within the GrF itself and the high content of the ultra-low density material within the composite is responsible for the declining density measurements as seen in Fig. 4.6.

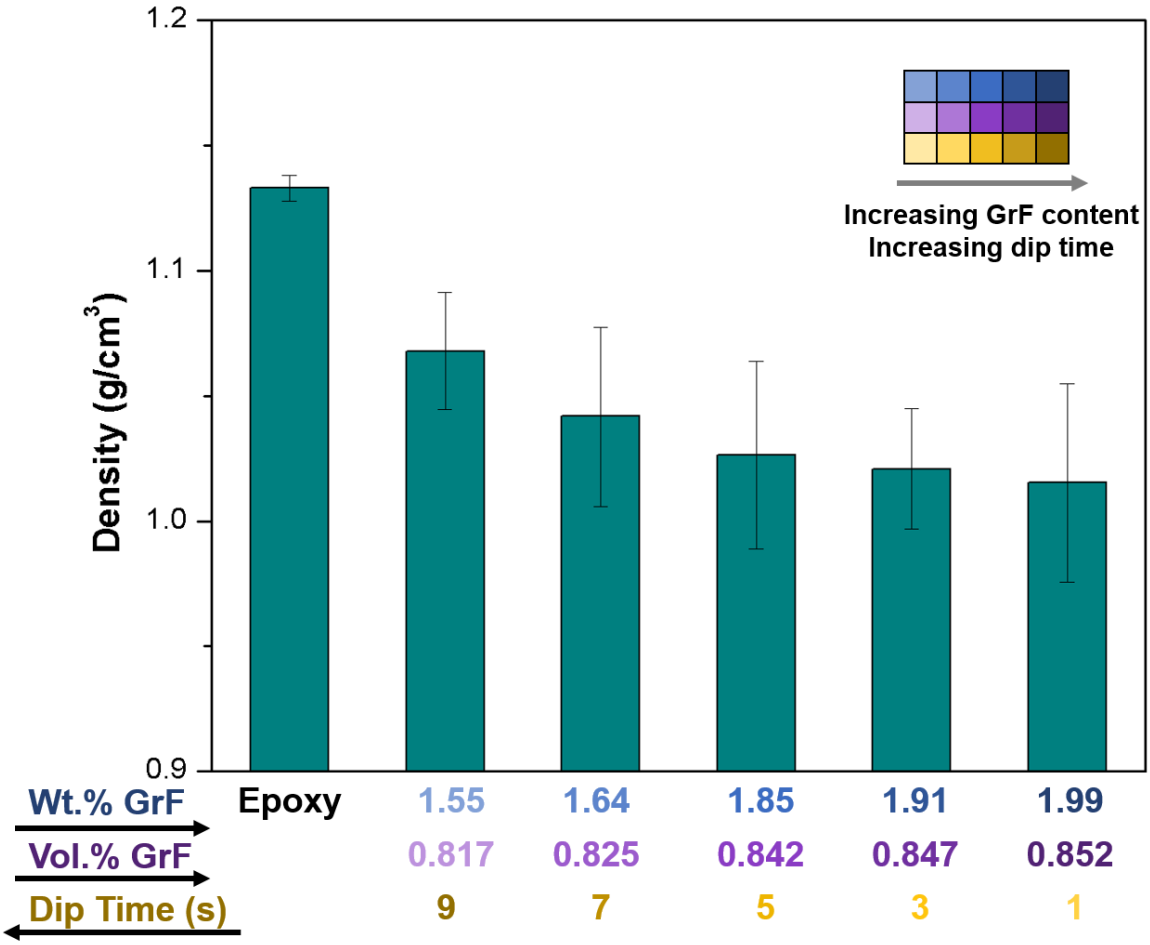

Fig. 4.5. Density values of pure epoxy and GrF-epoxy composites synthesized by dip coating technique.

SEM micrographs of the fracture surfaces of the composite samples are shown in Fig. 4.6. The interfacial spacing between GrF reinforcement and epoxy matrix was measured for each sample and plotted as a function of GrF content in Fig. 4.7.

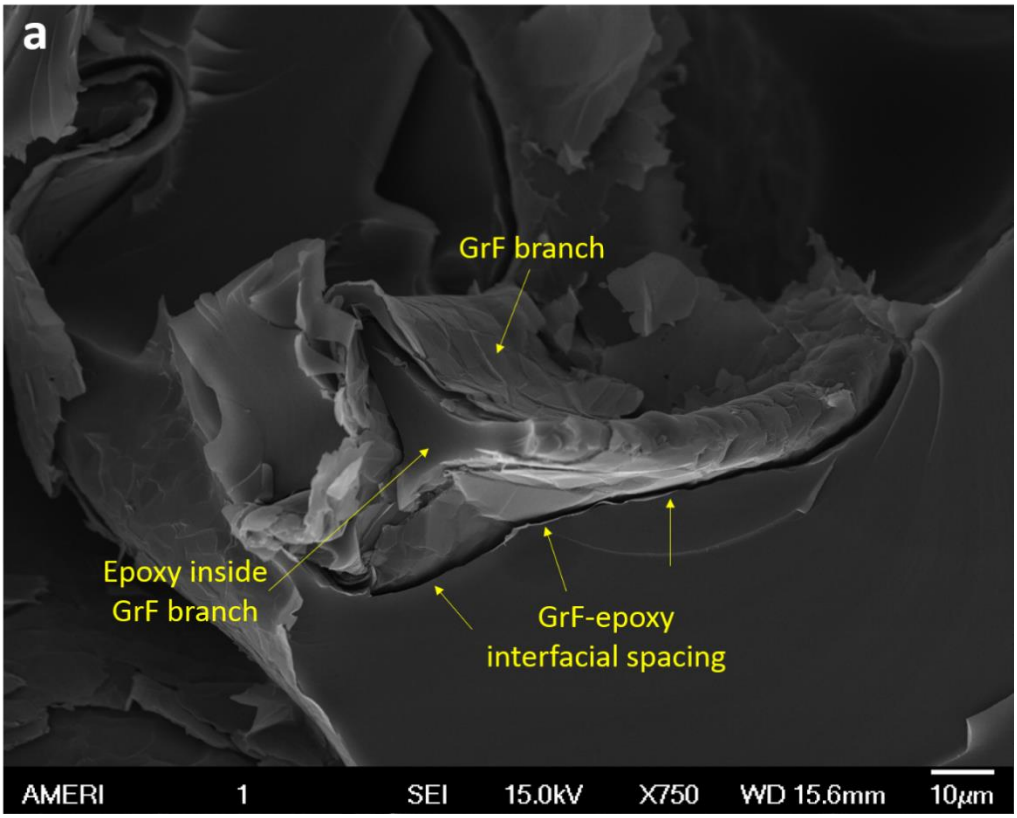
a
GrF branch
Epoxy inside
GrF branch
GrF-epoxy
interfacial spacing
AMERI 1 SEI 15.0kV X750 WD 15.6mm 10μm

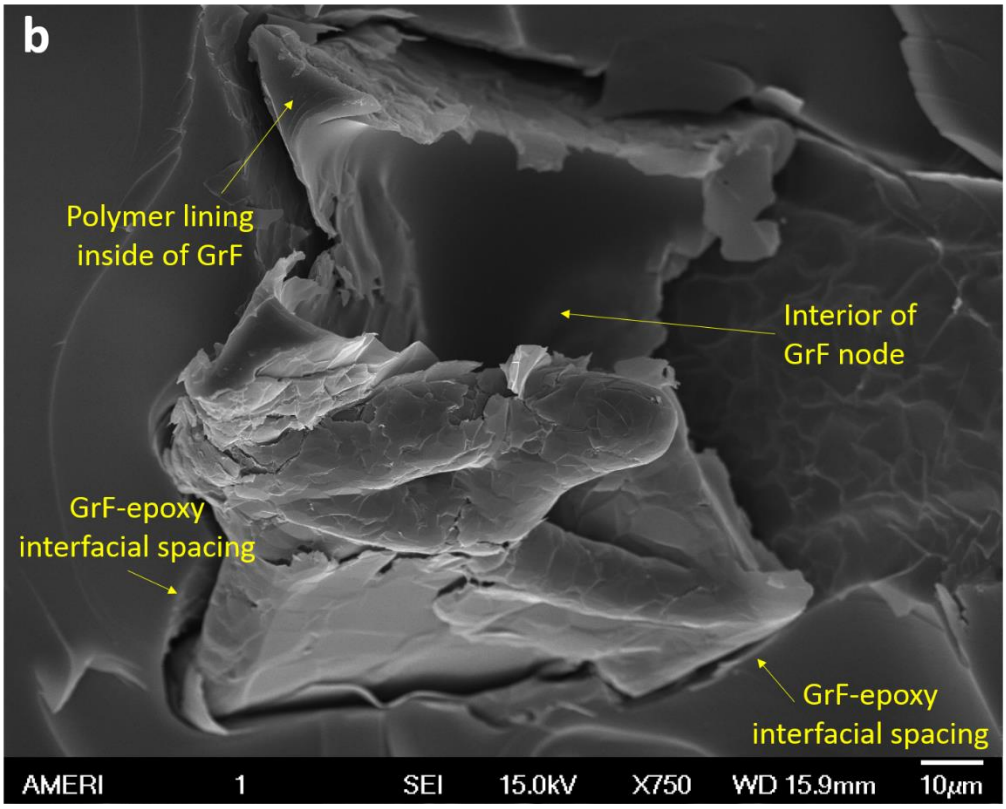
b
Polymer lining
inside of GrF
Interior of
GrF node
GrF-epoxy
interfacial spacing
GrF-epoxy
interfacial spacing
AMERI 1 SEI 15.0kV X750 WD 15.9mm 10μm

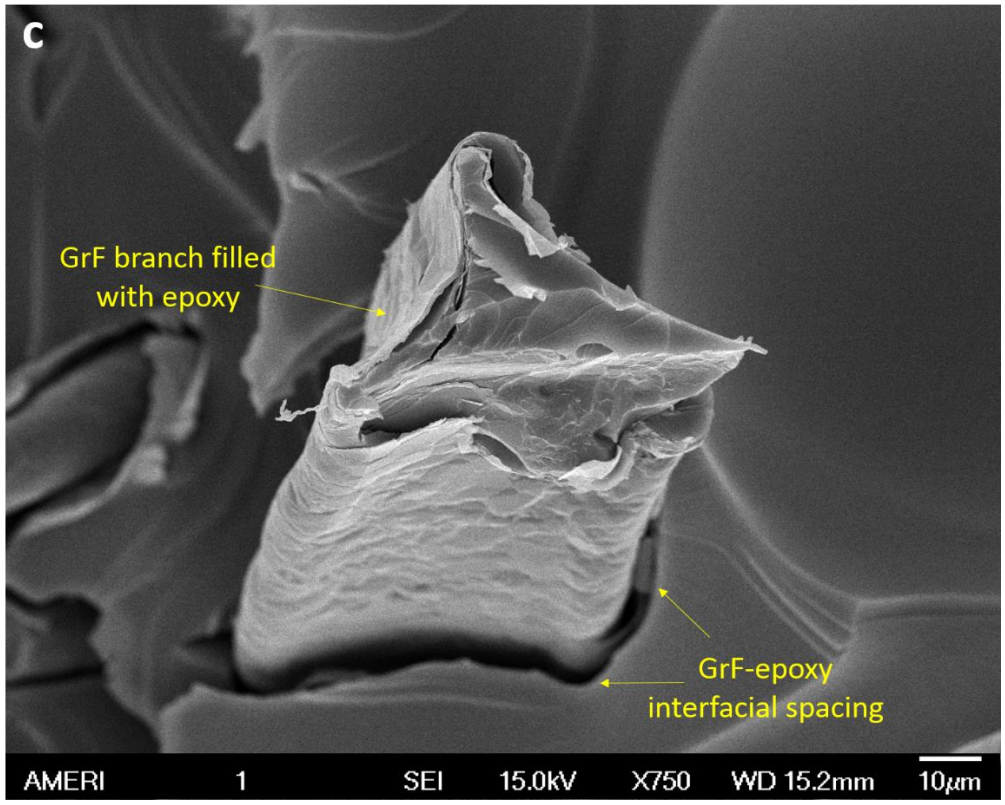
c
GrF branch filled with epoxy
GrF-epoxy interfacial spacing
AMERI 1 SEI 15.0kV X750 WD 15.2mm 10μm

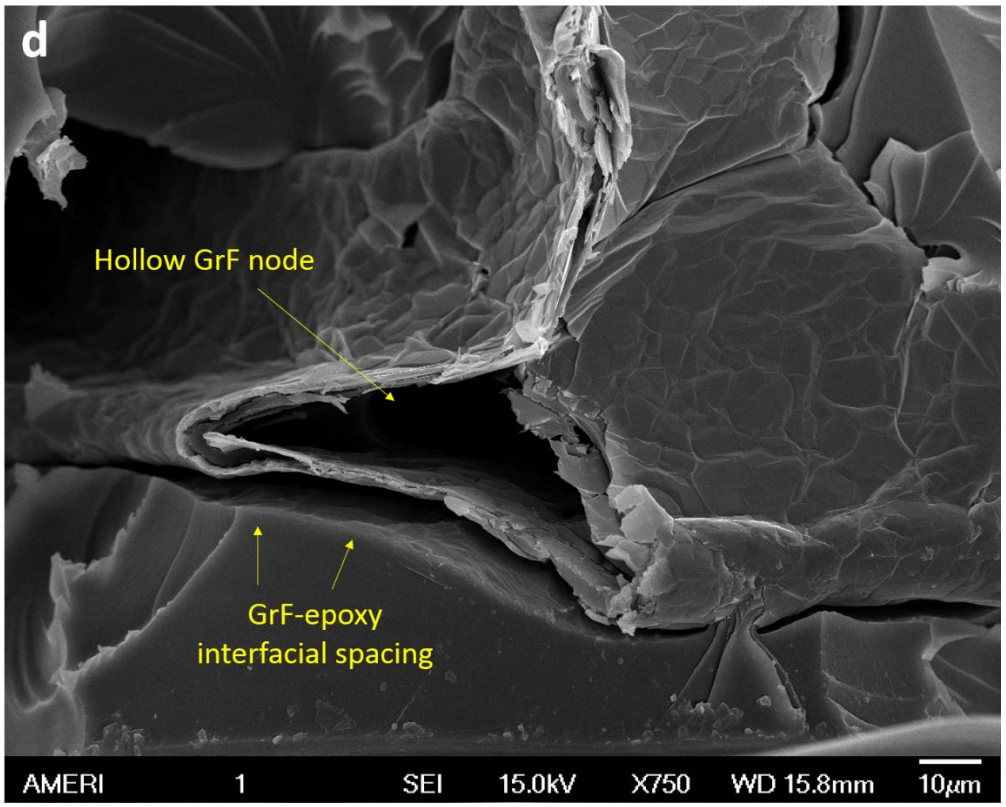
d
Hollow GrF node
GrF-epoxy interfacial spacing
AMERI 1 SEI 15.0kV X750 WD 15.8mm 10μm

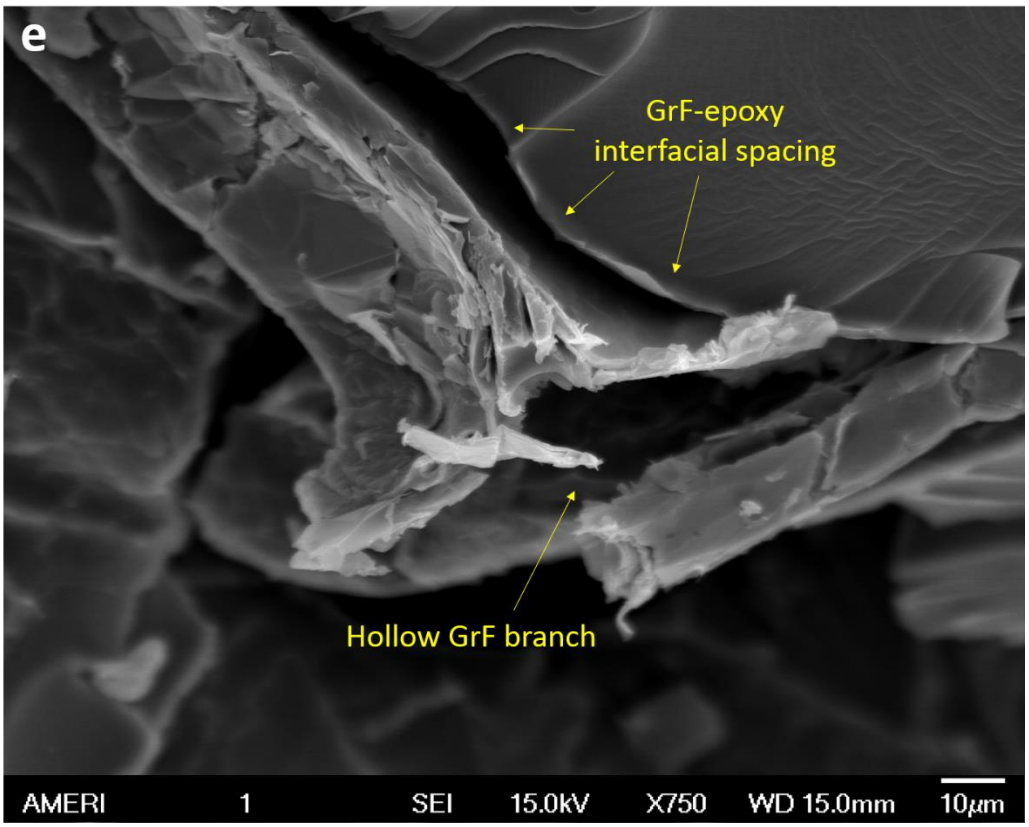

Fig. 4.6. SEM images showing GrF-epoxy matrix interfacial separation in dip coated samples for processing times (a) 1 s (1.99 wt.% GrF), (b) 3 s (1.91 wt.% GrF), (c) 5 s (1.85 wt.% GrF), (d) 7 s (1.64 wt.% GrF), and (e) 9 s (1.55 wt.% GrF).

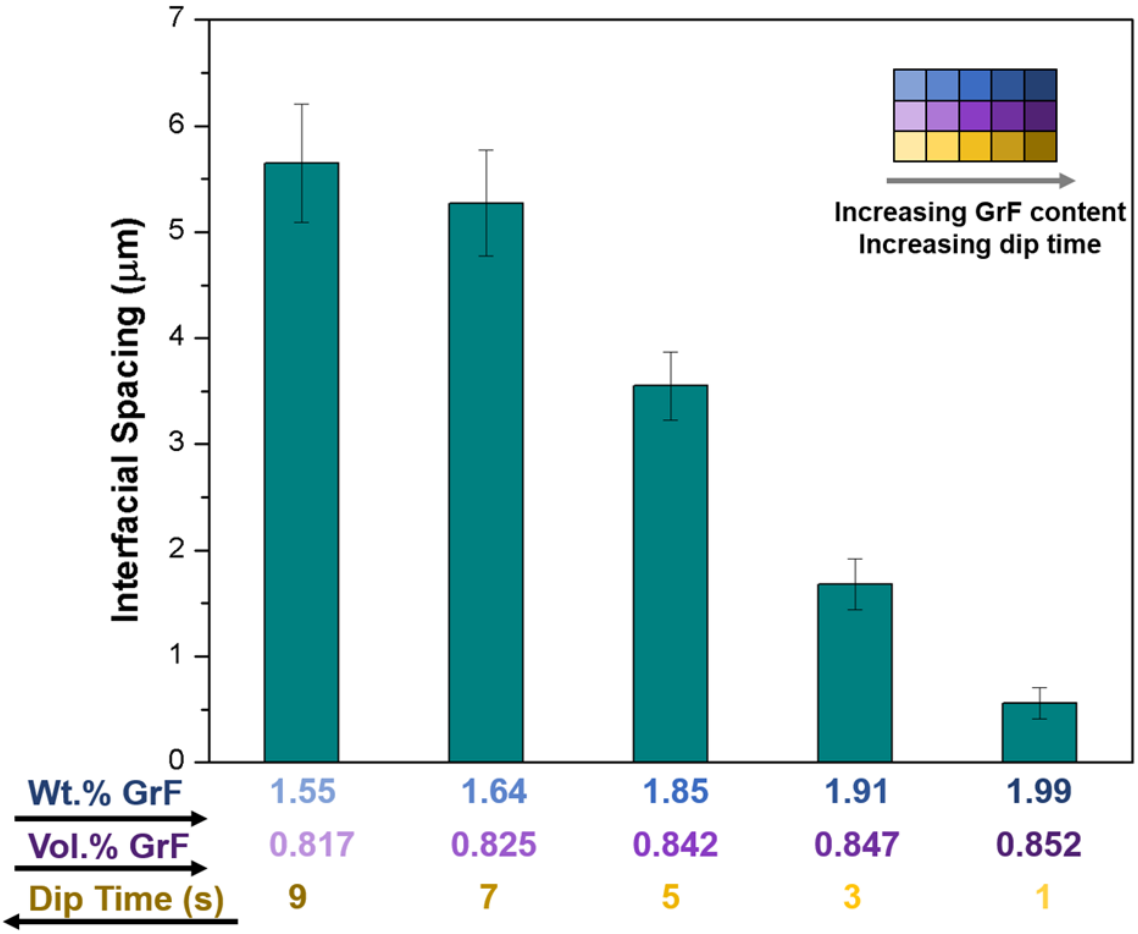

Fig. 4.7. Average interfacial spacing of dip coated GrF-epoxy composite samples.

The dip coated samples show decreasing average interfacial spacing with increasing polymer content. This is strictly attributed to polymer shrinkage, also known as cure shrinkage. After the components of the thermosetting polymer were mixed, an exothermic polymerization reaction was initiated. Initially, the polymer "swells" due to rigorous movement of the polymer chains as they start to connect and lock into place. As the reaction continues, more polymer chains settle onto one another and consequently take up less space than before. As a result, more initial polymer chain cross-linking leads to

greater movement at the beginning of the reaction, leading to increased polymer shrinkage by the end of the reaction. As the polymer chains settle in, a retraction of material away from the GrF occurs, resulting in increased interfacial spacing. The dip coating synthesis technique facilitates capillary filling of GrF branches by epoxy polymer which is clearly shown in Fig. 4.8. Epoxy is drawn up into the interior of the triangular GrF branches although the central portion of the branches are hollow. Furthermore, the high GrF weight percent in dip coated samples acts as barriers against polymer chain formation, leading to less heat generation and therefore less swelling during the polymerization process.

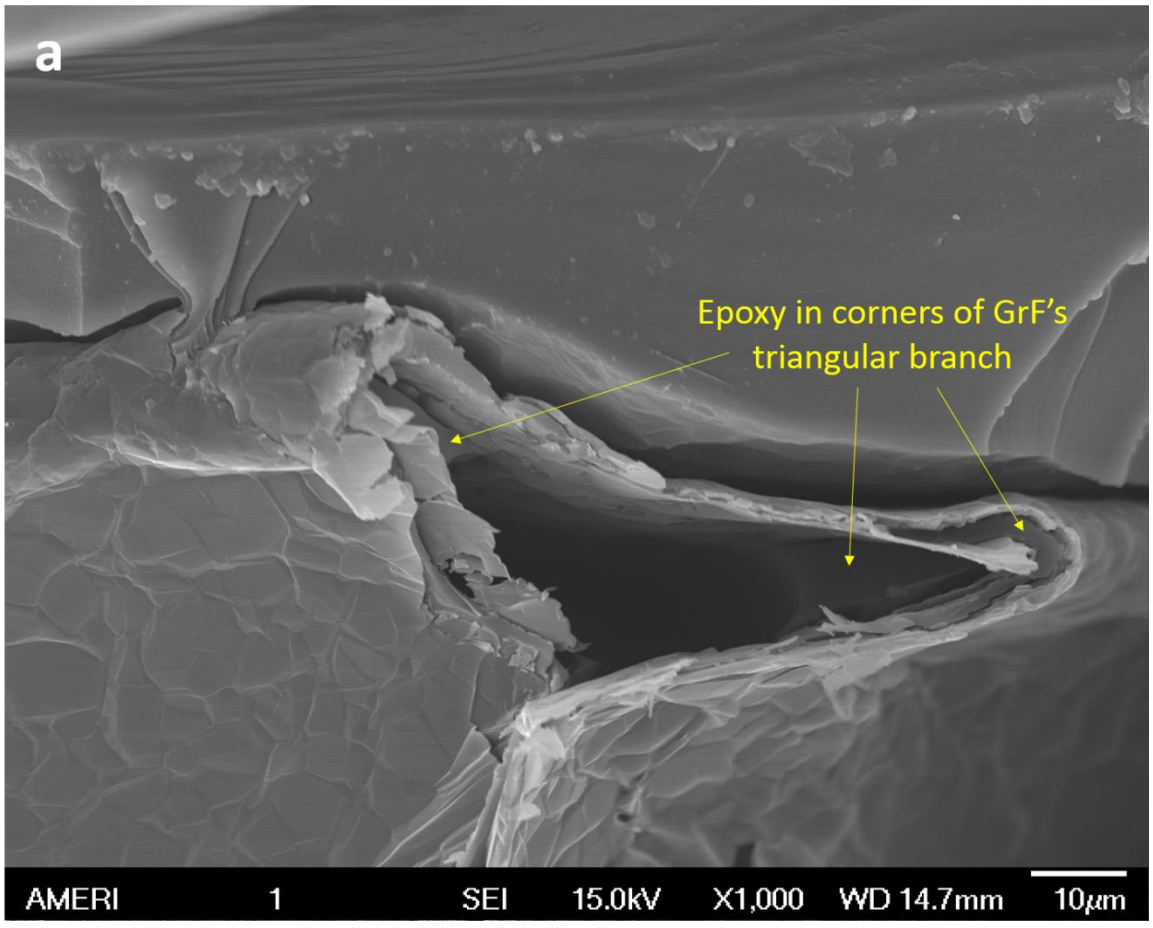

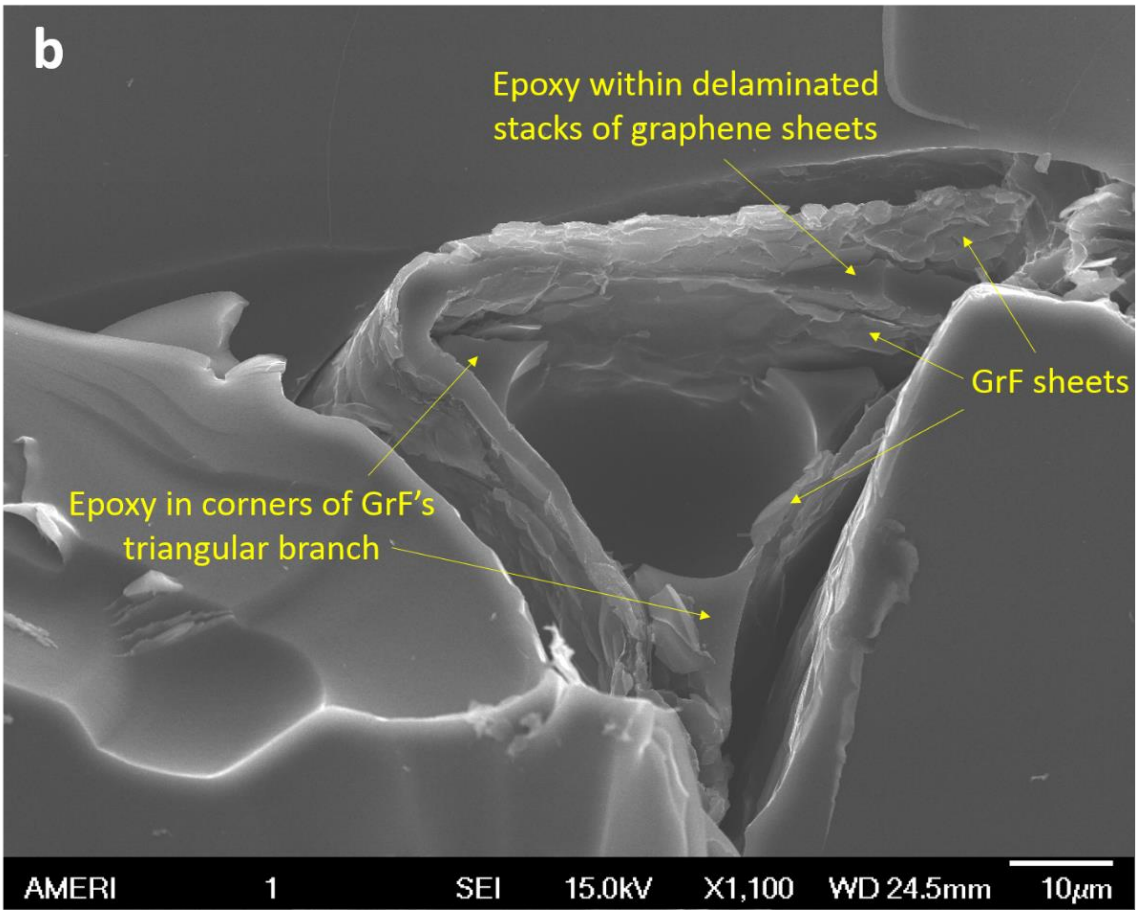

Fig. 4.8. Capillary pulling of epoxy into GrF branches demonstrated by (a) epoxy lining the corners of triangular GrF branches and (b) central circular hollow region formed by epoxy within GrF branch.

4.1.2. Mold Cast Technique

The mold casting technique allows for further GrF content controllability with an altogether different microstructure while maintaining uniform dispersion and polymer infiltration into GrF epoxy cellular structure as shown in Fig. 4.9.

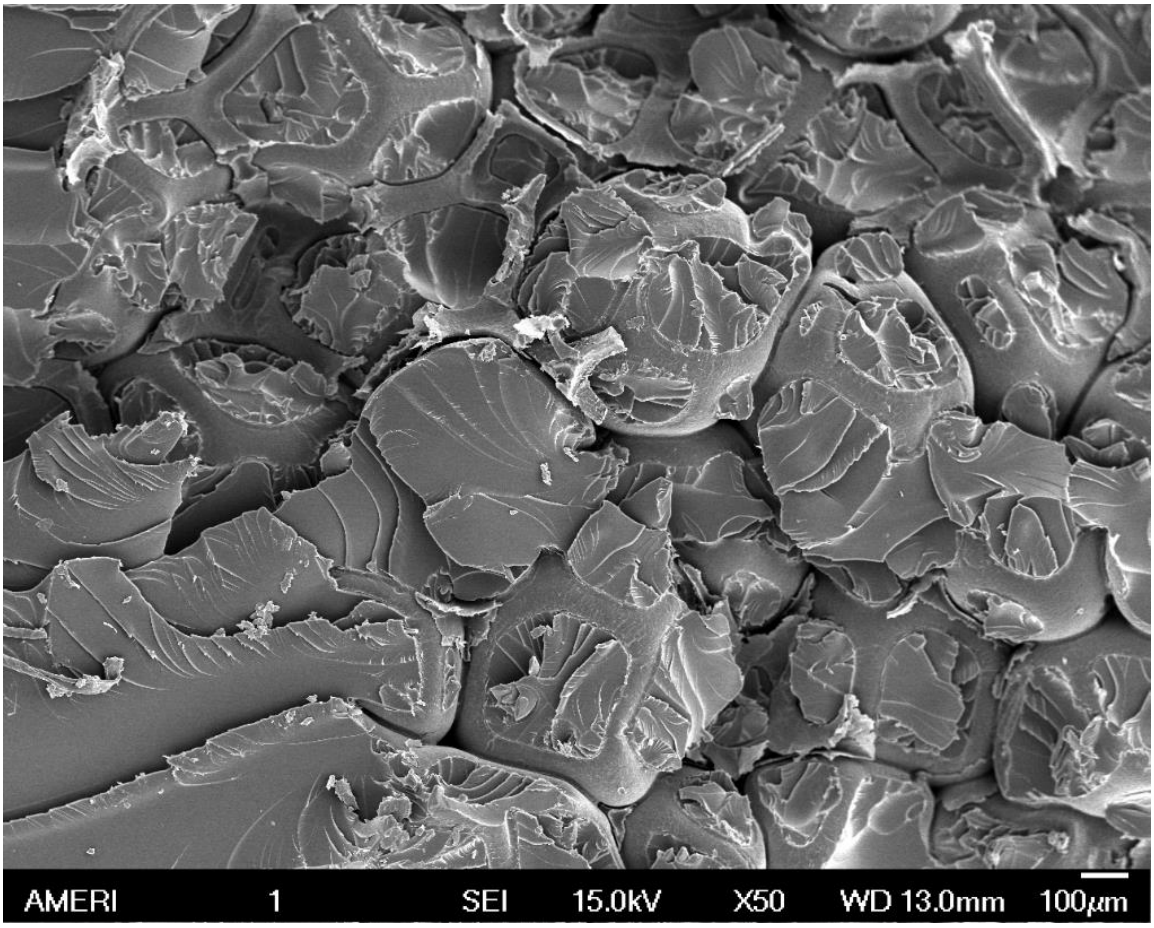

Fig. 4.9. SEM image of cross-sectional fracture surface demonstrating uniform dispersion of GrF inside epoxy matrix in mold casted sample.

The GrF-epoxy cast samples in Fig. 4.10 show almost no change in density with added GrF content. This can be attributed to the extremely small addition of mere 0.07 and 0.13 wt.% GrF to the epoxy. The density of pure epoxy (1.331 g/cm^3) is much higher than the GrF (4 mg/cm^3), and therefore, the extremely small GrF addition results in almost no change in overall composite density.

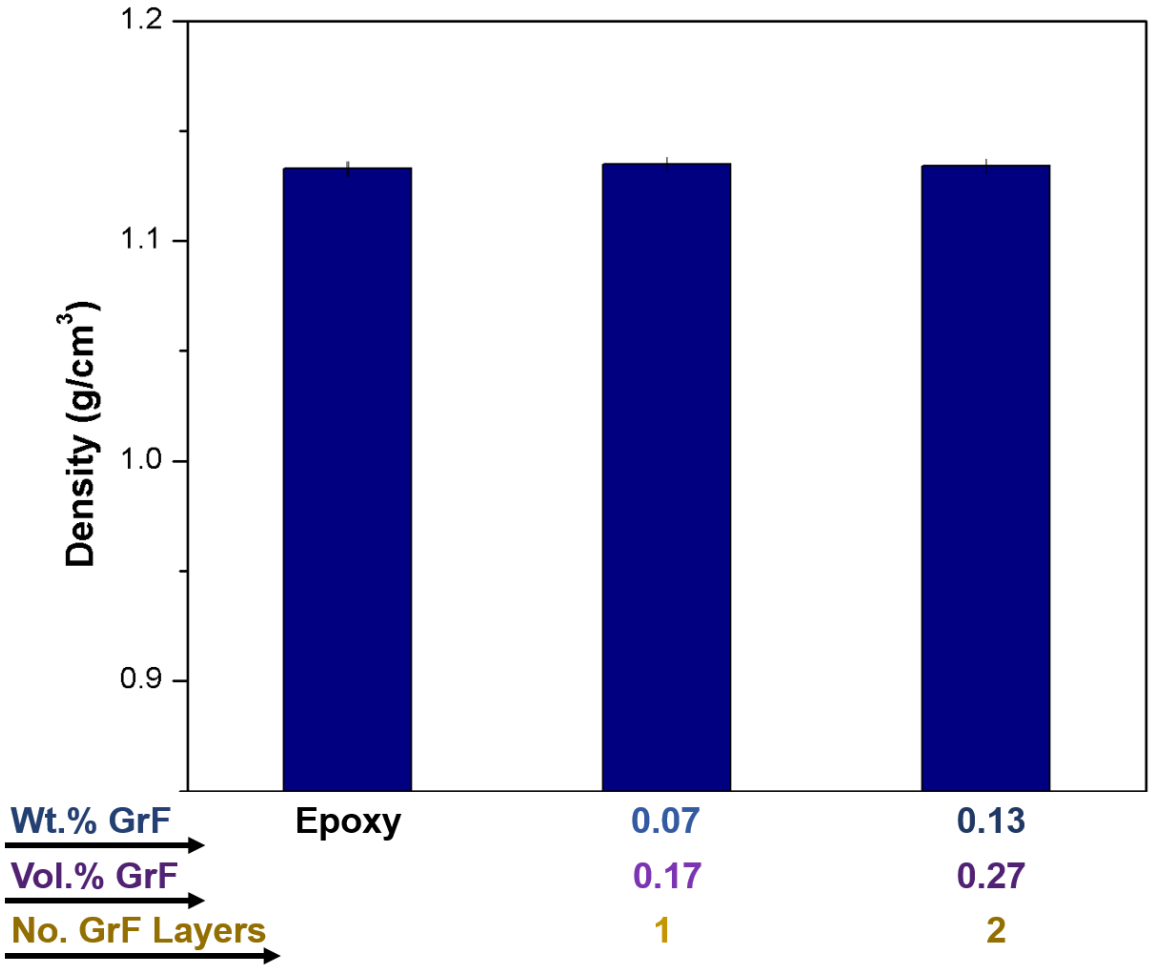

Fig. 4.10. Density of pure epoxy and GrF-epoxy composites synthesized by mold casting technique.

GrF-epoxy cast composites were synthesized and the average interfacial spacing was approximately 10 microns for both 0.07 and 0.13 wt.% GrF-epoxy samples. Fig. 4.11 shows SEM images of the GrF-epoxy cast samples. The average interfacial spacing for GrF-epoxy cast samples is roughly the same as seen in Fig. 4.12. The increased interfacial spacing as compared to the dip coated samples is a result of polymer shrinkage due to the further increased polymer content in the composite. As shown in Fig. 4.11 a, not every GrF

branch will be completely filled with epoxy. Epoxy polymer infiltrates through broken branches, however, many of the pristine GrF branches are still structurally sound.

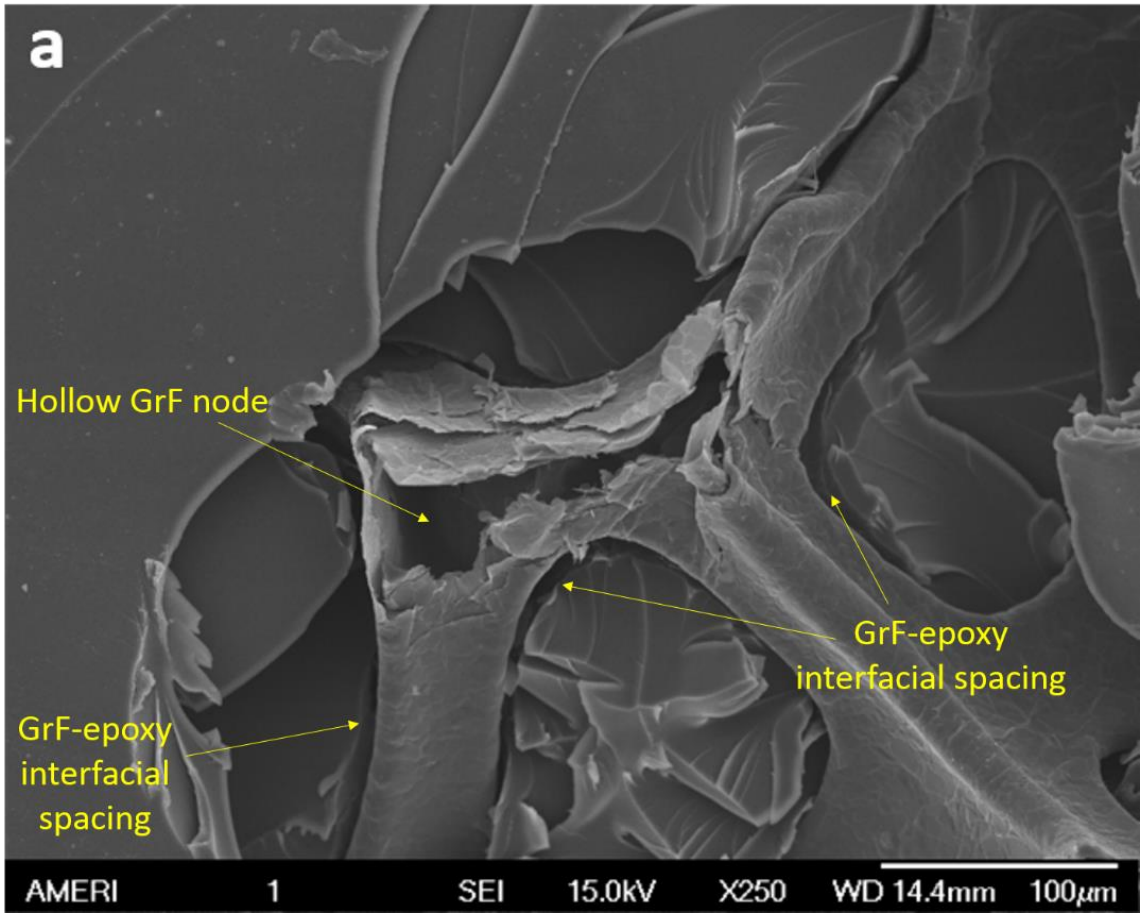

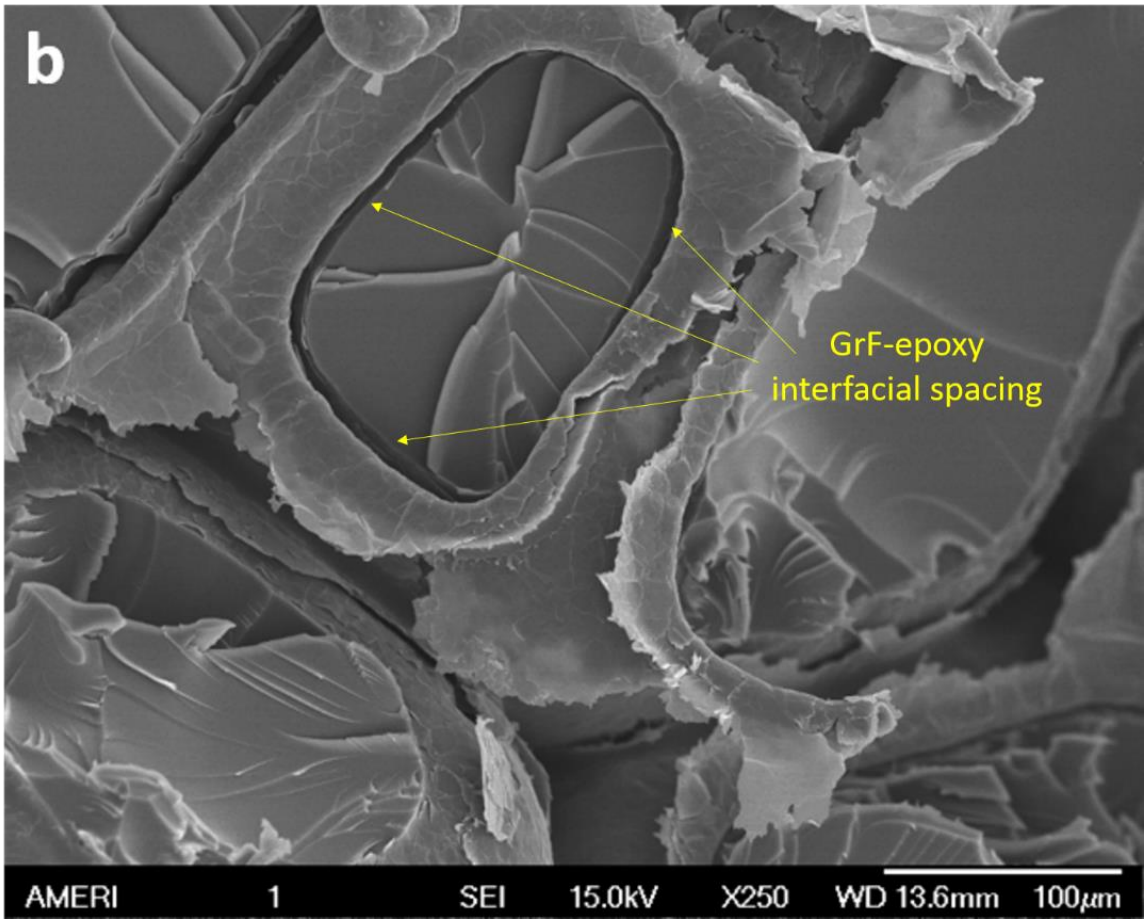

Fig. 4.11. Comparative SEM images demonstrating near equal interfacial separation between (a) 0.07 wt.% and (b) 0.13 wt.% GrF-epoxy cast composites.

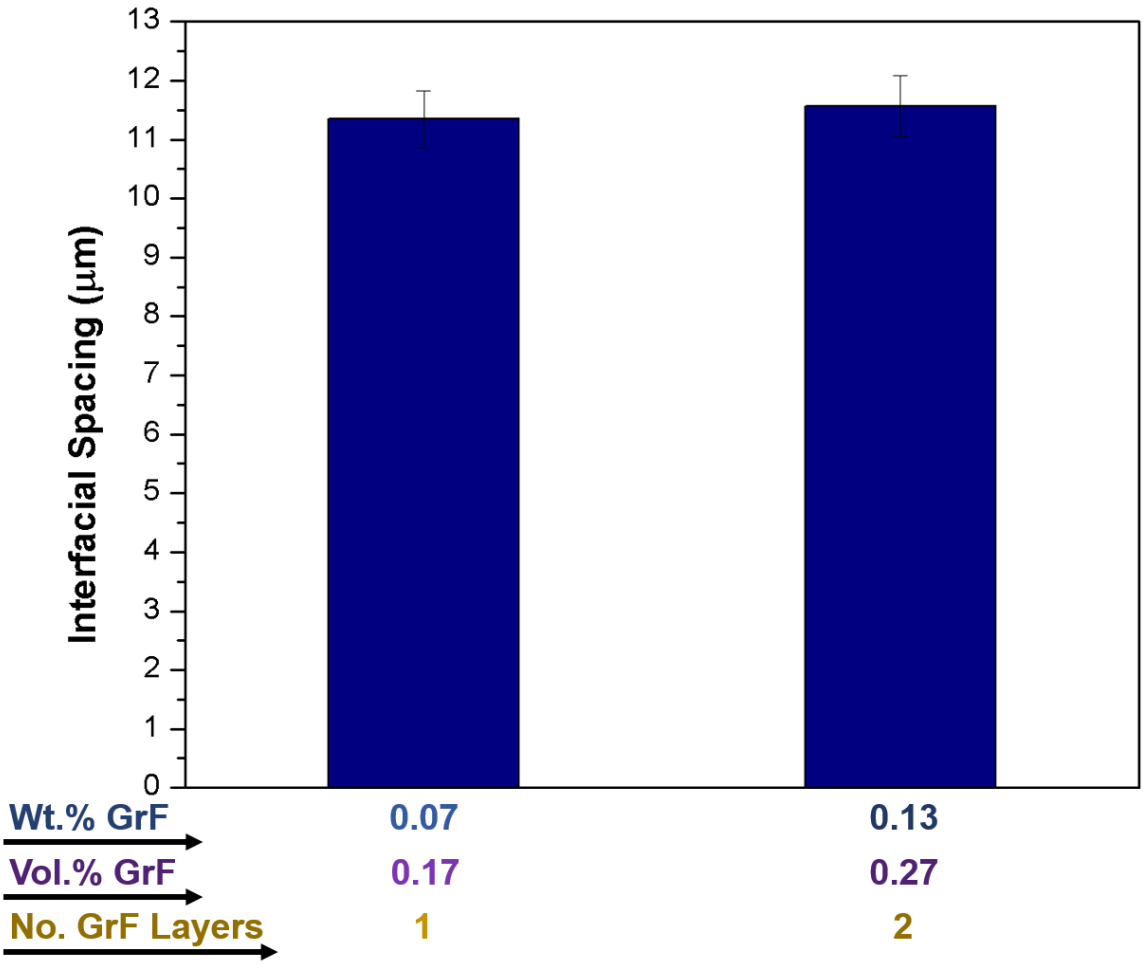

Fig. 4.12. Average interfacial spacing observed for GrF-epoxy cast composites.

Further analysis is done to characterize the mechanical, thermal, and electrical properties of both sets of GrF-epoxy composites.

4.2. Effect of Graphene Foam Addition on Thermal Stability of Epoxy

In a polymer or polymer composite, the glass transition temperature (Tg) describes a thermal stability or polymer chain movement. In this study, the glass transition temperature is evaluated as a function of GrF content for both processing techniques. Pure epoxy's Tg was measured to be 106^{o}C. Upon evaluating the GrF-epoxy dip coated samples,

a remarkable 43°C enhancement was observed with the addition of only 1.5 wt. % GrF. The Tg also continued to rise to above 160°C with further GrF addition of up to 2 wt.% (Fig. 4.13). An impressive 12°C rise in Tg was observed with addition of just over 0.1 wt.% GrF in cast samples (Fig. 4.14).

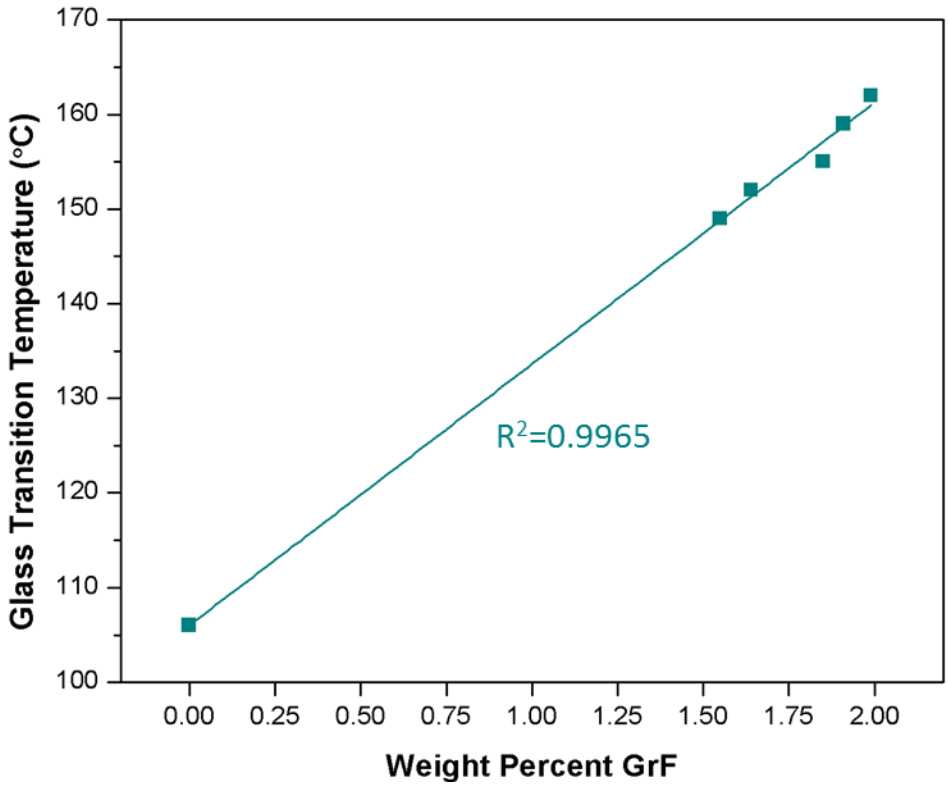

Fig. 4.13. Glass transition temperature of dip coated GrF-epoxy composites as a function of GrF weight percent.

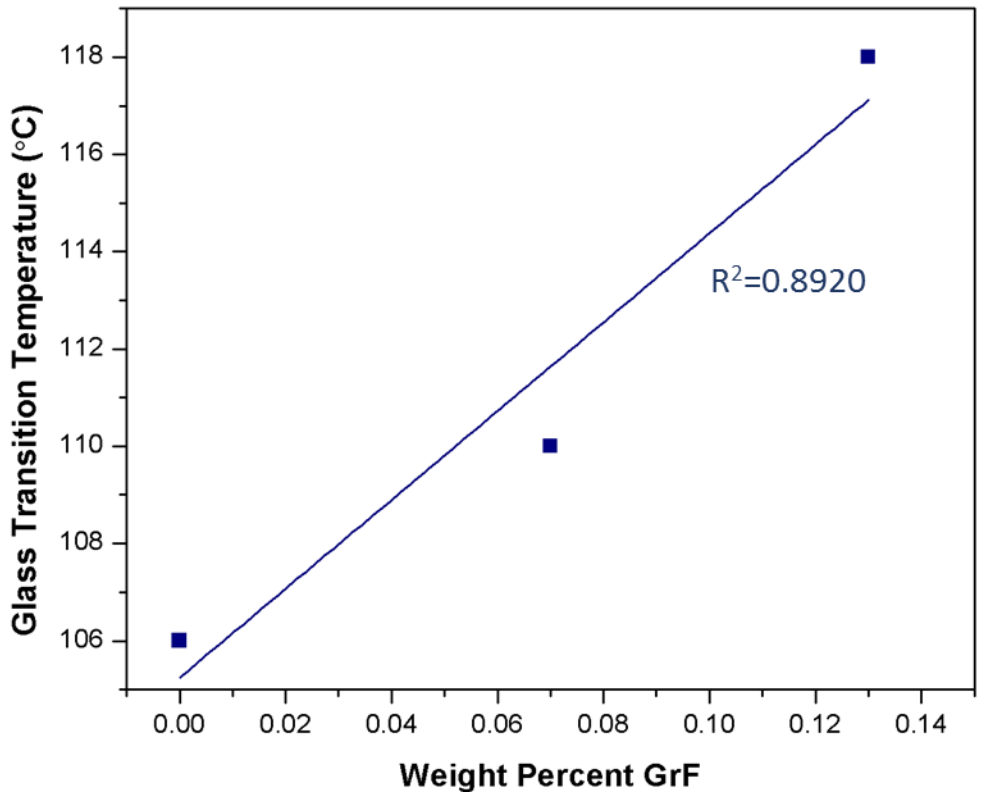

Fig. 4.14. Glass transition temperature as a function of weight percent GrF for mold casted GrF-epoxy composites.

This demonstrates GrF's ability to inhibit polymer chain movement. The polymer molecules may wiggle in place or wrap around the branches of the GrF, but the pre-defined 3D GrF architecture does not move in response to increasing temperature, especially considering graphene is stable at temperatures up to 2300°C [94]. The 53% enhancement in Tg with mere 2 wt.% GrF is also attributed to GrF's ability to transport phonons away from the polymer matrix through its seamless, three-dimensional network. Interfacial interaction enhances epoxy to GrF phonon transport, with the GrF acting as a heat vessel absorbing thermal energy from the polymer. This interaction allows the GrF-epoxy composite to be used at elevated temperature as compared to pure epoxy. By controlling the GrF content

within the epoxy matrix and therefore controlling the composite's Tg, the material may be tailored to fit the necessary applications for particular operating temperature conditions.

4.3. Mechanical Properties of 3D Graphene Foam-Epoxy Composites

4.3.1. Damping Behavior

Vibrations are often problematic for materials requiring dynamic integrity as well as fatigue and impact resistance ranging from large aircraft structural components down to small, functional, precision electronics. Damping behavior is essentially a viscoelastic material's ability to absorb and dissipate energy by converting mechanical energy to thermal energy. In order to quantify damping behavior, the loss tangent, or tan δ, value must be calculated. Tan δ is the ratio of the material's loss modulus to the storage modulus exhibited in response to impact loading:

$$tan\ \delta = \frac{E''}{E'} \qquad \text{(Eqn. 4.1)}$$

The storage modulus (E') is a measure of the material's stored energy and represents the elastic portion, while the loss modulus (E") represents the material's viscous portion and is responsible for the mechanical energy dissipated in the form of heat [95]. A schematic for understanding damping behavior is illustrated below in Fig. 4.15.

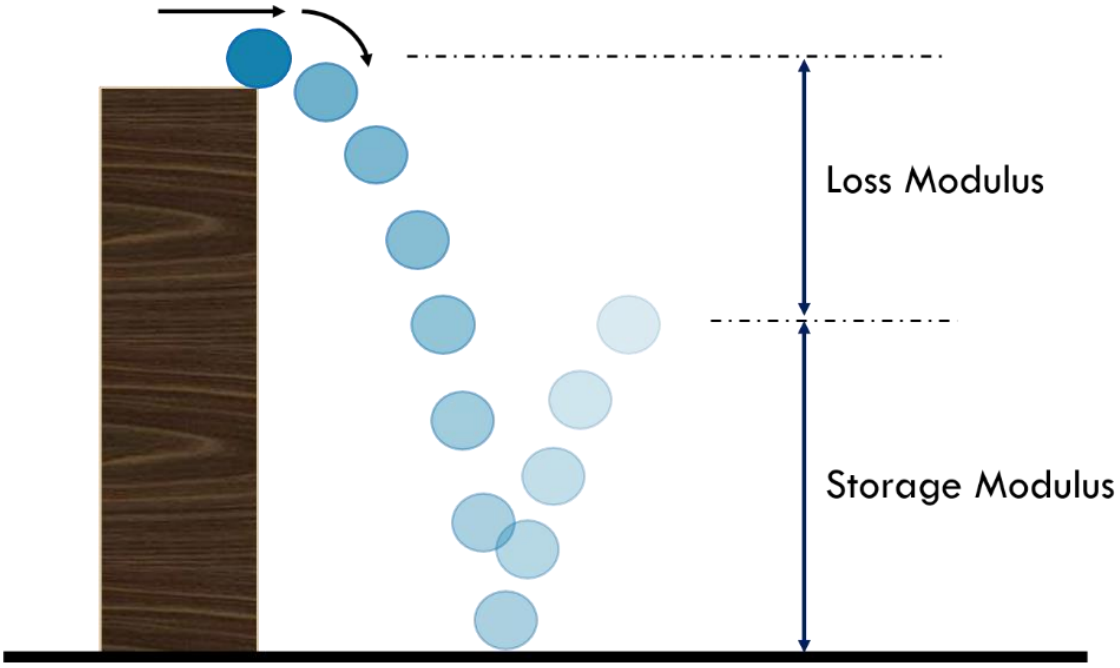

Fig. 4.15. Visualization of damping behavior in terms of storage and loss moduli.

GrF was tested for damping behavior at a number of loads varying from 1-10 mN, and the results are shown in Fig. 4.16. GrF possesses impressive damping capabilities, with tan δ values as high as 0.57 (for 1 mN load). Previous studies have found that damping in graphene is a result of weak van der Waals forces between graphene sheets as well as graphene's intrinsic ability to form waves, or ripples, in response to applied compressive loading [90]. As the waves propagate through the material, mechanical energy is absorbed and dissipated as thermal energy. The free-standing 3D node-branch network of GrF provides additional damping mechanisms since the wave propagation is not confined to a single plane as with graphene. The uniformity of GrF's cellular structure encourages nodal

splitting of the propagating wave, quickly and effectively diminishing the wave's amplitude.

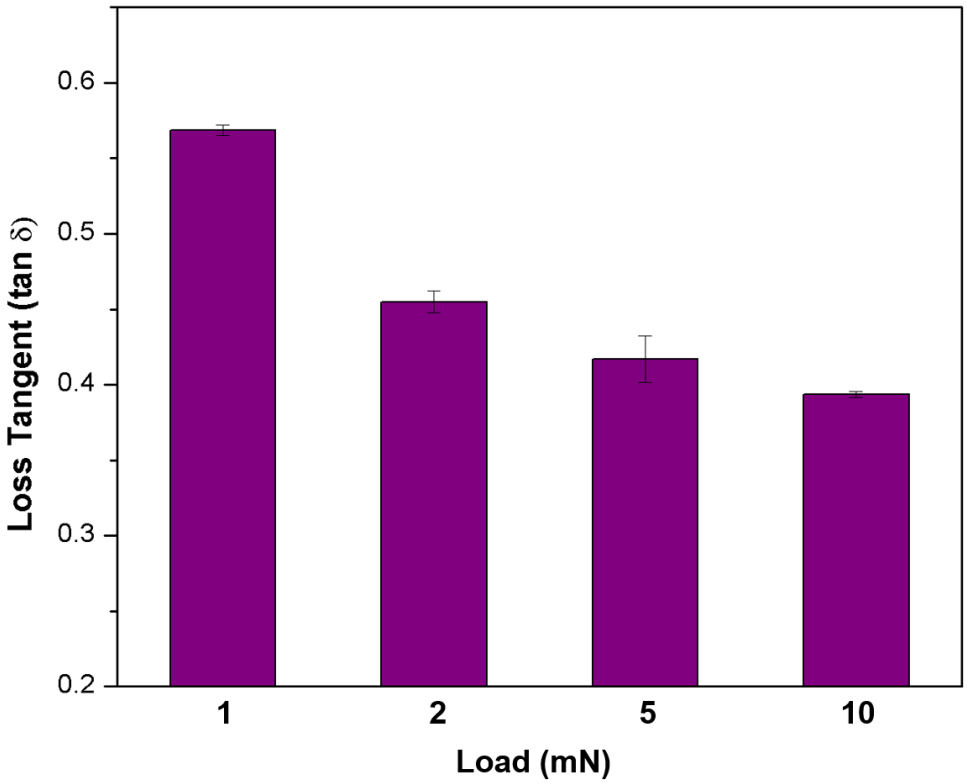

Fig. 4.16. Loss tangent values for GrF tested at various loads from 1-10 mN.

A type of beam "deflection damping" may be another mechanism employed by GrF during impact loading [96]. The GrF branches are likened to structural beams being supported at each end, with the nodes being the fixed supports. Upon impact loading, the "beam" or branch undergoes deflection where the impacted surface experiences compression and the lower surface is put in tension. The inherent structure of GrF allows for bending, kinking, and buckling in response to compressive loads. Studies done on 3D graphene sponge found that energy absorption in response to compressive strain is

dissipated by the load transfer bending to and reversible buckling of graphene sponge sidewalls [97].

As the graphene sheets in GrF undergo compression during impact loading, the inherent interlayer separation is reduced. To absorb the mechanical energy from the applied load, the ~3.4 Å interlayer spacing is utilized to produce an oscillating "spring-like" motion. At higher loads, the compression reduces the interlayer spacing to the extent the van der Waals forces no longer can accommodate the impact loading. With the out-of-plane graphene interlayer spacing at a minimum, the stress of the load is transferred to graphene's in-plane direction. However, the in-plane sp^2 hybridized bonding (bond length ~1.4 Å) being much stronger than the out-of-plane van der Waals forces does not contribute towards energy dissipation. In this case, GrF's in-plane elastic behavior dominates the out-of-plane viscoelastic behavior, leading to diminished loss tangent values and therefore reduced damping capabilities.

Highly impressive damping properties of GrF makes it a promising nanofiller for polymers to induce superior damping. It is noteworthy that unlike pure GrF, which is a free-standing nanomaterial, the composite structure is capable of withstanding higher impact loads due to rigid polymer matrix. Hence, dynamic behavior of composites is examined at higher loads than pure GrF, to gauge the true structural damping. The dynamic tests were conducted for dip coated samples for loads varying from 1 to 50 mN (Fig. 4.17). For the dip coated samples, with increasing GrF content, enhanced loss tangent values were observed. When compared with pure epoxy, at low loading (1 mN), 140% increase in loss tangent was observed with addition of mere 2 wt.% GrF to the epoxy matrix. At higher

loading of 50 mN and at same 2 wt.% GrF content, an 80% enhancement in loss tangent values was measured when compared to pure epoxy. The increase in damping behavior is due to the weak van der Waals forces allowing a spring like action between GrF layers in addition to the good GrF-epoxy interfacial interaction facilitating effective epoxy to GrF load transfer. The drastic increase in loss tangent values at higher loads is a result of the epoxy's infiltration into GrF providing GrF with structural support yielding repeated up-and-down motion of GrF without collapsing its branches. Furthermore, the enhanced energy dissipation comes from the fact that there is simply more energy introduced into the system by the impact load. Effective energy dissipation of 50 mN load means that GrF-epoxy dip coated composites are primarily tapping the van der Waals forces without needing to dissipate any of the energy into GrF's planar direction. No shear sliding is indicated by the excellent energy dissipation exhibited by the damping behaviors up to 50 mN.

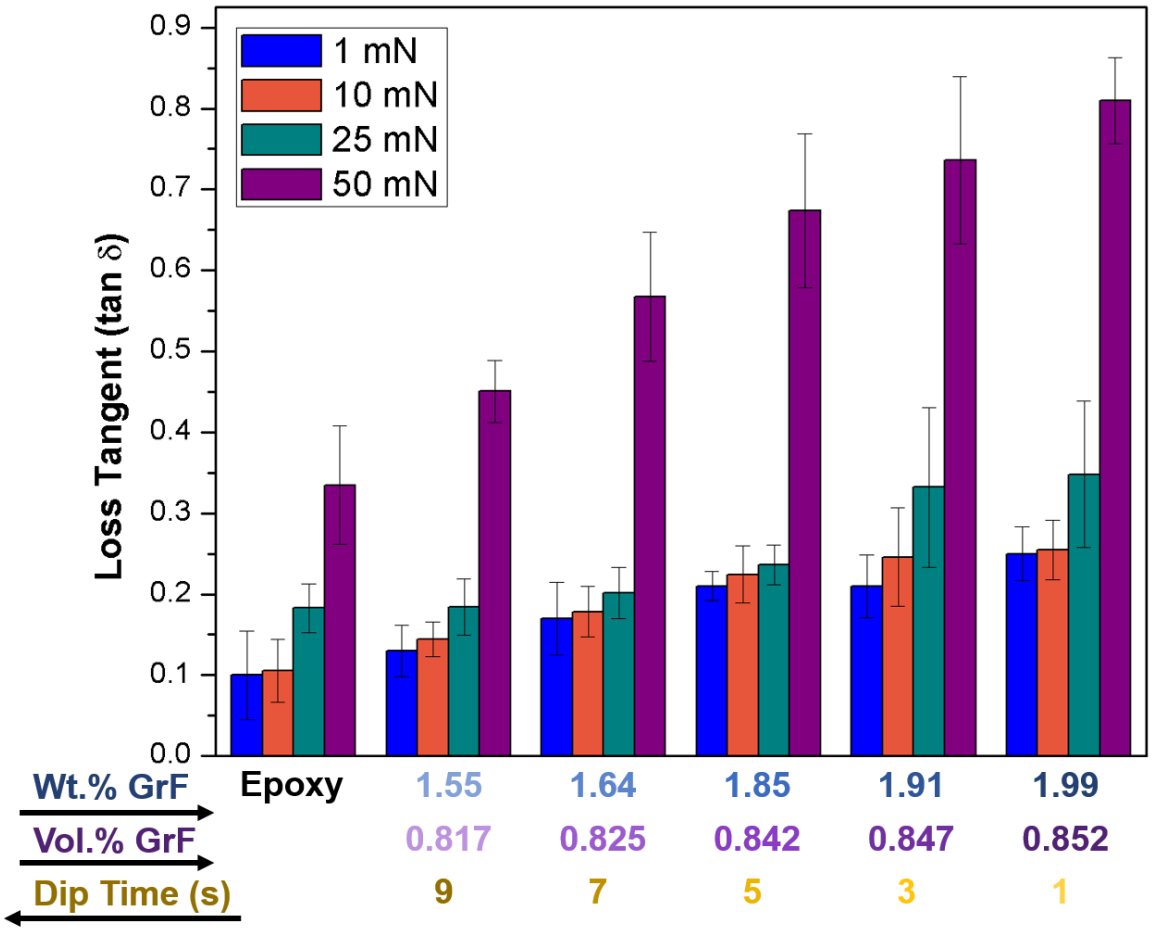

Fig. 4.17. Loss tangent values for pure epoxy and GrF-epoxy dip coated samples at loadings of 1, 10, 25, and 50 mN.

Unlike dip coated samples which are rich in graphene content, cast composites are rich in polymeric phase. Hence, to be able to truly capture the damping mechanics due to graphene foam reinforcement, the damping tests for mold casted samples (Fig. 4.18) were conducted for higher loads (up to 90 mN). The same trend was observed for cast GrF-epoxy composites. Higher GrF loading facilitated higher loss tangent values. Although the cast samples had much lower GrF content than the dip coated samples, the damping capabilities were nonetheless impressive. At same impact loading, mere 0.06 wt.% and

0.17 wt.% GrF resulted in 30% and 60% enhancement in loss tangent values, respectively. Minimal interfacial separation of only 10 microns in the synthesized composites allows effective transfer of mechanical energy from polymer to GrF reinforcement. Hence, superior damping properties of GrF is effectively harnessed, allowing impressive improvement in epoxy's damping capability even when nanofiller content is very low. Progressive enhancement in loss tangent with increasing load signifies excellent high load impact tolerance of these composites.

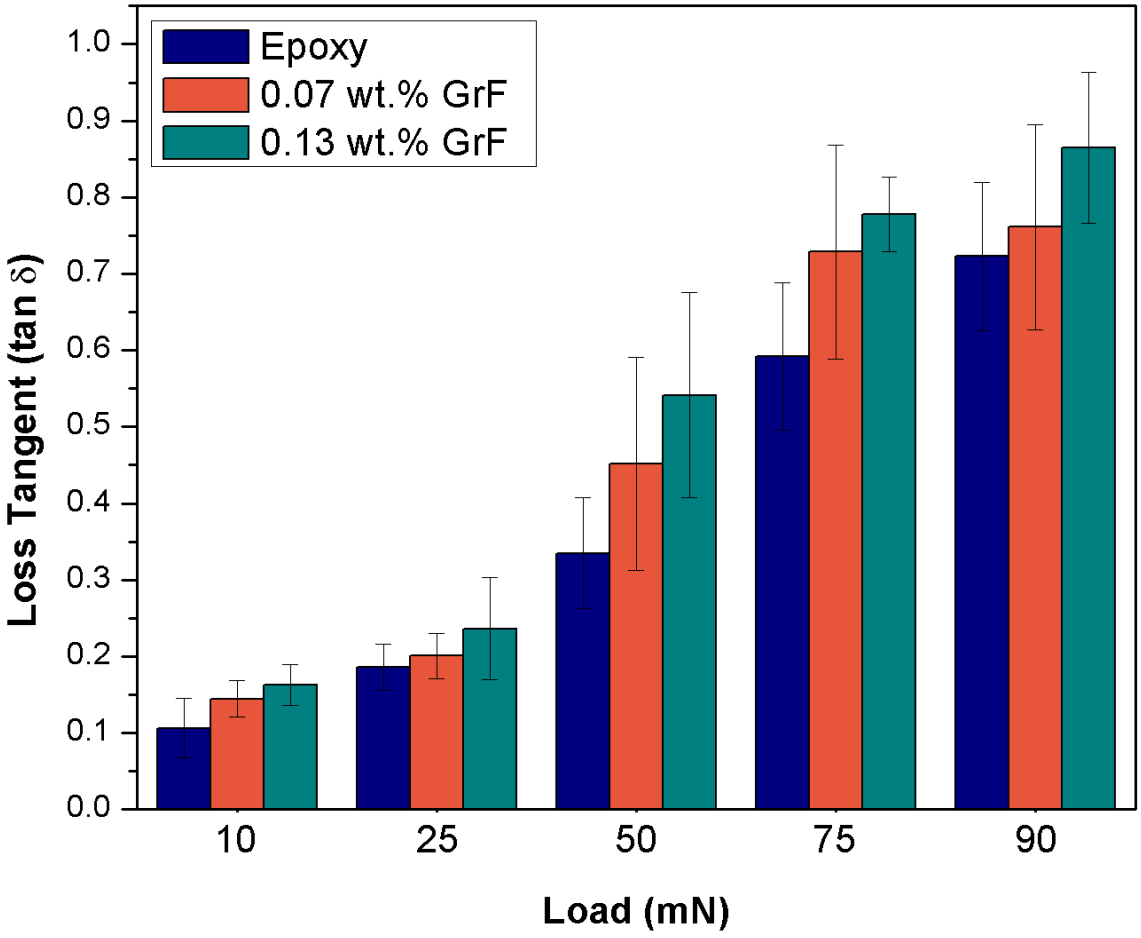

Fig. 4.18. Loss tangent values of pure epoxy and GrF-epoxy cast samples at loadings of 10, 25, 50, 75, and 90 mN.

Multilayer graphene has intrinsic damping capabilities owing to its interlayer weak van der Waals forces between stacked graphene sheets allowing a "spring-like" motion in response to compressive loading. Intrinsic ripples in the pure GrF structure welcome wave propagation from impact loading which results in effective energy dissipation away from the impact site.

The polymers themselves have good damping properties due to the polymer chains' hysteresis properties promoting polymer chain settling onto and sliding past one another in response to applied loads [98-99]. The composite components may also work together to exhibit excellent damping behavior by reinforcement to matrix boundary sliding [100]. As the polymer chains crosslink around the GrF during curing process, they are lengthening and taking up a lot of space. Upon curing, the polymer chains settle and result in an overall shrinking. The GrF works as a heat conductor to remove some of the heat away from the polymer chains, ultimately reducing the polymer shrinkage. This leads to minimal interfacial spacing between the GrF and epoxy. Good interfacial interaction between the composite components allows effective transfer of mechanical energy from polymer to GrF reinforcement. The small separation between the GrF and polymer allows the GrF to move adjacent to the applied load, permitting wave propagation through the sample, further dissipating the mechanical energy.

The polymer chains' abilities to bend, flex, and slide in conjunction with the in-plane and out-of-plane movements of the carbon atoms of the GrF employ wave ripple propagation as the primary dampening mechanism for effective energy absorption and dissipation. The pure polymer's damping capabilities are highlighted because the tan delta values for pure epoxy also proved extraordinary. However, the combined notable damping

characteristics of both GrF and epoxy led to the highest loss tangent value observed in this study. The synthesis techniques of the cast samples allowed more GrF branch infiltration with epoxy, providing the branches with added structural integrity. Additionally, with more epoxy infiltration, there is added GrF to epoxy surface area which leads to improved epoxy to GrF stress transfer upon compressive loading.

Although GrF suggests to have superior damping capabilities, pure GrF cannot withstand large impact loads as a free-standing structure. If the impact loading compresses the graphene layers too much, the van der Waals forces will be overly stressed and a shear sliding will begin to take effect. Since graphene has intermolecular strong π-π bonds, they will resist the shear sliding, leading to diminished damping behavior of GrF. Pure epoxy can withstand higher impact loadings due to the long chains' ability to move and slide to accommodate stress from impact loading.

The composites in this study demonstrated potential for use for high vibrational applications as the tan delta continually increased with not only added GrF content but also with increased impact loading. By selecting specific fabrication methods and tailoring the reinforcement to polymer ratio, the Tg and composite toughness may be enhanced to further improve damping behavior for the desired operating conditions of the material.

4.3.2. Flexural Strength

Flexural strength of GrF-epoxy cast composites are evaluated by 3-point bend flexural testing. Evaluation of flexural strength by 3-point bend testing requires materials with rigidity, therefore the flexible dip coated samples were not characterized for flexural strength. 3-point bend testing revealed that with mere 0.30 and 0.63 wt.% GrF addition to

epoxy, a remarkable 25% and 56% enhancement in flexural strength as compared to pure epoxy was observed (Fig. 4.19). The flexural stress-strain curve demonstrates that the flexural strength is enhanced with increasing GrF content. Although the pure epoxy fails at a higher strain, the addition of GrF has an obvious effect on the strength of the epoxy matrix.

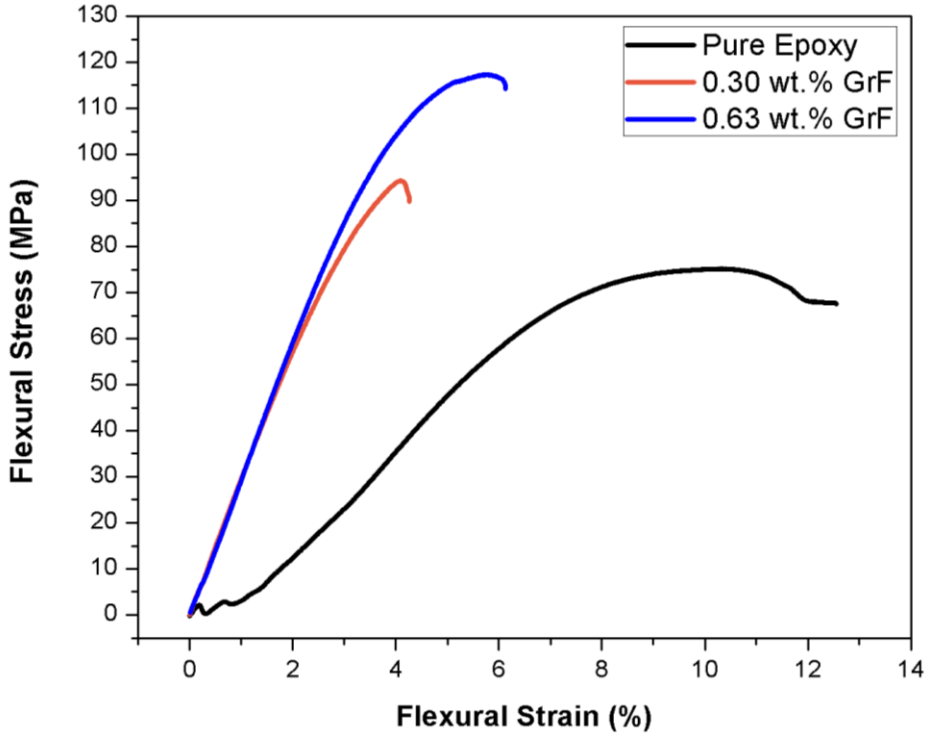

Fig. 4.19. Flexural stress-strain curve resulting from 3-point bend test for pure epoxy and GrF-epoxy mold casted composites.

The marked improvement is a result of the synthesis technique, good interfacial interaction, high polymer content within the GrF branches and nodes, GrF *compromising its structure in response to applied load*, and GrF deflecting crack propagations of the epoxy.

The mold casting synthesis technique gives rise to a microstructure which provides for enhanced flexural properties with minimal GrF content. By allowing the GrF to "soak" in the epoxy during the curing cycle, there is higher infiltration into the pores, branches, and nodes (Fig. 4.20) of the GrF providing the nanofiller with added structural stability.

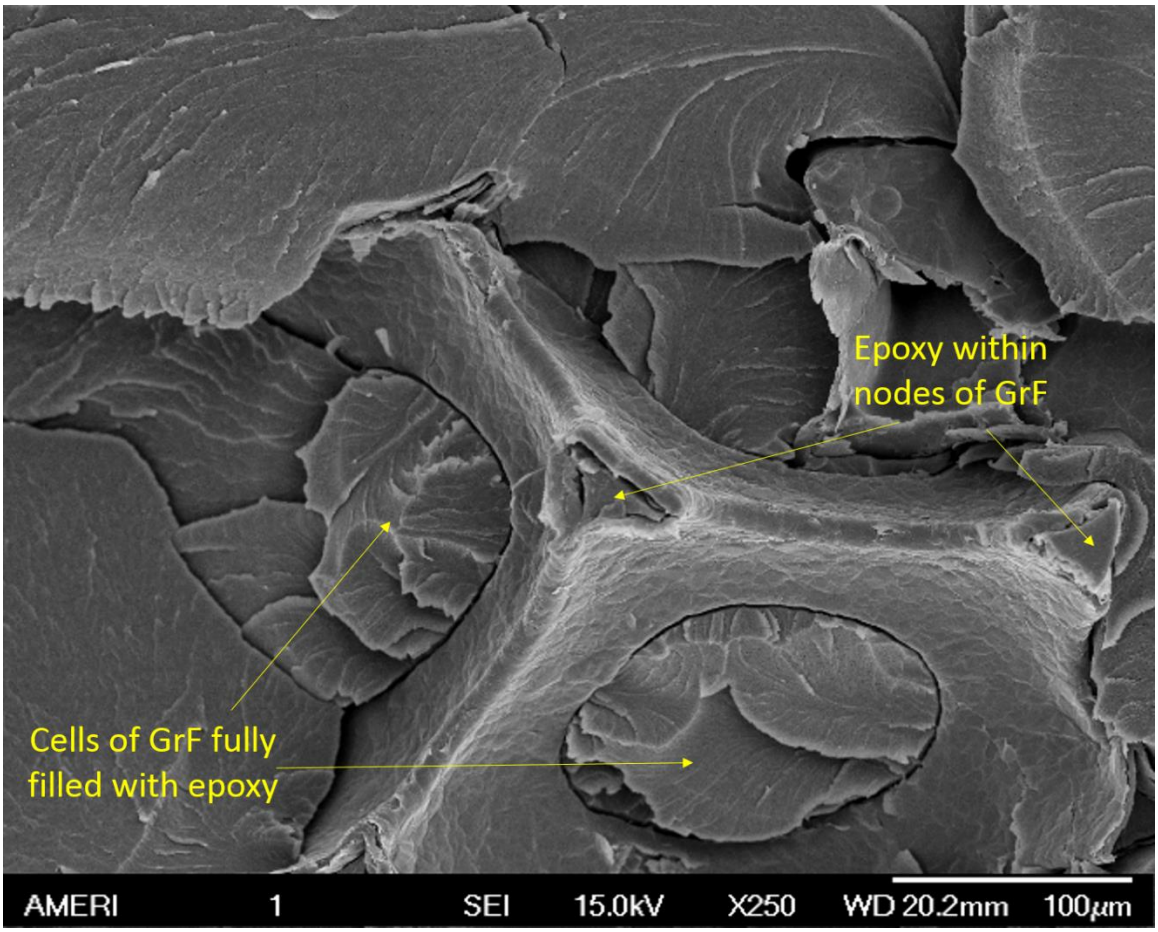

Fig. 4.20. Epoxy filling the nodes and cells of GrF.

Filled with epoxy, the GrF branches are more likely to bend, rotate, and twist rather than crush or collapse under loading conditions (Fig. 4.21 a-c). Minimal interfacial separation allows effective stress transfer from epoxy to GrF in response to the applied flexural load. GrF tends to wrinkle or kink as a means to alleviate the stress from the epoxy

matrix. Fig. 4.22 shows GrF's ability to stretch in order to resist failure. Note the inside of the GrF is lined with a thin layer of epoxy, allowing the GrF fragment to withstand higher flexural stress upon loading as shown in Fig. 4.20.

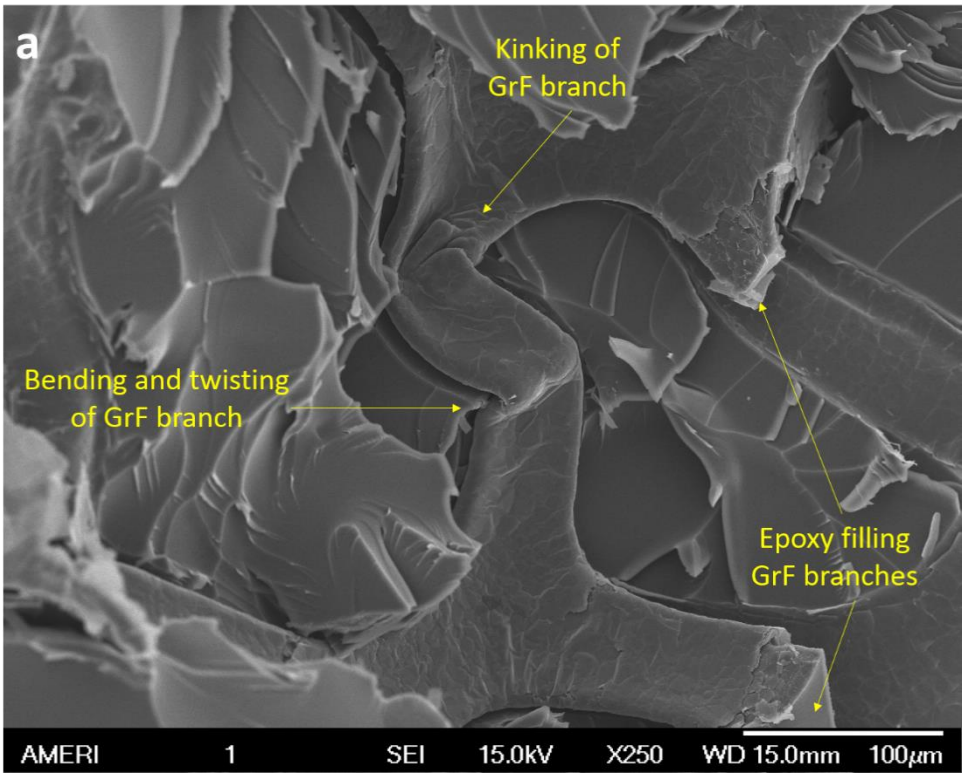

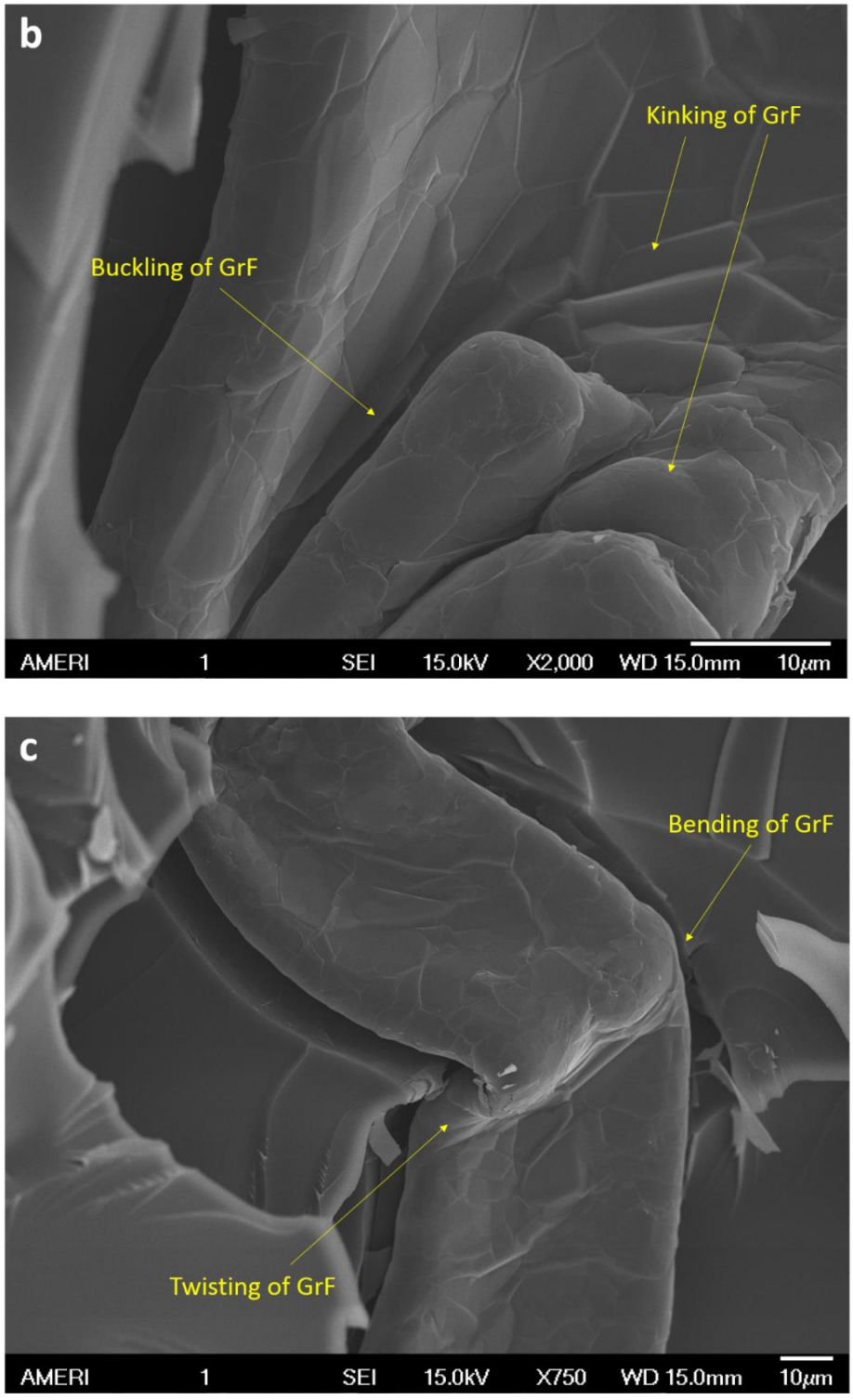

Fig. 4.21. SEM micrographs at (a) low magnification and (b-c) high magnification of epoxy filled GrF branches bending, kinking, twisting, and buckling in response to applied load.

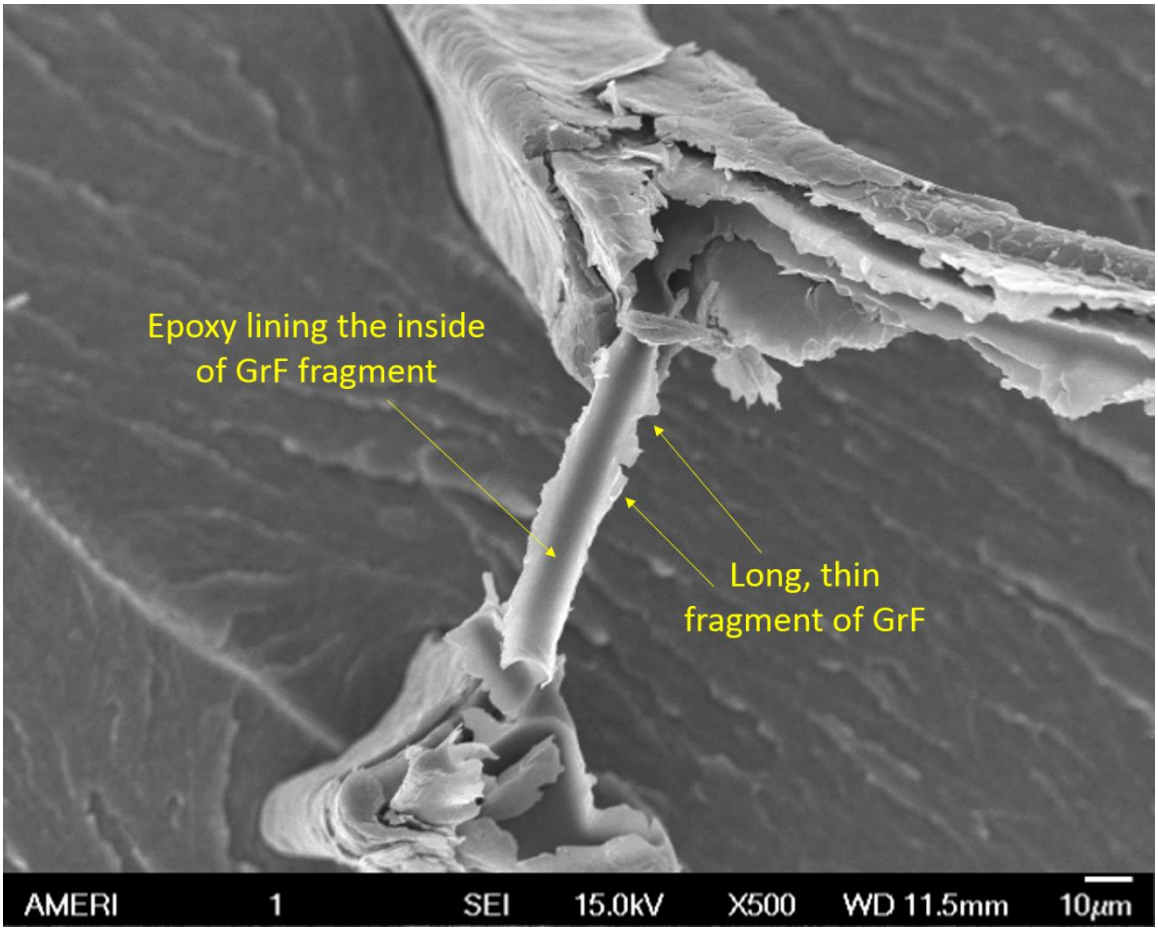

Fig. 4.22. Fragment of GrF lined with epoxy stretching to resist failure.

Micrographs of the post-tested composite reveal multi-directional fracture surface features caused by the GrF reinforcement blunting the advancing polymeric crack propagations. Fig. 4.23 shows the paths of the advancing cracks are forced to travel around GrF branches due to the crack deflection. .

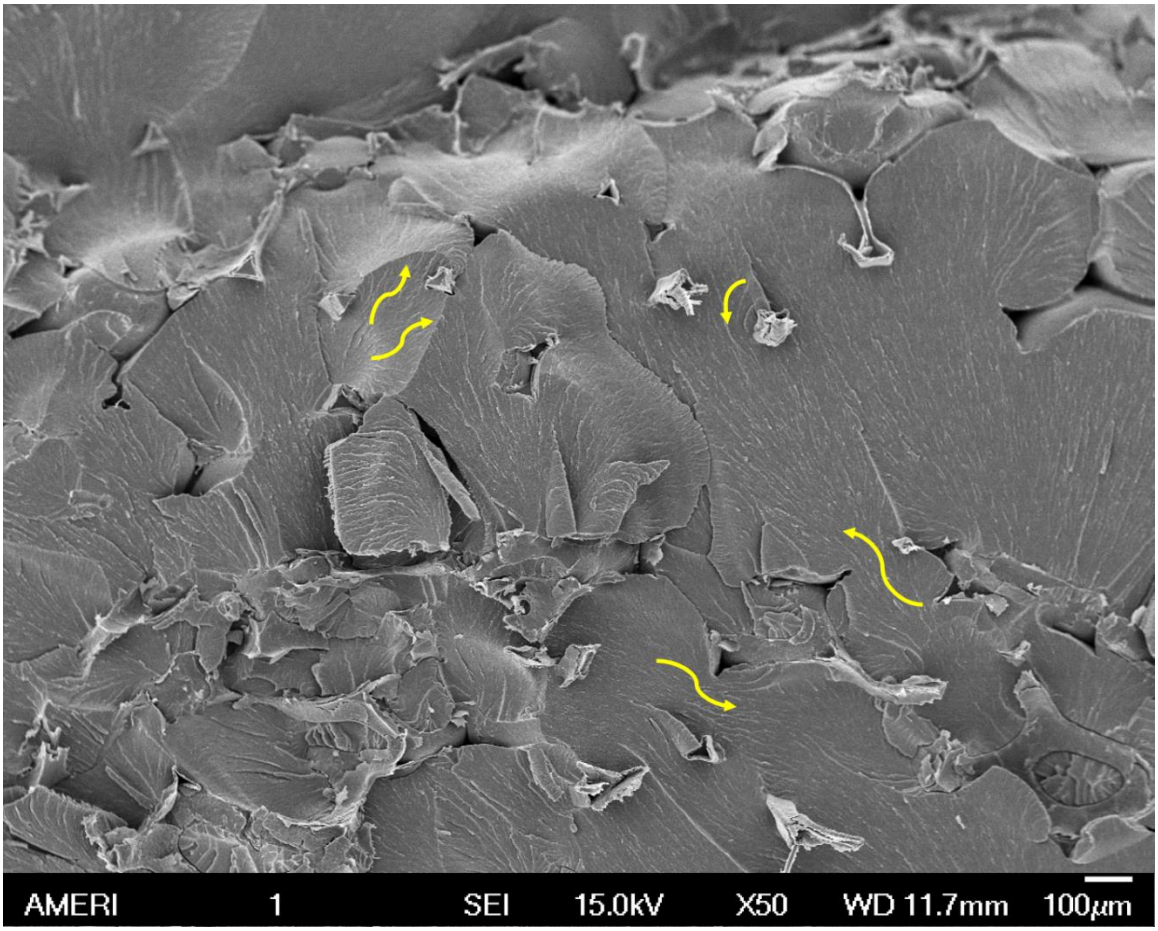

Fig. 4.23. SEM image of GrF-epoxy composite with fracture surface features revealing GrF deflecting polymer crack propagations.

The many strengthening mechanisms demonstrated in the flexural tests demonstrate the magnitude of the potential GrF can have as an epoxy reinforcement. The polymer's intrinsic failure mechanisms are blunted by GrF's crack deflection capabilities. The properties of each composite component synergistically work together to yield enhanced flexural properties for a variety of applications requiring lightweight, flexible, and structurally sound materials.

4.4. Electrical Properties of 3D Graphene Foam-Epoxy Composites

4.4.1. Electrical Conductivity

Insulating epoxy matrix was made electrically conductive by reinforcing with 3D GrF. Pure GrF, pure epoxy, and each of the GrF-epoxy samples were tested for electrical resistivity, and the electrical conductivity was calculated. The pure GrF as well as the epoxy composites showed superior electrical conductivity over pure epoxy. Fig. 4.24 shows epoxy to have a very low electrical conductivity of 10^{-9} S/m. The addition of mere 1.55 wt.% GrF boosted the electrical conductivity to 164 S/m, 9 orders of magnitude higher than pure epoxy in dip coated composite samples. As expected, as electrical properties improved with increasing GrF content. There are multiple reasons for the excellent electrical conductivity exhibited by the dip coated samples. First, the GrF itself displays excellent intrinsic electronic properties due to the unique bonding structure of the carbon atoms and the relativistic electron transport as previously discussed. The large surface area of GrF maximizes the contact made between the GrF and epoxy. The three-dimensional network allows for effortless electron mobility in all directions, reducing the probability of electron collision and scattering. Good interfacial interaction confirmed through SEM imaging of cross-sectional surfaces also contributes to the notable electronic properties of the GrF-epoxy composites. Easily observed is the decrease in electrical conductivity as GrF content decreases, or in other words as polymer content increases. Added polymer content results in increased interfacial spacing, and although the spacing is not significant, the result is slightly diminished electrical conductivity. As electrons scatter away from the GrF, they enter a void which slows them down until they experience a collision with the polymer molecules. Higher spacing at the interface gives the electrons more time to slow

down prior to the collision, leaving less energy for the electrons to bounce back to the GrF. Therefore, less interfacial spacing means the electrons do not slow as much before hitting the polymer interface, resulting in a higher chance of traveling back onto the GrF network. The inexpensive dip coat synthesis technique does not require costly equipment, and it also preserves the three-dimensional structure, minimizing damage to GrF's branches and nodes. The percolation limit of GrF-epoxy seems to occur starting at approximately 5 seconds dipping time.

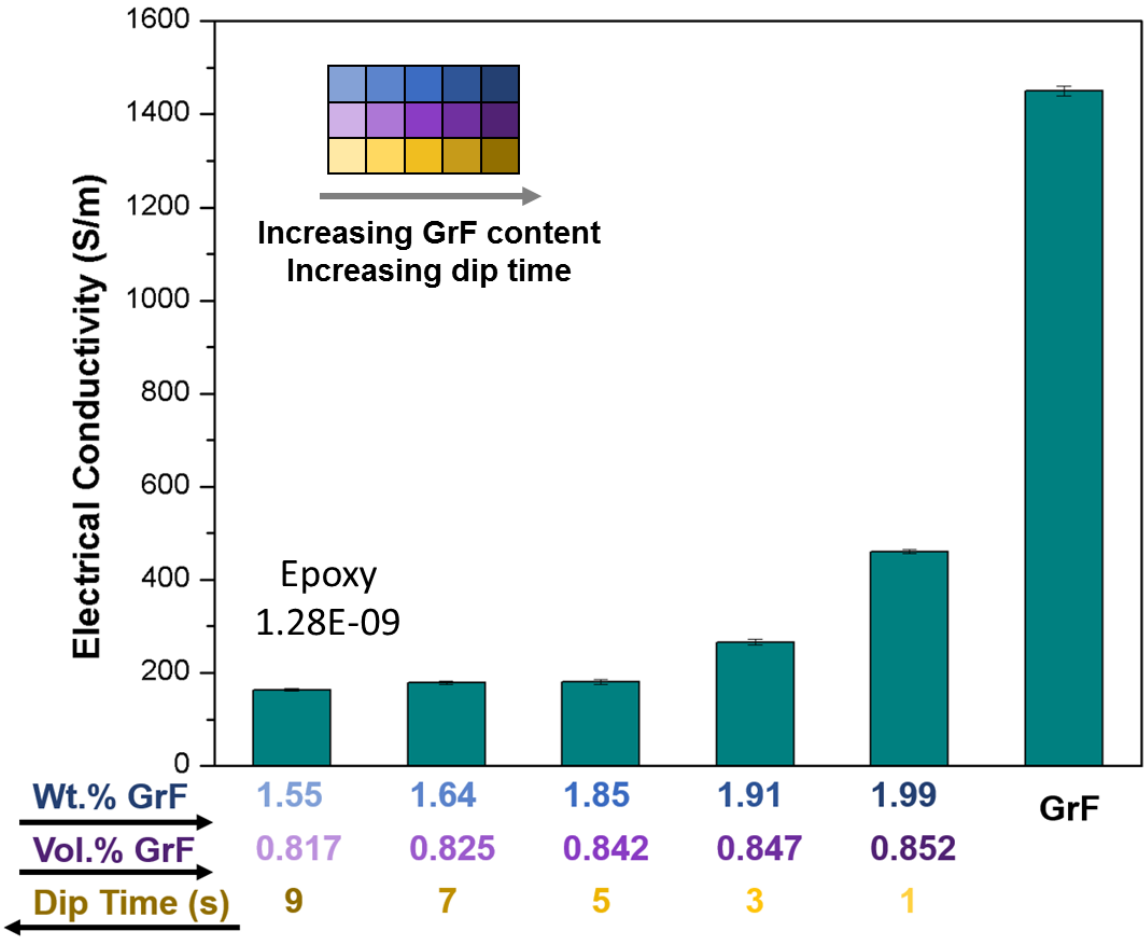

Fig. 4.24. Electrical conductivity measurements of dip coated GrF-epoxy composites with pure epoxy and pure GrF as comparison.

The 0.07 and 0.13 wt.% GrF-epoxy samples made by casting were also tested for electrical conductivity and found to be 85 and 109 S/m, respectively. This synthesis technique proved to be effective in achieving a comparable electrical conductivity measurement to the dip coated samples even at a much lower GrF content. This method allows the GrF nodes and branches to be more fully filled with epoxy throughout the sample, maximizing GrF to polymer contact, resulting in impressive electrical conductivity values despite the extremely low GrF content. The two synthesis techniques proved to be successful in achieving high electrical conductivity while allowing tailorable GrF to epoxy polymer ratios.

4.4.2. Electrical Resistance Retention as a Function of Tensile Strain

It is important for a structural, electrically conductive material to maintain its electrical performance under various mechanical stresses. Electrical conductivity of dip coated and cast epoxy/GrF composites samples was measured under tensile strain. Since the microstructure and interfacial spacing did not change much after 7 seconds of dipping, the 1.91 wt.% GrF sample was used for this particular testing. Therefore, the upper limits of a stabilized microstructure were taken into consideration when choosing which samples to test. The 1.91 wt.% GrF-epoxy dip coated sample impressively showed only a 12% increase in electrical resistance at 5% tensile strain (Fig. 4.25). In Fig. 4.26 the 0.1 wt.% GrF-epoxy mold cast composite demonstrated a 41% jump in electrical resistance at 17% tensile strain.

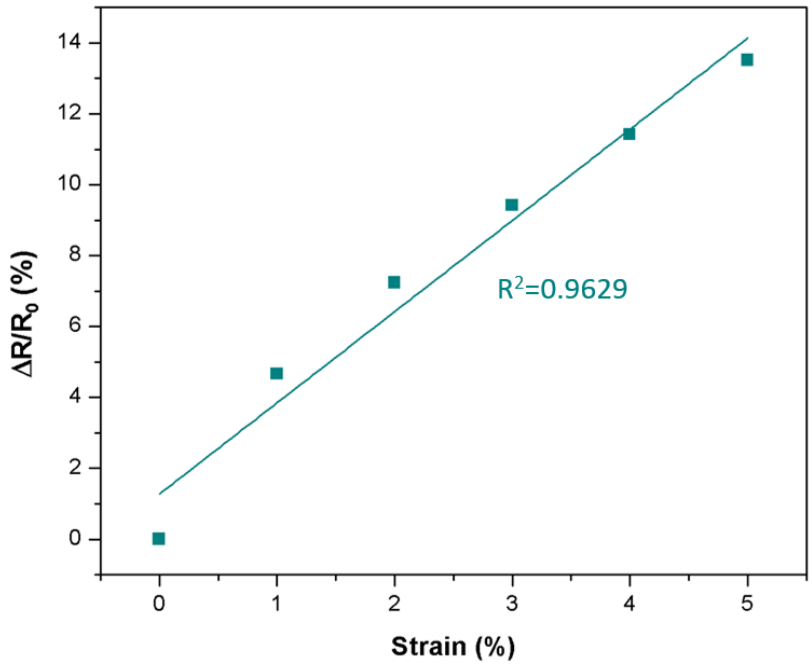

Fig. 4.25. Resistance retention as a function of tensile strain for 1.91 wt.% GrF-epoxy dip coated composite.

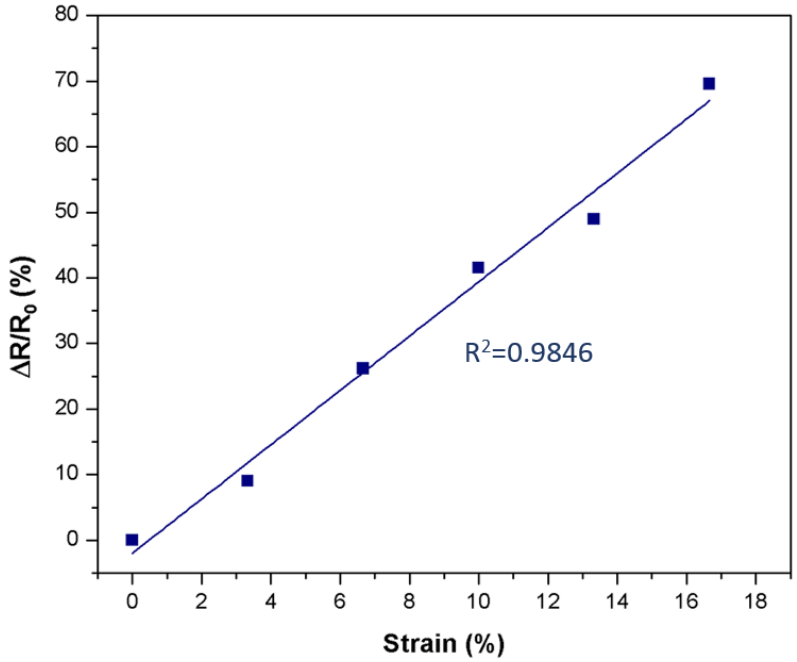

Fig. 4.26. Resistance retention as a function of tensile strain for 0.13 wt.% GrF-epoxy mold casted composite.

The dip coated sample retained its electrical properties under tensile strain, while the mold casted composite showed high sensitivity to deformation. This finding is impressive in both regards. While it is important for a structural material to retain its properties while undergoing deformation (such as the dip coated sample), the high sensitivity of the mold cast composite could prove beneficial for applications such as strain sensors. The mold cast sample shows impressive deformation capabilities since GrF and GrF-polymer composites have repeatedly demonstrated failure at only 5% tensile strain [15, 101]. Although the mold casted sample's electrical properties were not highly preserved as seen in the dip coated sample, the composite allowed 17% tensile strain before reaching failure. In the first case, the composite material demonstrates the ability to effectively conduct electricity despite undergoing deformation. Although the GrF-epoxy composite was being stretched, GrF compromised its hexagonal lattice shape but not its electrical capabilities. Furthermore, the mold casted composite continued to conduct electricity while accommodating significant tensile strain through effective polymer to reinforcement stress transfer. This demonstrates the material's ability to undergo higher strains before failure, indicating the possibility for impressive properties at high deformation. The electrical tests further prove GrF-epoxy composites as candidate materials to be used in conditions calling for a variety of multi-functional purposes. Different synthesis techniques and more precise GrF reinforcement to polymer ratio may be chosen based on the specific applications for which the materials must be utilized.

The electro-mechanical sensitivity of the composite was determined by evaluating the gauge factor, which is defined as:

$$\text{Gauge factor} = \frac{\Delta R/R_o}{\varepsilon} \qquad \text{(Eqn. 4.2)}$$

Both dip coat and mold cast composites showed similar sensitivities, with gauge factors 2.4 and 2.411, respectively. This suggests that the electromechanical sensitivity of GrF based polymer composites is independent of composite fabrication method. These findings are evident that GrF-epoxy composites synthesized by facile dip coating and mold casting methods are electromechanically robust materials with a wide range of potential applications.

CHAPTER V

CONCLUSIONS AND MAJOR FINDINGS

In this thesis, graphene foam reinforced epoxy composites are successfully synthesized using facile dip coating and mold casting processing methods. GrF demonstrates the ability to provide a structurally intact, three-dimensional continuous network eliminating issues such as nanoparticle agglomeration and material anisotropy typically observed in polymer composites reinforced with 1D and 2D carbon-based materials. The addition of GrF is shown to increase the polymer's glass transition temperature, damping behavior, and 3-point bend flexural strength. Electrical properties are characterized, and the addition of GrF to epoxy matrix allows accomplishment of epoxy polymer composites with high electrical conductivity even when subjected to deformation by tensile strain. The specific outcomes of reinforcing epoxy matrix with 3D GrF are presented below:

- Composite materials with tailorable structural and functional characteristics may be achieved by employing facile dip coating and mold casting synthesis techniques.
- Hollow GrF branches and interlayer spacing between stacks of graphene layers induce capillary filling of epoxy resin inside the GrF providing more polymer to reinforcement interfacial interaction.
- Predetermined GrF structure within the epoxy matrix hinders polymer chain movement with increasing temperatures resulting in as high as a 51% enhancement in glass transition temperature (2 wt.% GrF-epoxy surged to 160^{o}C Tg from the 106^{o}C Tg of pure epoxy).

- Mechanical energy dissipation and absorption upon impact loading occurs due to graphene's interlayer van der Waals forces and intrinsic ripple wave propagation as well as epoxy's polymer chain flexion and shear sliding. With mere 2 wt.% GrF content addition, 140% and 80% enhancements in loss tangent were observed at low impact loads (1 mN) and higher impact loads (50 mN), respectively.
- Effective load transfer from epoxy to GrF reinforcement takes place when undergoing tensile and compressive loading as demonstrated by bending, twisting, and kinking of GrF within the epoxy matrix. Mere 0.6 wt.% GrF addition increased flexural strength 65% as compared to pure epoxy.
- GrF's 3D regularly spaced, interconnected network provides continuous pathways within the composites allowing effective electron transport. Addition of 1.5 wt.% GrF improved electrical conductivity by 11 orders of magnitude over pure epoxy.
- Both dip coated and mold casted composites showed gauge factors of 2.4 and 2.411, respectively. Therefore, the electromechanical sensitivity of GrF based polymer composites is independent of composite fabrication method. The impressive gauge factor indicates dip coated and mold casted GrF-epoxy to be an electromechanically robust composite material.

CHAPTER VI

FUTURE RESEARCH

Based on the conclusions and major findings of this research, following recommendations for continuing research may be made.

- For both synthesis techniques employed, observation of interfacial spacing was observed throughout the samples. Surface treatment of GrF and/or chemical modification of epoxy resin could eliminate interfacial spacing by inducing stronger bonding between reinforcement and matrix materials.
- Alternate sample preparations as well as variations in curing conditions should initially be explored. Further optimizing curing temperature and time may lead to reduced polymer shrinkage which would reduce the interfacial separation.
- *In situ* mechanical testing could be performed to understand the deformation mechanisms of GrF-epoxy composites in real time at high magnifications.
- The electrical resistance retention for mold casted composites could be evaluated as a function of cyclic bending, further investigating the possibility of potential high sensitivity strain gauge applications.
- A potential application for GrF-epoxy is anti-ice fuselage and wing coatings for aerospace applications. Carrying out testing and characterization on cooled or frozen composite samples to simulate icy conditions could provide crucial information regarding the feasibility of this application.

REFERENCES

[1] Deepak, V., et al. "Mechanical, Thermal, Electrical and Morphological Properties of Graphene Reinforced Polymer Composites: A Review". Transactions of the Indian Institute of Metals **2014,** *67* (6), 803-816.

[2] Garcia, M. G., et al. "Effect of the Particle Size and Particle Agglomeration on Composite Membrane Performance". Journal of Applied Polymer Science **2010,** *118* (4), 2417-2424.

[3] Zhao, Y., et al. "Highly Compression-Tolerant Supercapacitor Based on Polypyrrole-Mediated Graphene Foam". Advanced Materials **2013,** *25* (4), 591-595.

[4] Chen, Z., et al. "Three-Dimensional Flexible and Conductive Interconnected Graphene Networks Grown by Chemical Vapour Deposition". Nature Materials **2011,** *10*, 424-428.

[5] Chen, Z., et al. "Lightweight and Flexible Graphene Foam Composites for High-Performance Electromagnetic Interference Shielding". Advanced Materials **2013,** *25* (9), 1296-1300.

[6] Kurahatti, R. V., et al. "Defense Applications of Polymer Nanocomposites". Defense Science Journal **2010,** *60* (5), 551-563.

[7] Breuer, O., Sundararaj, U. "Big Returns From Small Fibers: A Review of Polymer/Carbon Nanotube Composites". Polymer Composites **2004,** *25* (6), 603-645.

[8] Singh, V., et al. "Graphene Based Materials: Past, Present, and Future". Progress in Materials Science **2011,** *56*, 1178-1271.

[9] Liu, Y., Kumar, S. "Recent Progress in Fabrication, Structure, and Properties of Carbon Fibers". Polymer Reviews **2012,** *52* (3), 234-258.

[10] Qiu, Y., et al. "Hierarchical Assembly of Tungsten Spheres and Epoxy Composites in Three-Dimensional Graphene Foam and Its Enhanced Acoustic Performance as a Backing Material". ACS Applied Materials & Interfaces **2016,** *8*, 18496-18504.

[11] Glenn Research Center. https://www.grc.nasa.gov (accessed September 14).

[12] Cassanova, R., . A. "Solid State Aircraft". NASA Phase II Technical Report **2005,** *5* (3110).

[13] Choub, T. W., et al. "An Assessment of the Science and Technology of Carbon Nanotube-Based Fibers and Composites". Composites Science and Technology **2010,** *2010* (70), 1.

[14] Papageorgiou, D. G., et al. "Graphene/Elastomer Nanocomposites". Carbon **2015,** *95*, 460-484.

[15] Nieto, A., et al. "Three Dimensional Graphene Foam/Polymer Hybrid as a High Strength Biocompatible Scaffold". Advanced Functional Materials **2015,** *25* (25).

[16] Li, N., et al. "Three-Dimensional Graphene Foam as a Biocompatible and Conductive Scaffold for Neural Stem Cells". Scientific Reports **2013,** *3* (1604).

[17] Ma, Y., Chen, Y. "Three-Dimensional Graphene Networks: Synthesis, Properties and Applications". National Science Review **2015,** *2* (1), 40-53.

[18] Wang, J. K., et al. "Polymer-Enriched 3D Graphene Foams for Biomedical Applications". ACS Applied Materials & Interfaces **2015,** *7*, 8275-8283.

[19] Yang, Z., et al. "Preparation of 3D Graphene-Based Architectures and Their Applications in Supercapacitors ". Progress in Natural Science: Materials International **2015,** *25*, 554-562.

[20] Qin, Z., et al. "Effect of Wrinkles on the Surface Area of Graphene: Toward the Design of Nanoelectronics". Nano Letters **2014,** *14*, 6520-6525.

[21] Ke, Q., Wang, J. "Graphene-Based Materials for Supercapacitor Electrodes - A review". Journal of Materiomics **2016,** *2*, 37-54.

[22] Kuilla, T., et al. "Recent Advances in Graphene Based Polymer Composites". Progress in Polymer Science **2010,** *35* (11), 1350-1375.

[23] Bong, J., et al. "Dynamic Graphene Filters for Selective Gas-Water-Oil Separation". Scientific Reports **2015,** *5*, 14321-14327.

[24] Gadipelli, S., Guo, Z. X. "Graphene-Based Materials: Synthesis and Gas Sorption, Storage and Separation". Progress in Materials Science **2015,** *69*, 1-60.

[25] Yavari, F., et al. "High Sensitivity Gas Detection Using a Macroscopic Three-Dimensional Graphene Foam Network". Scientific Reports **2011,** *1* (166).

[26] Divya, H. V., et al. "Processing Techniques of Polymer Matrix Composites - A Review". International Journal of Engineering Research and General Science **2016,** *4* (3), 357-362.

[27] Ashby, M. F. "Technology of the 1990s: Advanced Materials and Predictive Design". Philosophical Transactions of the Royal Society of London **1987,** *A322*, 393-407.

[28] Balandin, A. A. "Thermal Properties of Graphene and Nanostructured Carbon Materials". Nature Materials **2011,** *10* (8), 569-580.

[29] Johnson, D. W., et al. "A Manufacturing Perspective on Graphene Dispersions". Current Opinion in Colloid & Interface Science **2015,** *20* (5-6), 367-382.

[30] Morgan, P., *Carbon Fibers and Their Composites*. CRC Press: Boca Raton, FL, 2005.

[31] Karger-Kocsis, J., et al. "Recent Advances in Fiber/Matrix Interphase Engineering for Polymer Composites". Progress in Materials Science **2015,** *73*, 1-43.

[32] Callister, J., W. D. , Composites. In *Materials Science and Engineering: An Introduction*, 8th ed.; John Wiley & Sons, Inc.: Hoboken, NJ, 2010.

[33] Aqel, A., et al. "Carbon Nanotubes, Science and Technology Part (I) Structure, Synthesis and Characterisation". Arabian Journal of Chemistry **2012,** *5*, 1-23.

[34] Boehm, H. P. "The First Observation of Carbon Nanotubes". Carbon **1997,** *35*, 581-584.

[35] Monthioux, M. "Who Should Be Given the Credit for the Discovery of Carbon Nanotubes?". Carbon **2006,** *44*, 1621-1623.

[36] Geim, A. K. "Random Walk to Graphene". Reviews of Modern Physics **2011,** *83*, 851-862.

[37] Endo, M. "Grow Carbon Fibers in the Vapour Phase". Chemtech **1988,** *18*, 568.

[38] Minus, M. L., Kumar, S. "The Processing, Properties, and Structure of Carbon Fibers". Journal of Materials **2005,** *57*, 52-58.

[39] Iijima, S. "Single-Shell Carbon Nanotubes of 1-nm Diameter". Nature **1993,** *363*, 603-605.

[40] Nieto, A., et al. "Synthesis and Properties of Bulk Graphene Nanoplatelets Consolidated by Spark Plasma Sintering". Carbon **2012,** *50* (11), 4068-4077.

[41] Chand, S. "Carbon Fibers for Composites". Journal of Materials Science **2000,** *35*, 1303-1313.

[42] Huang, X. "Fabrication and Properties of Carbon Fibers ". Materials **2009,** *2*, 2369-2403.

[43] Ovid'ko, I. A. "Mechanical Properties of Graphene". Reviews on Advanced Materials Science **2013,** *34*, 1-11.

[44] Eatemadi, A., et al. "Carbon Nanotubes: Properties, Synthesis, Purification, and Medical Applications". Nanoscale Research Letters **2014,** *9*, 393-406.

[45] Szabo, A., et al. "Synthesis Methods of Carbon Nanotubes and Related Materials". Materials **2010,** *3* (5), 3092-3140.

[46] Tsubokawa, N. "Preparation and Properties of Polymer-Grafted Carbon Nanotubes and Nanofibers". Polymer Journal **2005,** *37* (9), 637-655.

[47] Kumar, D., et al. "Microwave Assisted Synthesis and Characterization of Graphene Nanoplatelets". Applied Nanoscience **2015,** *6*, 97-103.

[48] Shokrieh, M., et al. "Effects of Graphene Nanoplatelets and Graphene Nanosheets on Fracture Toughness of Epoxy Nanocomposites". Fatigue & Fracture of Engineering Materials & Structures **2014,** *37*, 1116-1123.

[49] Wang, Y., et al. "Enhanced Thermal and Electrical Properties of Epoxy Composites Reinforced with Graphene Nanoplatelets". Polymer Composites **2015,** *36* (3), 556-565.

[50] Kaur, J., et al. "Producing High-Quality Precursor Polymer and Fibers to Achieve Theoretical Strength in Carbon Fibers: A Review". Journal of Applied Polymer Science **2016,** *133* (38), 43963-43977.

[51] Thostenson, E. T., et al. "Advances in the Science and Technology of Carbon Nanotubes and Their Composites: A Review". Composites Science and Technology **2001,** *61*, 1899-1912.

[52] Tiwari, A., Syvajarvi, M., *Graphene Materials: Fundamentals and Emerging Applications*. Scrivener Publishing: Beverly, MA, 2015.

[53] Reina, A., et al. "Large Area, Few-Layer Graphene Films on Arbitrary Substrates by Chemical Vapor Deposition". Nano Letters **2009,** *9* (1), 30-35.

[54] Hawaldar, R., et al. "Large-Area High-Throughput Synthesis of Monolayer Graphene Sheet by Hot Filament Thermal Chemical Vapor Deposition". Scientific Reports **2012,** *2: 682*.

[55] Lee, C., et al. "Measurement of the Elastic Properties and Intrinsic Strength of Monolayer Graphene". Science **2008,** *321*, 385-388.

[56] Frank, I. W., et al. "Mechanical Properties of Suspended Graphene Sheets". Journal of Vacuum Science and Technology B **2007,** *25* (6), 2558-2561.

[57] Jun, Y. S., et al. "Highly Conductive Interconnected Graphene Foam Based Polymer Composites". Carbon **2015,** *95*, 653-658.

[58] Yan, D., et al. "Enhanced Mechanical and Thermal Properties of Rigid Polyurethane Foam Composites Containing Graphene Nanosheets and Carbon Nanotubes". Polymer International **2012,** *61* (7), 1107-1114.

[59] Zhao, Y. H., et al. "Study on Thermal Properties of Graphene Foam/Graphene Sheets Filled Polymer Composites". Composites: Part A **2015,** *72*, 200-206.

[60] Osswald, T., *Understanding Polymer Processing: Processes and Governing Equations*. Hanser: Cincinnati, OH, 2010.

[61] Bakshi, S. R., et al., *Carbon Nanotubes Reinforced Metal Matrix Composites*. CRC Press Boca Raton, FL, 2011.

[62] Moniruzzaman, M., Winey, K. I. "Polymer Nanocomposites Containing Carbon Nanotubes". Macromolecules **2006,** *39*, 5194-5205.

[63] Anwar, Z., et al. "Advances in Epoxy/Graphene Nanoplatelet Composite with Enhanced Physical Properties: A Review". Polymer-Plastics Technology and Engineering **2016,** *55* (6), 643-662.

[64] Lahiri, D., et al. "Nanotribological Behavior of Graphene Nanoplatelet Reinforced Ultrahigh Molecular Weight Polyethylene Composites". Tribology International **2014,** *70*, 165-169.

[65] Jia, J., et al. "3D Network Graphene Interlayer for Excellent Interlaminar Toughness and Strength in Fiber Reinforced Composites". Carbon **2015,** *95*, 978-986.

[66] Li, C., Shi, G. "Three-Dimensional Graphene Architectures". Nanoscale **2012,** *4*, 5549-5563.

[67] Magni, S., et al. "FIB/SEM Characterization of Carbon-Based Fibers". Scanning **2007,** *29* (4), 185-195.

[68] Chen, M., et al. "Three-Dimensional Porous Stretchable and Conductive Polymer Composites Based on Graphene Networks Grown by Chemcial Vapour Deposition and PEDOT:PSS Coating". Chemical Communications **2015,** *51*, 3169-3172.

[69] Fang, Q., et al. "Synthesis, Decoration and Properties of Three-Dimensional Graphene-Based Macrostructures: A Review". Chemical Engineering Journal **2015,** *264*, 753-771.

[70] Lv, L., et al. "Solution-Processed Ultraelastic and Strong Air-Bubbled Graphene Foams". Small **2016,** *12* (24), 3229-3234.

[71] Parobek, D., Liu, H. "Wettability of Graphene". 2D Materials **2015,** *2*, 32001-32010.

[72] Qin, Y., et al. "Lightweight, Superelastic, and Mechanically Flexible Graphene/Polyimide Nanocomposite Foam for Strain Sensor Application". ACS Nano **2015,** *9* (9), 8933-8941.

[73] Hu, C., et al. "Scalable Preparation of Multifunctional Fire-Retardant Ultralight Graphene Foams". ACS Nano **2016,** *10*, 1325-1332.

[74] Chen, G., et al. "Fabrication of Three-Dimensional Graphene Foam with High Electrical Conductivity and Large Adsorption Capability". Applied Surface Science **2014,** *311*, 808-815.

[75] Zhang, H. B., et al. "Tough Graphene-Polymer Microcellular Foams for Electromagnetic Interference Shielding ". ACS Applied Materials & Interfaces **2011,** *3* (3), 918-924.

[76] Zhang, X., et al. "Dispersion of Graphene in Ethanol Using a Simple Solvent Exchange Method". Chemical Communications **2010,** *46*, 7539-7541.

[77] Park, S., Ruoff, R. S. "Chemical Methods for the Production of Graphenes". Nature Nanotechnology **2009,** *4*, 217-224.

[78] Xiao, X., et al. "Lithographically Defined Three-Dimensional Graphene Structures". ACS Nano **2012,** *6* (4), 3573-3579.

[79] Huang, X., et al. "Functional Nanoporous Graphene Foams with Controlled Pore Sizes". Advanced Materials **2012,** *24*, 4419-4423.

[80] Jia, J., et al. "Exceptional Electrical Conductivity and Fracture Resistance of 3D Interconnected Graphene Foam/Epoxy Composites". ACS Nano **2014,** *8* (6), 5774-5783.

[81] Du, X., et al. "Ultrafast Synthesis of Multifunctional N-Doped Graphene Foam in an Ethanol Flame". ACS Nano **2016,** *10*, 453-462.

[82] Sha, J., et al. "Preparation of Three-Dimensional Graphene Foams Using Powder Metallurgy Templates". ACS Nano **2016,** *10*, 1411-1416.

[83] Chen, W., Yan, L. "In Situ Self-Assembly of Mild Chemical Reduction Graphene for Three-Dimensional Architectures". Nanoscale **2011,** *3*, 3132-3137.

[84] Deng, W., et al. "Hydrothermal Self-Assembly of Graphene Foams with Controllable Pore Size". RSC Advances **2016,** *6*, 20843-20849.

[85] Min, Z., et al. "Preparing three-dimensional graphene architectures: Review of recent developments". Chinese Physical Society **2013,** *22* (9), 1-8.

[86] Samad, Y. A., et al. "Novel Graphene Foam Composite with Adjustable Sensitivity for Sensor Applications". ACS Applied Materials & Interfaces **2015,** *7*, 9195-9202.

[87] Reddy, S. K., et al. "Highly Compressive Behavior of Polymer Mediated Three Dimensional Network of Graphene Foam". RSC Advances **2014,** *4*, 50074-50080.

[88] Zhao, Y.-H., et al. "High Thermal Conductivity of Flexible Polymer Composites Due to Synergistic Effect of Multilayer Graphene Flakes and Graphene Foam". Composites: Part A **2016,** *85*, 148-155.

[89] Xu, R., et al. "Facile Fabrication of Three-Dimensional Graphene Foam/Poly(dimethylsiloxane) Composites and Their Potential Application as Strain Sensor". ACS Applied Materials & Interfaces **2014,** *6*, 13455-13460.

[90] Lahiri, D., et al. "Unfolding the Damping Behavior of Multilayer Graphene Membrane in Low Frequency Regime". ACS Nano **2012,** *6* (5), 3992-4000.

[91] Supermarket, G. https://graphene-supermarket.com/3D-Multilayer-Freestanding-Graphene-Film-2-x2-Foam-2x2.html (accessed February 01).

[92] Rudolf, C. C. Microstructure and Mechanical Properties of Nanofiller Reinforced Tantalum-Niobium Carbide Formed by Spark Plasma Sintering. Florida International University, 2016.

[93] Materials, A. MTI Instruments SEMtester. http://www.azom.com/equipment-details.aspx?EquipID=1777.

[94] Kim, K., et al. "High-Temperature Stability of Suspended Single-Layer Graphene". Physica Status Solidi **2010,** *4* (11), 302-304.

[95] Agrawal, R., et al. "Nanoscale Damping Characteristics of Boron Nitride Nanotubes and Carbon Nanotubes Reinforced Polymer Composites". ACS Applied Materials & Interfaces **2013,** *5*, 12052-12057.

[96] Nautiyal, P., et al. "Harnessing Three Dimensional Anatomy of Graphene Foam to Induce Superior Damping in Hierarchical Polyimide Nanostructures". Small **2017**, 1-8.

[97] Wu, Y., et al. "Three-Dimensionally Bonded Spongy Graphene Material with Super Compressive Elasticity and Near-Zero Poisson's Ratio". Nature Communications **2015,** *6*, 6141.

[98] Heijboer, J. "Modulus and Damping of Polymers in Relation to Their Structure". British Polymer Journal **1969,** *1*, 3-14.

[99] Geethamma, V. G., et al. "Vibration and Sound Damping in Polymers". Resonance **2014,** *19* (9), 821-833.

[100] Kroisova, D., An Internal Damping in Epoxy Composite Systems. In *ISMA*, 2010; pp 1207-1218.

[101] Nieto, A., et al. "Multi-Scale Intrinsic Deformation Behavior of Free-Standing 3D Graphene Foam". Carbon **2015,** *85*, 299-308.